



UNIVERSITAT DE
BARCELONA

Analysis and design of heating systems for advanced automotive Radomes

Marc Torres Sacristan

ADVERTIMENT. La consulta d'aquesta tesi queda condicionada a l'acceptació de les següents condicions d'ús: La difusió d'aquesta tesi per mitjà del servei TDX (www.tdx.cat) i a través del Dipòsit Digital de la UB (diposit.ub.edu) ha estat autoritzada pels titulars dels drets de propietat intel·lectual únicament per a usos privats emmarcats en activitats d'investigació i docència. No s'autoritza la seva reproducció amb finalitats de lucre ni la seva difusió i posada a disposició des d'un lloc aliè al servei TDX ni al Dipòsit Digital de la UB. No s'autoritza la presentació del seu contingut en una finestra o marc aliè a TDX o al Dipòsit Digital de la UB (framing). Aquesta reserva de drets afecta tant al resum de presentació de la tesi com als seus continguts. En la utilització o cita de parts de la tesi és obligat indicar el nom de la persona autora.

ADVERTENCIA. La consulta de esta tesis queda condicionada a la aceptación de las siguientes condiciones de uso: La difusión de esta tesis por medio del servicio TDR (www.tdx.cat) y a través del Repositorio Digital de la UB (diposit.ub.edu) ha sido autorizada por los titulares de los derechos de propiedad intelectual únicamente para usos privados enmarcados en actividades de investigación y docencia. No se autoriza su reproducción con finalidades de lucro ni su difusión y puesta a disposición desde un sitio ajeno al servicio TDR o al Repositorio Digital de la UB. No se autoriza la presentación de su contenido en una ventana o marco ajeno a TDR o al Repositorio Digital de la UB (framing). Esta reserva de derechos afecta tanto al resumen de presentación de la tesis como a sus contenidos. En la utilización o cita de partes de la tesis es obligado indicar el nombre de la persona autora.

WARNING. On having consulted this thesis you're accepting the following use conditions: Spreading this thesis by the TDX (www.tdx.cat) service and by the UB Digital Repository (diposit.ub.edu) has been authorized by the titular of the intellectual property rights only for private uses placed in investigation and teaching activities. Reproduction with lucrative aims is not authorized nor its spreading and availability from a site foreign to the TDX service or to the UB Digital Repository. Introducing its content in a window or frame foreign to the TDX service or to the UB Digital Repository is not authorized (framing). Those rights affect to the presentation summary of the thesis as well as to its contents. In the using or citation of parts of the thesis it's obliged to indicate the name of the author.

Tesi doctoral

Analysis and design of heating systems for advanced automotive Radomes

Marc Torres Sacristan



UNIVERSITAT DE
BARCELONA

A handwritten signature in blue ink, consisting of several overlapping loops and lines.

Marc Torres Sacristan

A handwritten signature in blue ink, featuring a large, stylized 'J' and 'E' followed by a long horizontal stroke.

Joan Esteve Pujol

Analysis and design of heating systems for advanced automotive Radomes

Programa de doctorat en Física U.B.

Autor/a: **Marc Torres Sacristan**

Director/a: Joan Esteve Pujol

Tutor/a: Artur Carnicer Gonzalez

Universitat de Barcelona



UNIVERSITAT DE
BARCELONA

*Aquesta tesi ha sigut possible gràcies al
programa de Doctorats Industrials de la
Generalitat de Catalunya.*



Agraïments

En primer lloc, agrair a l'empresa, Zanini Autogrup SA, la possibilitat que m'han donat de dur a terme aquest projecte de recerca amb ells i la confiança dipositada en mi. Igualment a l'equip d'innovació i al seu director, August Mayer, i especialment als meus companys dels equips de Radomes i de Nanocoatings.

Agrair al meu director, en Joan Esteve, tot el temps dedicat en tutories, proves i experiments, correccions i organització de calçotades i sopars. Als companys i professors que han col·laborat amb mi del Departament de Física Aplicada.

Per últim i l'agraïment més important, als meus pares, perquè sense ells res d'això hagués estat possible. A la Cristina, pel seu suport durant aquests anys de tesi. I a la Maria i als que vindran per haver-m'ho fet més complicat del què seria.

Abstract

The main purpose of this thesis is to study how we could obtain a transparent heating system for a Radome. In the context of this thesis, transparent have two different meanings that are tied due to the objective of our research. First, transparent means that the heating system have not to disturb the electromagnetic radiation from the radar. And, secondly, and because of the industrial nature of this thesis, the heating system have not to be seen by an external observer, or, we can also say that it has not to disturb the aspect of the exterior decoration of the Radome.

After previous studies of different possible options, we get focus on Transparent Conductive Oxides (TCO) applications to get a heating system different from these that already exist to warm, defrost, and avoid ice on the surface of Radomes used on some vehicles [1], [2], [3]. Different elements and concepts needed to be considered for the developing of the TCO:

- How to deposit TCO
- Optimal sheet resistance
- Optimal circuit designs
- Effect of radar polarization
- Attenuation of radar electromagnetic waves
- Adhesion of the TCO on the substrate
- Heating and attenuation requirements from vehicle's companies
- Electrical connection and Power supply

Considering all the points mentioned we will be able to design two different heating systems based on TCO's that are transparent to the human eye and minimize the attenuation of electromagnetic radiation of the radar.

The TCO depositions are used in two different ways depending on how important the polarization of the radar radiation is for the heating system, this way we can differentiate two heating systems:

First, we see from previous studies made at the company, [REDACTED] [REDACTED] is almost transparent to the radar and [REDACTED] [REDACTED]. So, it is not conditioned by the polarization of the radar radiation. In this part of the thesis, we develop thin film coatings of [REDACTED] [REDACTED] at the Univeristy of Barcelona and at the University of Zaragoza. The development of this system is explained in chapter 3.

Secondly, we developed a system [REDACTED] that are not visible for human eye and that are placed on the surface of the Radome. In this way we improve the thermal efficiency of the heating system with respect to copper wires systems since our heating system is almost in direct contact to ice and water, solely a film of few microns of varnish would protect the system from the outside in a real case. In this case the attenuation of radar radiation caused by the heating system is [REDACTED]

The development of this system is explained in chapter 5.

Resum en català

El principal propòsit d'aquesta tesi és estudiar com podem aconseguir un sistema d'escalfament transparent per a un Radome. En el context de la tesi, transparent té dos significats diferents però lligats degut als objectius de la recerca. Primer, transparent es refereix a que el sistema d'escalfament no ha de destorbar la radiació electromagnètica del radar. I, segon, i degut a la naturalesa industrial de la tesi, el sistema d'escalfament no ha de ser visible per un observador exterior, o, dit d'una altra manera no pot destorbar l'aspecte de la decoració exterior del Radome.

Després d'un estudi previ de diferents possibles opcions, ens hem centrat en l'ús de Òxids Conductors Transparents (o TCO per les sigles en anglès) per tal d'aconseguir un sistema d'escalfament diferent als que existeixen per escalfar, descongelar i evitar el gel a la superfície dels Radomes utilitzats en alguns vehicles [1],[2],[3]. Per fer-ho necessitem prendre en consideració diferents elements i conceptes:

- Com dipositar un TCO
- Una resistència superficial òptima
- Disseny òptim del circuit
- Efectes de la polarització
- Atenuació de la radiació electromagnètica
- Adhesió del TCO en el substrat
- Requeriments d'escalfament i atenuació per part de les companyies de vehicles
- Connectors i subministrament d'energia

Considerant tots els punts anomenats serem capaços d'obtenir dos sistemes d'escalfament basats en TCOs que són invisibles a l'ull humà i que minimitzen l'atenuació de la radiació electromagnètica causada pel mateix sistema.

La manera com hem utilitzat els dipòsits de TCO es poden diferenciar a partir de com d'important és la polarització de la radiació del radar pel sistema d'escalfament, d'aquesta manera podem diferenciar dos sistemes d'escalfament:

Primer, a partir de resultats d'estudis fets prèviament a l'empresa, [REDACTED]

[REDACTED] En aquest cas el punt més important és [REDACTED]. Per tant, aquest sistema no estaria condicionat per la polarització de la radiació del radar. En aquesta part de la tesi, [REDACTED]

Content

Chapter 0.....	17
Introduction.....	17
0.1 Historical Context of the Thesis.....	18
0.2 Sensors and ADAS system.....	19
0.3 Aesthetics	22
0.4 State of the art	22
0.5 Outline & Objective	28
0.5.1 Main objective.....	29
0.5.2 Outline.....	29
Chapter 1.....	32
Basic concepts.....	32
1.1 Basics of wave propagation.....	32
1.1.1 Electromagnetic waves propagation.....	32
1.1.2 Plane wave Reflection and Transmission at a dielectric interface	38
1.1.3 Polarization.....	39
1.2 Heating systems based on Joule’s effect.....	41
1.2.1 View of a common Radome with a heating system based on metallic wires.....	41
1.2.2 Radome with a heating system based on TCO.....	42
1.3 Substrate Thickness adaptation	44
1.4 Materials for Transparent Conductive Oxides (TCO).....	45
1.4.1 Optical properties of TCO thin films	46
1.4.2 Electrical conductivity of TCO thin films	48
1.4.3 ABC.....	49
1.5 EM wave transmission through multiple layer films	50
1.6 About the simulation software – CST Studio Suite	52
1.7 Minimum energy requested to melt ice on a Radome surface	52
Chapter 2.....	56
Instruments and methods.....	56
2.1 Magnetron Sputtering.....	56
2.1.1 Sputtering system at the University of Zaragoza (UZag).....	57
2.1.2 Sputtering system at the University of Barcelona (UB).....	58
2.2 Thickness Measurements	60
2.2.1 Profilometer.....	60
2.2.2 Focused ion beam (FIB).....	61

2.3 Resistance Measurements	62
2.3.1 Four-point probe with Jandel RM3	62
2.3.2 Hand-made system for measuring square Resistance of samples	64
2.3.3 Confocal Microscope - Sensofar PL μ 2300	65
2.4 Attenuation and Reflectivity microwave measurements (UPC)	66
2.4.1 Scattering parameters (S-parameters)	66
2.4.2 Attenuation system	68
2.4.3 Reflectivity set-up	69
2.5 Climate Chamber - Weiss WKL 100	70
2.6 Optical measurements of Transmission Spectra	71
Chapter 3.....	76
TCO films	76
3.1 Introduction	76
3.1.1 Background	76
3.2 Properties of [REDACTED] deposited at the University of Zaragoza.....	78
3.2.1 Thin film parameters	78
3.2.2 MW transmission, reflection, and absorption measurements.....	79
3.3 Properties of [REDACTED] deposited at the University of Barcelona (UB)	82
3.3.1 [REDACTED]	82
3.3.2 Deposition of [REDACTED]	82
3.4 Thin film homogeneity.....	85
3.5 Heating test.....	86
3.6 Summary and comments	89
Chapter 4.....	92
Characterization of commercial samples	92
4.1 Introduction	92
4.2 Characterization of the samples	92
4.2.1 Sheet Resistances	93
4.2.2 Profilometer measurements.....	93
4.2.3 FIB and SEM measurements.....	94
4.2.4 Transmission Spectra	96
4.2.5 Radar measurements	99
4.3 Simulations.....	101
4.4 Summary and comments	103
Chapter 5.....	105
[REDACTED] etched circuit.....	105
5.1 Introduction	105

5.1.1 Designed circuit.....	107
5.2 Preliminary test	108
5.2.1 Samples	108
5.2.2 ████ etching.....	109
5.2.3 Tests	110
5.3 Optimization of samples and results	112
5.3.1 Laser expansion.....	112
5.3.2 Simulations.....	117
5.4 Real samples results	119
5.4.1 Attenuation.....	120
5.4.2 Real samples vs Simulated samples	122
5.5 Heating tests	124
5.6 Summary and comments	127
6 Conclusions	130
REFERENCES	134

Chapter 0

Introduction

This thesis is oriented on the improvement of the radar system applied in the automotive industry for autonomous vehicles. Nowadays the safety of the occupants of the vehicles is the main reason of the application and development of technology for transportation. Human conduction is subject to many constraints and imperfections due to the nature of the human being: fatigue, stress, tension, distraction ... and, of course, the behavior of each one before and during the driving time. All of this together with the limitation of information we can perceive and process and other interferences that can occur during driving time, makes human conduction risky. We can see this just looking at the number of accidents in the urban and interurban areas in Catalonia during 2017 as an example:

— Dades d'accidentalitat per àmbits —

Zona	Àmbit	Accidents amb víctimes	Accidents mortals	Morts	Morts i ferits greus	Ferits greus	Ferits lleus
Interurbana	Barcelona	5.622	63	72	471	399	8.067
	Girona	1.255	27	33	145	112	1.731
	Lleida	942	32	34	176	142	1.273
	Tarragona	1.136	23	29	154	125	1.503
	Total	8.955	145	168	946	778	12.574
Urbana	Barcelona	15.364	44	44	702	658	18.490
	Girona	1.421	10	10	126	116	1.657
	Lleida	449	2	2	64	62	522
	Tarragona	863	12	16	113	97	973
	Total	18.097	68	72	1.005	933	21.642

— Condició de les víctimes en els accidents de trànsit —

Zona	Condició	Morts	Morts i ferits greus	Ferits greus	Ferits lleus
Interurbana	Conductor	129	712	583	8.602
	Passatger	33	195	162	3.655
	Vianant	5	24	19	78
	Altres	1	15	14	239
	Total	168	946	778	12.574
Urbana	Conductor	38	570	532	14.606
	Passatger	7	61	54	2.250
	Vianant	27	341	314	2.927
	Altres	0	33	33	1.859
	Total	72	1.005	933	21.642

Fig1 – Statistic yearbook of traffic accidents Catalunya 2017

The growing of safety requirements by the clients and governments push companies of the transportation sector to introduce and develop technologies to reduce all this numbers to zero. So, the idea of an “entity” that replace human drivers to improve the safety of the occupants of a vehicle becomes each year more real with the application of new technologies coming from different sectors like sensing, data processing and machine learning. These technologies would

let vehicles understand their surroundings and communicate between them sharing information with other sensors and traffic signals that makes easier to take a safety choice when driving. Taking all of this into account, firms have created standards to regulate these technologies and define different levels of autonomy of the vehicles to define the path to get the objective of the total autonomous driving. The set of different systems that help de driver in the driving process is called ADAS (Advanced Driving Assistance System).

0.1 Historical Context of the Thesis

The Information given by sensors needs to be clear to be processed by the vehicle to take the correct decision each time with no human factors involved. So, we need to protect sensors of the vehicle, but this protection cannot disturb the information received by the sensor. In this context the improvement of the sensors is allows tied to protection system that makes the sensors receive good and clear information is a key factor on the development of a self-driving system. Also, sensors and protections need to adapt to the legislation of the governments.

The first trials took place in New York City in 1925 [1] when a radio equipment firm, Houdina Radio Control, drove a radio-controlled car [2] from a car that follows the guided car. It was an elementary trial but was a prove that with the correct an optimal sensor working in a good way a car was able to be driven by no one in any weather conditions.



Fig2 -Radio News, November 1925, americanradiohistory.com

Other experiments between 1939 to 1980 were developed implying different electric and magnetic devices imbedded on the roadway to guide the vehicle like Normand Bel Geddes's at the World Fair of 1939 sponsored by GM (General Motors). Or RCA Labs in 1953, the Transport and Road Research Laboratory tested a Citroen DS that interacted with magnetic cables embedded in the road. Then in 1980, a vision guided driverless Mercedes-Benz robotic van designed by Ernst Dickmanns at the Bundeswehr University of Munich achieved a speed of 63 km/h on the streets without traffic. That was the first vision guided system used with no need of embedded devices on the road [2].

Today the most important firms are testing right now their driver-less vehicles General Motors, Mercedes Benz, Volkswagen, Audi, Nissan, Toyota, BMW, and Volvo. A driverless taxi is being tested in the roads of a residential area in Dubai. Companies like Tesla have started to sell completely autonomous vehicles that you can test at their stores and one can already see on the road. In the USA these Tesla vehicles have no restriction for driving without human help, in Europe legislation makes the driver to have his hands on the steering wheel even if the human being is doing nothing to control the car.



Fig3 – Klejj Times Dubai

0.2 Sensors and ADAS system

Different sensors take part during the decision making, each sensor is used to collect a part of the surrounding information, depending on the characteristics of the information a different sensor needs to be used, of course, they are working all together at the same time. This way we have:

- Long Range Radar: Adaptive Cruise Control. It works between 76 GHz and 77 GHz radar range and it is used to detect distant objects like controlling the distance between the car in front, it has low angularity, but it works well in any weather conditions.
- LIDAR: a LIDAR sensor continually fires off beams (up to 150.000 beams per second) [3] of laser light, and then measures how long it takes for the light to return to the sensor. By firing off millions of beams of light per second, the measurements from the LIDAR sensor enable a visualization of the world that is truly 3D. They work at the infrared range. Emergency braking and pedestrian detection are some of its uses.
- Cameras: they work at the visible range and they are used for traffic sign recognition, Park assistance, ... It has more accurate angularity, but it has many problems of light absorption.
- Short/Medium- Range Radar: Like the first one it works at the radar range for Cross traffic alert.
- Ultrasounds – Are basically used for very short distance when parking the car.

Figure 4 Gives us an idea of the different systems working and is an overview of the different sensors included in the ADAS system:

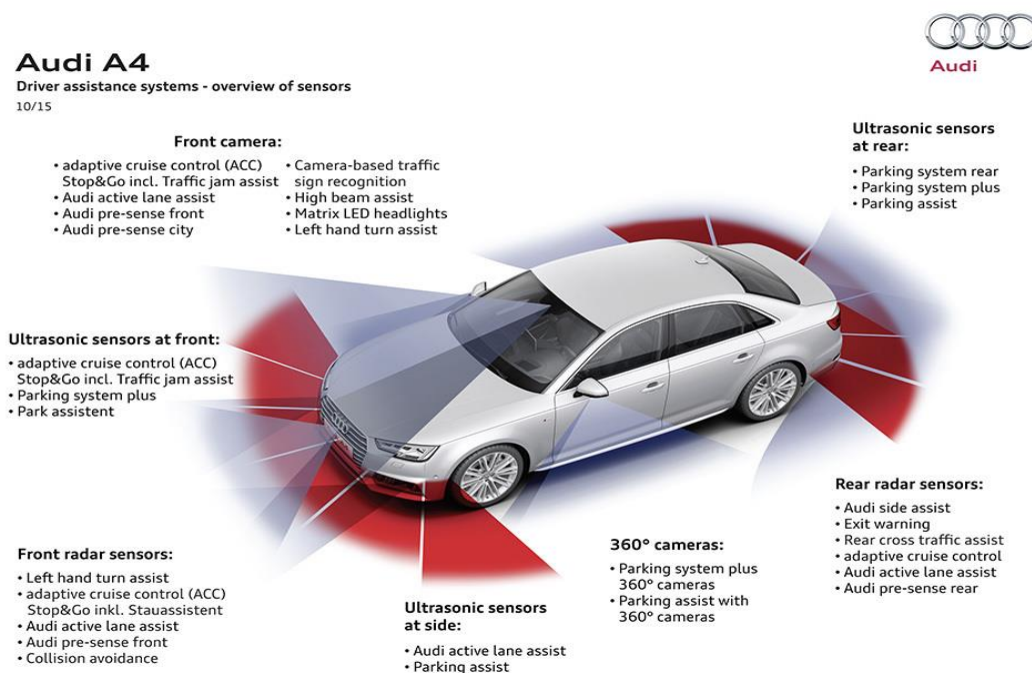


Fig4 – Source: Forum-Audi.com

The ADAS system needs to work all the time no matter the weather conditions and each sensor needs to be protected against external aggressions. In this thesis we will focus on Radar sensors

and its protection that its call Radome (Radar Dome). Radome needs to be transparent to the radar radiation in order not to disturb the measurements of this sensor. The most important problem is when water, ice, or snow particles are stuck on the surface of the Radome then the capacity of measurements of the Radome drops notably. From [4] we can see in figure 5 and schematic representation of radar radiation going through a Radome with a water-film in front and in figure 6 from [5] the effect of the thickness of the film of water on the transmissivity of the radar signal depending on the frequency used.

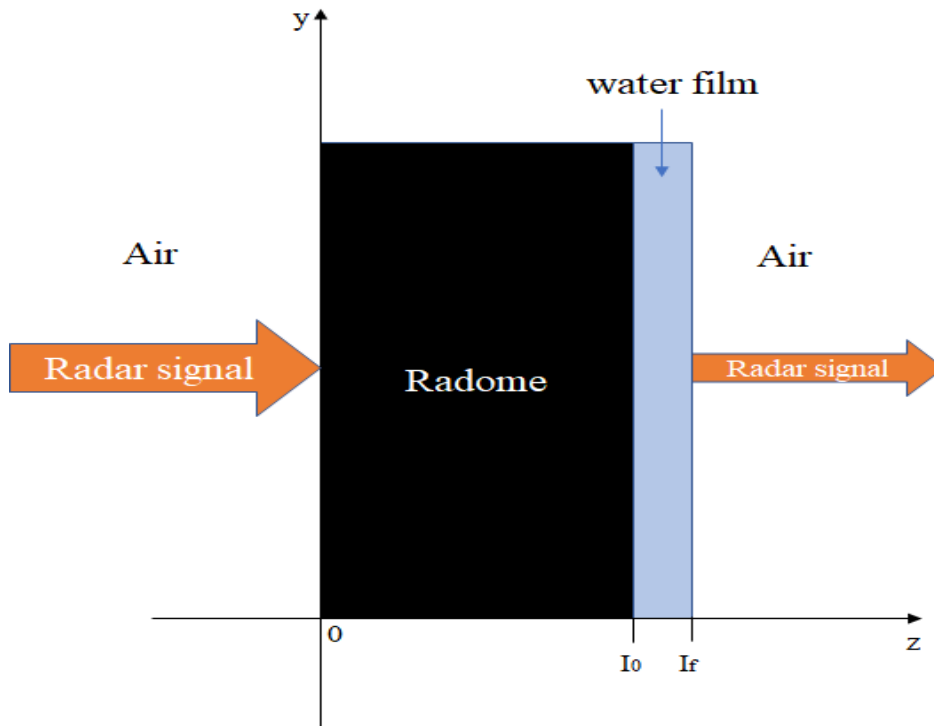


Fig5. Schematic representation of a Radome with a water-film in front of it

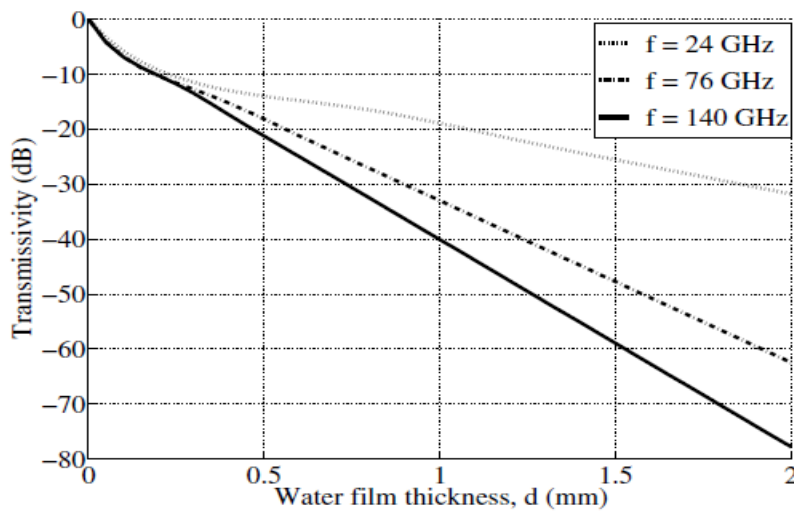


Fig6. Transmissivity through water film at 20 °C. [5]

From these data one concludes that radar sensor gets completely blind when a film of water is placed in front of the Radome. So, avoiding the stuck of water particles on the surface of the Radome is a key factor for the good function of the radar sensor, especially in cold countries.

0.3 Aesthetics

For the automotive companies, the esthetics of its creations is very important, since considering the car nice is an important reason to buy a car. Furthermore, the most optimal position to place the radar to operate suitably is, in most cases, in the same place where the emblem of the firm is placed. So, the emblem of the firm is used as the Radome and at the same time it is the symbol that represents the company, so, it must be nice, and the image of the firm must not be affected by sensors or protections. This means that any kind of system trying to avoid ice and fogg in the surface of the Radome needs to respect the quality and esthetics standards of the firms.

This is also the reason why the emblems of the firms have changed its design and composition in the last years. As an example:



Fig7. – Images of different emblems of mercedes taken from internet

0.4 State of the art

Today all the system required by automotive companies to avoid water films on the Radomes are based on heating systems. Hydrophobic coatings are also used but they are limited in function and their properties degrade in short time compared with the required life of a Radome that is between 10 and 15 years. Hydrophobic properties can help heating systems to erase water-films but cannot work alone against ice and fogg as well as heating systems. So, the main tasks of the

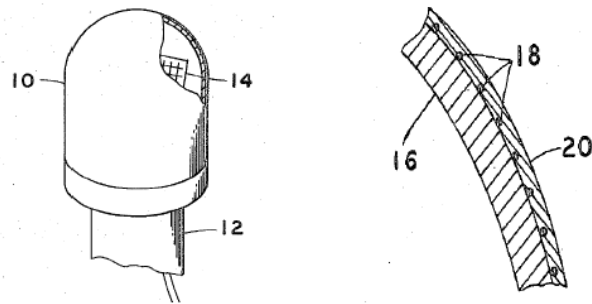
heating systems are defrosting and deicing the Radome surfaces to maintain the operativity of the radar sensors. As an Esthetic requirement from firms this heating system should be very difficult to see for human eye or even completely invisible in order not to affect the design of the car. As a functional requirement, the heating system should not affect the radar signal. In practice this is almost impossible, so the limit of affectation of all the Radome, including the heating system is on -3 dB. But this requirement is becoming more restrictive each time as well as the requirements of safety gets higher, then the radar detection would have to be more precise.

Theses heating systems that exist today are all based on electric heater, so metallic wires are embedded in the Radome to heat it when it is needed. Some of them are already used in car emblems, some others are just developments of firms that has been patented but not used. The basic ideas come from Radomes that already exist and used in military equipment or in aeronautic industry where radar technology is a key factor for the security of the vehicles and the detection of external aggressions. Military and aeronautic industry have different functional requirements as well as they work in a different range of frequencies and the power supply is not limited to a battery car. Of course, in military and aeronautic industries there are no esthetic requirements. Some examples of heating systems in Radomes that already exist in the military and aeronautic industries are:

- Patent US-3805017 General Dynamics Corporation (Department of US Navy):

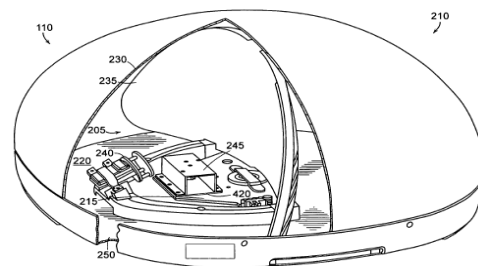
Patent of a cylindrical and spherical Radome with a resistance (18) around the structure of the Radome imbedded on the outer coating (20) that is thermally conductive.

The resistance is made of Nickel Chrome alloy.



- Patent US-2007/0120759 A1 KVH industries, Inc.

The surface of the Radome is heated by heating the air inside the dome, also a thermal isolator material is used on the base of the antenna in order to focus the thermal flux to the upper side of the dome



- Patent PCLO 219201000 Bell Helicopter Textron

An ice protection system (19) for a structure (25) has at least one electro-thermal heating element (23) carried by the structure (25) and a controller (21) for selectively controlling the operation of each heating element (23). The controller (21) operates each heating element (23) according to a selected duty cycle defined by a pattern of time intervals, the controller (21) selecting the duty cycle at least partially in response to measurements of ambient conditions about the structure (25).

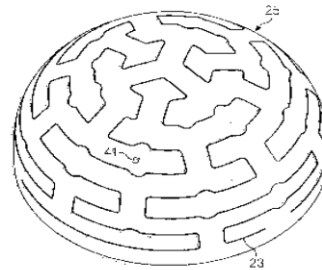


FIG. 4

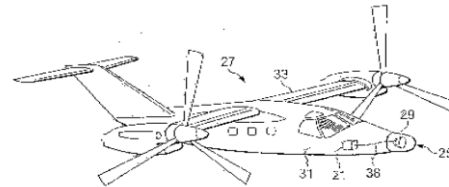
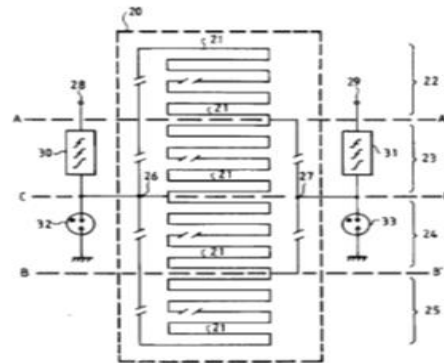


FIG. 5

- Patent PCLO 343704000 Thomson CSF

Anti-icer that can be used to neutralize the effects of a nuclear electromagnetic pulse or of parasitic electromagnetic fields coming from other radars transmitting in the vicinity. The anti-icer comprises a sheet of conductive wires positioned on a screen placed before the aperture of the radar antenna.



The most common Radome in aeronautic industry is placed on the front part of the plane, where weather radar scanner is placed:

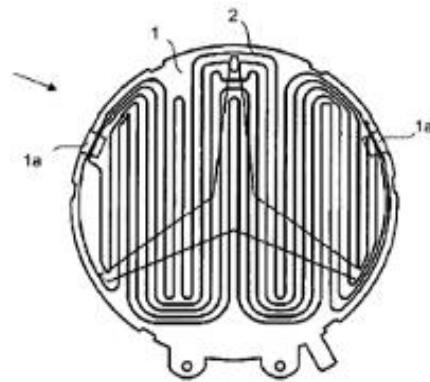


Fig 8 – radar and Radome of a military plane (left) and a comercial plane (right)

The main cars companies started to develop Radomes for cars and transport vehicles years ago. Some of these developments are right now on the street and some others are not. Some examples that we can already see are:

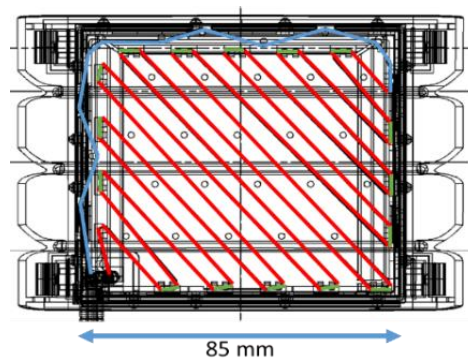
- Patent DE 102014002438 A1 Daimler AG

Patent of a fabrication process of heated Radome with a film with a conductive wire inside. The design of the circuit of the wire need to be adjusted to minimize attenuation of radar radiation and according to polarization. So, parallel parts of the wire must be separated between 3 and 10 mm preferable 5 mm. The wire has a diameter between 40 μm and 60 μm . The point where the wire contacts the power supply is made by thermocompression



- Patent DE 10156699 B4 Audi

This is a cover type Radome, so, it is not the emblem of the car is a cover with a heating system with also wires imbedded on the plastic part. Here wires are placed in diagonal and then polarization of the radar should be perpendicular to the wires

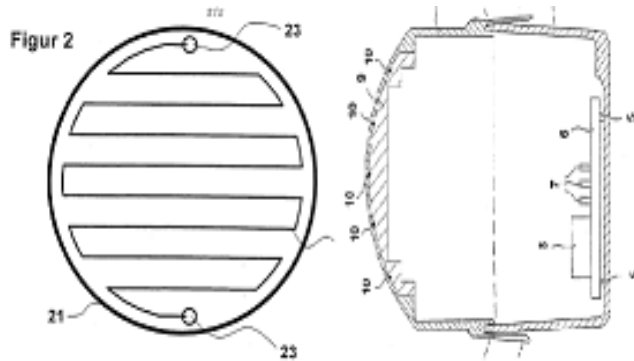




We can find other examples on the covers of the radar and some other patent that are developed and not used or still in development:

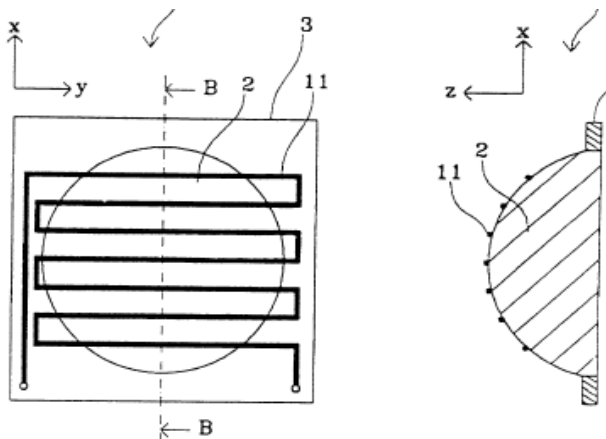
- Patent WO 0148509 A2 Robert Bosch GmbH

This patent is system of radar and Radome. The Radome not only have a heating system also it acts like a lens to focus electromagnetic radiation of the radar. The wires are made of a conductive material and placed parallels imbedded in the outer surface of the Radome



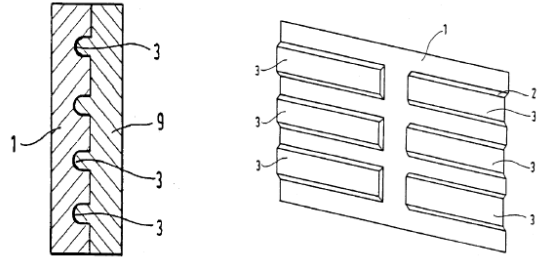
- Patent PCLO 343704000 Murata Manufacturing

Like the last one this invention provides a dielectric lens antenna having a lens comprising a dielectric material and a heating body disposed on a surface of the lens. The above dielectric lens antenna has a snow melting function, which allows no degradation in lens efficiency



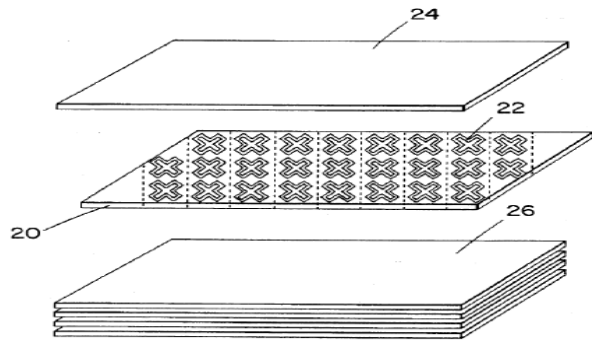
- Patent US 6433753 B1 Daimler Chrysler

Radome with thin metal layers (no specification of what kind of material). This patent is only referred to the design of the Radome.



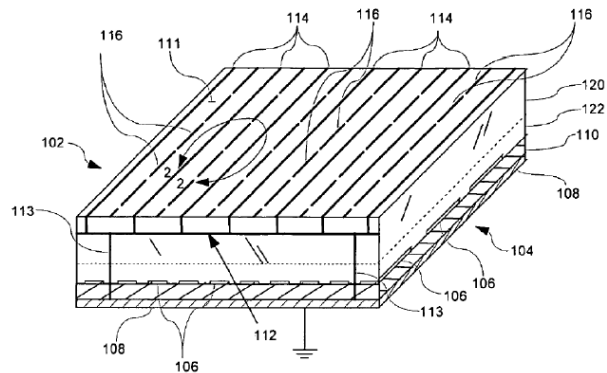
- Patent US 005528249 A no company, group of particular inventors

Radome with a selective surface. The selective surface is made of metal that can heats the Radome, with some periodical pattern that makes the metallic layer resonate at the frequency we want and let radar radiation go through the metallic layer with no attenuation and independent of polarization

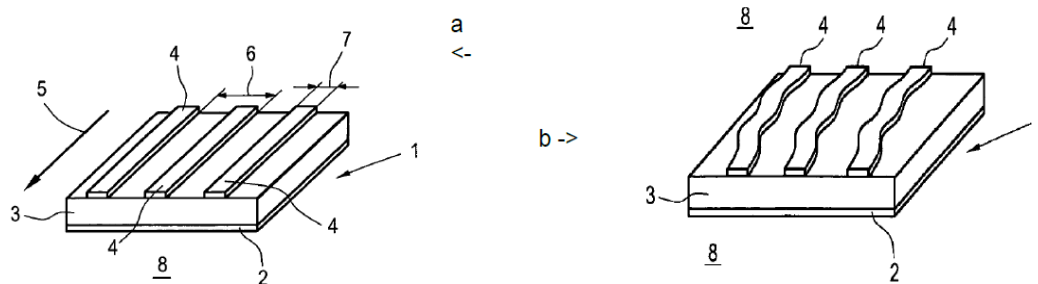


- Patent US 2007/0252775 A1 Harris Corporation

Patent of a method to improve the efficiency of the Radome, using a Radome with metallic wires to heat it, they introduce some capacitive elements to cancel the inductance of the wires. This way the Radome can correct the attenuation. This system is also independent of polarization



- Patent EP 2151889 A1 Audi AG



Capacitive and inductive elements are introduced also in this Radome to minimize attenuation. In this case the wires can be placed parallel between them or with some specific pattern.

As we mentioned just some of these heating systems are working right now on the emblems of some cars. Despite the benefits in attenuation of the rectifying heating systems they are not used right now so they can be still in development or perhaps they are just ideas that companies have not achieved.

0.5 Outline & Objective

Most important firms and companies in car sector have focused its interest in protecting sensors and make them operative in all weather conditions, so, development of heating systems for plastic parts to avoid icing and dicing without interaction with the sensor has become one of the most important areas of research in the automotive sector. The most intuitive method is to introduce metallic wires as a resistance as we have seen in different patents from the most important firms. A simple principle is used, when current passes the temperature grows up heating the plastic part. This simple system has some problems to solve:

- Electromagnetic transparency, the wires must be of specific size and be placed on specific positions in order to minimize absorption of the radiation due to electrical conductivity of the wires.
- Homogeneity of the heated surface, because of the separation of the wires the surfaces is not heated in a homogeneous way and together with the low thermal conductivity of the plastics used to make the Radome, high differences of temperature appears between the wire region and its surroundings.

- Efficiency, these wires are introduced inside the plastic part at some distance of the surface so thermal conductivity of the material is a key factor and an inconvenient for the efficiency of the heating system.
- Aesthetic, most of times the Radome is the emblem of the car firm because it is placed on a privileged area of the car for radar detection, wires inside should not be seen from the outside since they damage the main image of the company.
- Material problems, Wires also can damage the plastic part due to dilatation and contraction when they get heat and cold.

All these different factors are linked since the placement and size of the wires affects the efficiency, the esthetics and the electromagnetic transparency. At the same time, we need to consider the design of the Radome and the specifications of each radar used by different firms. So, right now a balance of all these parameters is needed and they constrain the capabilities of the heatable Radome. The heating system should adapt to the surface of the Radome maximizing the efficiency, minimizing attenuation, being transparent at the visible range and it should not be dependent of the polarization of the radar.

The use of conductive materials inside or on the surface of the Radome generates some attenuation of the radar signal due to the absorption of the electromagnetic (em) radiation by the conductors since the amplitude of an em wave is attenuated exponentially following:

$$e^{-\alpha z} \text{ where } \alpha = \sqrt{\omega\mu\sigma}$$

being σ the conductivity, ω the angular frequency of the electromagnetic radiation and μ is magnetic permeability so, briefly we can say that more conductivity implies more attenuation.

0.5.1 Main objective

Design a heating system that reduces the impact on the image of the company and, on the same time, improves its electromagnetic transparency, erases polarization dependence, improves homogeneity of the heated surface and avoid degradation of the Radome due to the heating system function.

0.5.2 Outline

Here we want to use Transparent Conductive Oxides (TCO) to improve some of the points commented in different ways depending on the properties of the TCO layers. Using TCOs the aesthetic problem could be solved since they are transparent in the visible range.

We use TCO in two different ways:

- First, we use [REDACTED] and to design a heating system [REDACTED]. In this case, [REDACTED] [REDACTED]. We have had to design these films and find the deposit conditions to avoid degradation. The most important advantage of this system is that [REDACTED], this is a very important point since in the future radars with multiple polarizations can be used to receive more information from outside of the car.
- Second, we use the TCO to do wires like the commercial Radomes but with a totally different design by changing placement and size to improve its efficiency. To do this, we needed [REDACTED] with a transmittivity in the visible range [REDACTED] to minimize damage on the aesthetics. The thin film has to be placed at the surface of the Radome to improve the thermal efficiency of the heating system. We have drawn the appropriated circuit using a laser etching technology to meet the requirements of attenuation for the heating system (-0.6 dB maximum).

To develop [REDACTED] TCO system, different samples have been made at the University of Barcelona (UB) and at the University of Zaragoza (UZag). Different thickness and different deposition conditions have been used to deposit ABC and ABC on polycarbonate substrate. Attenuation of the radar radiation were measured at the Nord Campus Laboratory of the Universitat Politècnica de Catalunya (UPC) and the square resistances and the coatings thickness were measured at the UB.

To design the TCO [REDACTED] we have performed electromagnetic simulations with CST studio-2019 software this way we could optimize the design and minimize the real samples made at the laboratory. We need also to optimize the [REDACTED] to improve its efficiency and the [REDACTED]. Because of the [REDACTED] by the material [REDACTED] the edges of the wires expand and create deformations on the edges of the TCO wires this effect needs to be consider when implementing the designs and optimized by simulation.

In both cases heating test had been performed with different measurements of the temperature of the heating system using a thermocouple and a climatic chamber. The tests had been performed inside the climatic chamber to reproduce the cold weather conditions where the systems should work.

Chapter 1

Basic concepts

1.1 Basics of wave propagation

The heating systems we have worked on, are based on different concepts (or solutions). All them require to be heated using an electric DC or AC current but, whichever should be the solution, they need to be simultaneously enough transparent to the Radar Electromagnetic Radiation and transparent to the visible light.

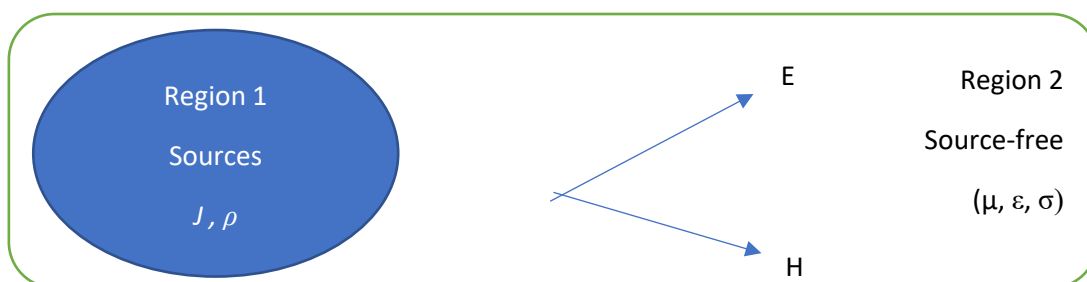
This chapter presents an essential summary about the propagation of the electromagnetic waves (em) radar signal, through a multi-layer media. First, we will start with the basics of propagation in two media, we will add a third medium, and then we will see a general formulation for n media.

We also will see how this propagation on different media affects attenuation depending on the nature of the media and how it is related to the em skin depth. However, for the concepts based on the heating through conductive wires, we will be also interested in the geometry of the wires and we will see, with the help of simulation, how em wave propagation is affected by them.

Some basics of TCO (Transparent Conducting Oxides) will be also commented, its characteristics and main properties, especially with ABC (ABC ABC ABC),

1.1.1 Electromagnetic waves propagation

Consider a linear, homogeneous, isotropic media characterized by μ, ϵ, σ in a source-free region (Region2) and a source region (Region1)



For the source-free region, instantaneous Maxwell's equations, written in terms of \mathbf{E} and \mathbf{H} only, are:

$$\nabla \times \mathbf{E} = -\mu \frac{\partial \mathbf{H}}{\partial t} \quad (1)$$

$$\nabla \times \mathbf{H} = \sigma \mathbf{E} + \epsilon \frac{\partial \mathbf{E}}{\partial t} \quad (2)$$

$$\nabla \cdot \mathbf{E} = 0 \quad (3)$$

$$\nabla \cdot \mathbf{H} = 0 \quad (4)$$

The decoupling of the Maxwell equations leads to obtaining the Instantaneous vector wave equations (Helmholtz equations)

$$\nabla^2 \mathbf{E} = \mu\sigma \frac{\partial \mathbf{E}}{\partial t} + \mu\epsilon \frac{\partial^2 \mathbf{E}}{\partial t^2} \quad (5)$$

$$\nabla^2 \mathbf{H} = \mu\sigma \frac{\partial \mathbf{H}}{\partial t} + \mu\epsilon \frac{\partial^2 \mathbf{H}}{\partial t^2} \quad (6)$$

For time-harmonic fields, the instantaneous (time-domain) vector \mathbf{F} is related to the phasor (frequency-domain) vector \mathbf{F}_s by:

$$\mathbf{F} \leftrightarrow \mathbf{F}_s$$

$$\frac{\partial \mathbf{F}}{\partial t} \leftrightarrow j\omega \mathbf{F}_s$$

$$\frac{\partial^2 \mathbf{F}}{\partial t^2} \leftrightarrow (j\omega)^2 \mathbf{F}_s$$

Using these relations, the instantaneous vector wave equations are transformed into the phasor vector wave equations:

$$\nabla^2 \mathbf{E}_s - \gamma^2 \mathbf{E}_s = 0 \quad (7)$$

$$\nabla^2 \mathbf{H}_s - \gamma^2 \mathbf{H}_s = 0 \quad (8)$$

The complex constant γ is defined as the propagation constant

$$\gamma = \sqrt{j\omega\mu(\sigma + j\omega\epsilon)} = \alpha + j\beta \quad (9)$$

The real part of the propagation constant α is defined as the attenuation constant while the imaginary part β is defined as the phase constant. The attenuation constant defines the rate at which the fields of the wave are attenuated as the wave propagates. An electromagnetic wave propagates in an ideal (lossless) media without attenuation $\alpha = 0$. The phase constant defines the

rate at which the phase changes as the waves propagates. Given the properties of the medium (μ , ϵ , σ), we can determine equations for the attenuation and phase constants and then:

$$\alpha = \omega \sqrt{\frac{\mu\epsilon}{2} \left[\sqrt{1 + \left(\frac{\sigma}{\omega\epsilon}\right)^2} - 1 \right]} \quad (10)$$

$$\beta = \omega \sqrt{\frac{\mu\epsilon}{2} \left[\sqrt{1 + \left(\frac{\sigma}{\omega\epsilon}\right)^2} + 1 \right]} \quad (11)$$

Units:

γ propagation constant (m^{-1})

α attenuation constant ($\frac{Np}{m}$)

β phase constant ($\frac{rad}{m}$)

The attenuation constant α is often expressed in decibels per meter (dB/m). The conversion between Nepers per meter and decibels per meter is obtained by examining the real exponential that represents an attenuation factor of the wave in a lossy medium. Since the factor represents the relative attenuation of the electric or magnetic field, its conversion to decibels (dB) is obtained by:

$$dB = 20 \log_{10}(e^{-\alpha z}) = 20(-\alpha z) \log_{10}(e) = -8.68(\alpha z) \quad (12)$$

Or

$$|\alpha (Np/m)| = \frac{1}{8.68} |\alpha (dB/m)| \quad (13)$$

Considering a uniform plane wave travelling in a lossy medium, the electric field is assumed to have an x component and the travelling waves are travelling in the z axis. The expression for the wave equation is:

$$E(z) = a_x E_x(z) = a_x (E_0^+ e^{-\alpha z} e^{-j\beta z} + E_0^- e^{+\alpha z} e^{+j\beta z}) \quad (14)$$

The magnetic field associated can be obtained using the Maxwell's equation:

$$H = -\frac{1}{j\omega\mu} \nabla \times E \quad (15)$$

$$H = a_y \sqrt{\frac{\sigma + j\omega\epsilon}{j\omega\mu}} (E_0^+ e^{-\gamma z} - E_0^- e^{+\gamma z}) = a_y \frac{1}{Z_w} (E_0^+ e^{-\gamma z} - E_0^- e^{+\gamma z}) \quad (16)$$

where, Z_w is the impedance of the wave and it takes the form of:

$$Z_w = \sqrt{\frac{\sigma + j\omega\epsilon}{j\omega\mu}} = \eta_c \quad (17)$$

which is equal to the intrinsic impedance η_c of the lossy medium.

- Skin depth (δ)

Skin depth defines the distance a wave must travel before its amplitude has decayed by a factor of $1/e$. The skin depth is the reciprocal of the attenuation constant α , then:

$$\delta = \frac{1}{\alpha} = \frac{1}{\omega} \sqrt{\frac{\mu\epsilon}{2} \left[\sqrt{1 + \left(\frac{\sigma}{\omega\epsilon}\right)^2} - 1 \right]} \quad (18)$$

Since β depends on the frequency and the physical properties of the media, so does the skin depth.

In the case we have $\epsilon\omega \ll \sigma$ (good conductor) the skin depth is approximately equal to:

$$\delta = \sqrt{\frac{2}{\omega\mu\sigma}} \quad (19)$$

assuming $\mu=\mu_0$ for a non-magnetic material and $\omega=2\pi f$ we obtain:

$$\delta \approx 503 \sqrt{\frac{1}{f\sigma}} \quad (20)$$

so, the skin depth decreases as the conductivity, frequency and permeability grows. In most cases magnetic properties are negligible.

In the case $\epsilon\omega \gg \sigma$ (good dielectric) and assuming $\mu=\mu_0$ for a non-magnetic material and using ϵ/ϵ_0 we obtain:

$$\delta \approx 0.0053 \frac{\sqrt{\epsilon_r}}{\sigma} \quad (21)$$

- **Loss tangent**

The total current on the right-hand side of Ampere's law consists of a current term and a displacement current term. These two terms can be combined into one using the concept of a complex-valued permittivity.

$$\nabla \times \mathbf{H} = \sigma \mathbf{E} + j\omega \epsilon \mathbf{E} = (\sigma + j\omega \epsilon) \mathbf{E} = j\omega \epsilon \left[1 - j \left(\frac{\sigma}{\omega \epsilon} \right) \right] \mathbf{E} = j\omega \epsilon_c \mathbf{E} \quad (22)$$

$$\epsilon_c = \epsilon \left[1 - j \left(\frac{\sigma}{\omega \epsilon} \right) \right] = \epsilon' - j\epsilon'' = |\epsilon_c| e^{-j\theta} \quad (23)$$

$$\epsilon' = \epsilon; \quad \epsilon'' = \frac{\sigma}{\omega} \quad (24)$$

The ratio of the imaginary part (ϵ'') to the real part (ϵ') of the complex permittivity is the ratio of the magnitude of the conduction current density to the magnitude of the displacement current density. This ratio is defined as the loss tangent of the medium. The loss tangent gives you the dielectric characteristics of the medium and let you choose what dielectric material is best to design a Radome.

- **Good Dielectric Materials *special case***

For source-free lossy media, Maxwell's equation in differential form derived from Ampere's law takes the form of

$$\nabla \times \mathbf{H} = \mathbf{J}_c + \mathbf{J}_d = \sigma \mathbf{E} + j\omega \epsilon \mathbf{E} = (\sigma + j\omega \epsilon) \mathbf{E} \quad (25)$$

Where \mathbf{J}_c and \mathbf{J}_d represent, respectively, the conduction and displacement current densities. When $\sigma/\omega \epsilon \ll 1$, the displacement current density is much greater than the conduction current density; when $\sigma/\omega \epsilon \gg 1$, the conduction current density is much greater than the displacement current density. For each of these two cases the exact forms of the field parameters can be approximated by simpler forms.

For good dielectric, $\sigma/\omega \epsilon \ll 1$, the exact expression for the attenuation constant can be written using the binomial expansion and it takes the form of

$$\alpha = \omega \sqrt{\frac{\mu \epsilon}{2} \left[\sqrt{1 + \left(\frac{\sigma}{\omega \epsilon} \right)^2} - 1 \right]} = \omega \sqrt{\mu \epsilon} \left\{ \frac{1}{2} \left[\left(1 + \frac{1}{2} \left(\frac{\sigma}{\omega \epsilon} \right)^2 - \frac{1}{8} \left(\frac{\sigma}{\omega \epsilon} \right)^4 \dots \right) - 1 \right] \right\}^{1/2} \quad (26)$$

$$\alpha \approx \omega \sqrt{\mu \epsilon} \frac{1}{2} \left[\frac{1}{4} \left(\frac{\sigma}{\omega \epsilon} \right)^2 \right]^{1/2} = \frac{\sigma}{2} \sqrt{\frac{\mu}{\epsilon}} \quad (27)$$

In a similar manner, it can be shown that the expression of β can be approximated to

$$\beta \approx \omega\sqrt{\mu\epsilon} \quad (28)$$

For good dielectrics the wave and intrinsic impedances can be approximated by

$$Z_w = \eta_c = \sqrt{\frac{j\omega\mu}{\sigma + j\omega\epsilon}} \approx \sqrt{\frac{\mu}{\epsilon}} \quad (29)$$

and the skin depth, $\delta = \frac{1}{\alpha} \approx \frac{2}{\sigma} \sqrt{\frac{\epsilon}{\mu}}$

- **Good conductor Materials special case**

For good conductor materials, the approximated expression for attenuation can be written using the binomial expansion and takes the form of:

$$\alpha = \omega \sqrt{\frac{\mu\epsilon}{2} \left[\sqrt{1 + \left(\frac{\sigma}{\omega\epsilon}\right)^2} - 1 \right]} = \omega\sqrt{\mu\epsilon} \left\{ \frac{1}{2} \left[\left(\frac{\sigma}{\omega\epsilon} + \frac{1}{2} \frac{1}{\sigma/\omega\epsilon} - \frac{1}{8} \frac{1}{(\sigma/\omega\epsilon)^3} \dots \right) - 1 \right] \right\}^{1/2} \quad (30)$$

$$\alpha \approx \omega\sqrt{\mu\epsilon} \left[\frac{1}{2} \frac{\sigma}{\omega\epsilon} \right]^{1/2} = \sqrt{\frac{\omega\sigma\mu}{2}} \quad (31)$$

and then

$$\beta \approx \sqrt{\frac{\omega\mu\sigma}{2}} \quad (32)$$

The intrinsic impedance:

$$Z_w = \eta_c = \sqrt{\frac{j\omega\mu}{\sigma + j\omega\epsilon}} \approx \sqrt{j \frac{\omega\mu}{\sigma}} = \sqrt{\frac{\omega\mu}{\sigma}} (1 + j) \quad (33)$$

and the skin depth:

$$\delta = \frac{1}{\alpha} \approx \sqrt{\frac{2}{\omega\mu\sigma}} \quad (34)$$

1.1.2 Plane wave Reflection and Transmission at a dielectric interface

When a plane wave propagating through a homogenous medium finds an interface with a different medium, a part of the wave is reflected from the interface while the remaining wave is transmitted. The reflected and transmitted waves can be determined by applying the boundary conditions at the media interface. Then, a flat wave uniformly polarized according to the X direction, and propagating in the Z direction, normally incident on a plane interface oriented according to the X - Y plane, is decomposed into a reflected wave and a transmitted wave whose fields can be expressed as:

Incident Wave	$E^i = E_0 e^{-\gamma_1 z} a_x$	$H^i = \frac{E_0}{\eta_1} e^{-z\gamma_1} a_y$
Reflected wave	$E^r = rE_0 e^{\gamma_1 z} a_x$	$H^r = -r \frac{E_0}{\eta_1} e^{z\gamma_1} a_y$
Transmitted Wave	$E^t = \tau E_0 e^{-\gamma_2 z} a_x$	$H^t = \tau \frac{E_0}{\eta_1} e^{-z\gamma_1} a_y$
r- Reflection coefficient		τ - Transmission coefficient

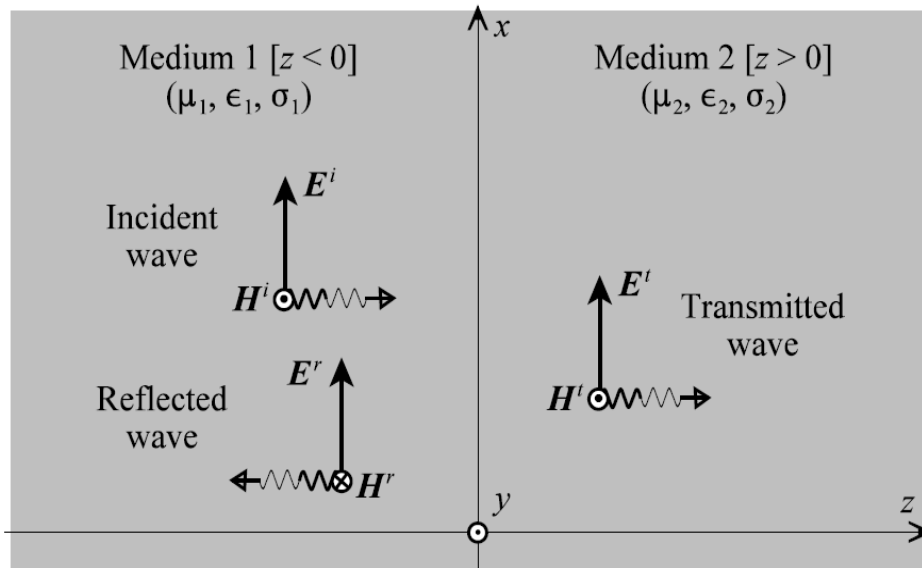


Fig1- Incident, transmitted and reflected wave between two media

The application of continuity conditions at the interface to the transverse electric and magnetic fields, provides:

$$\Gamma = \frac{\eta_2 - \eta_1}{\eta_2 + \eta_1} \quad \text{Reflection Coefficient (35)}$$

$$\tau = \frac{2\eta_2}{\eta_2 + \eta_1} \quad \text{Transmission Coefficient} \quad (36)$$

The total fields in the two media become:

$E_1 = E^i + E^r = E_0(e^{-\gamma_1 z} + \Gamma e^{-\gamma_1 z})a_x$	Fields in region 1
$H_1 = H^i + H^r = \frac{E_0}{\eta_1}(e^{-\gamma_1 z} + \Gamma e^{-\gamma_1 z})a_x$	
$E_2 = E^t = E_0 \tau e^{-\gamma_2 z} a_x$	Fields in region 2
$H_2 = H^t = \frac{E_0}{\eta_2} \tau e^{-\gamma_2 z} a_y$	

1.1.3 Polarization

Polarization represents the orientation of how wave is oscillating. This is especially important if the Radome heating is based on wires. Conventionally, the direction of the vector of oscillation of the electric field is used. A plane wave, that is the equation we use all the thesis, will have components just in a plane so, we will have a linearly polarized wave. In a non-polarized wave, the electric field oscillates in all normal directions to the propagation direction.

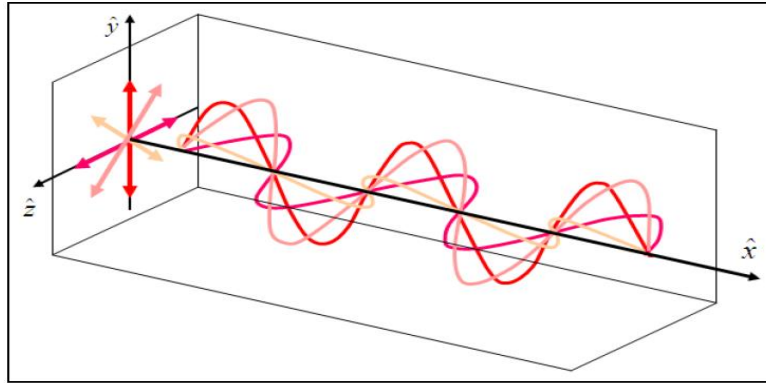


Fig 2. Non-polarized wave, E field is oscillating in all directions.

In this thesis, we will always suppose a normal incidence of the wave, but with a preferred direction, so we do not need to change wave equations and introduce the influence of an oblique incidence. But we need to consider that the radar signal is polarized in the X direction or Y direction depending not only on the company that fabricates the radar but also on each different car model. This point is very important for a heating system based on wires since if the wires are parallel to polarization the attenuation of the Radome will increase, on the contrary, if the wires are placed perpendicular to polarization the attenuation of the Radome will be minimized.

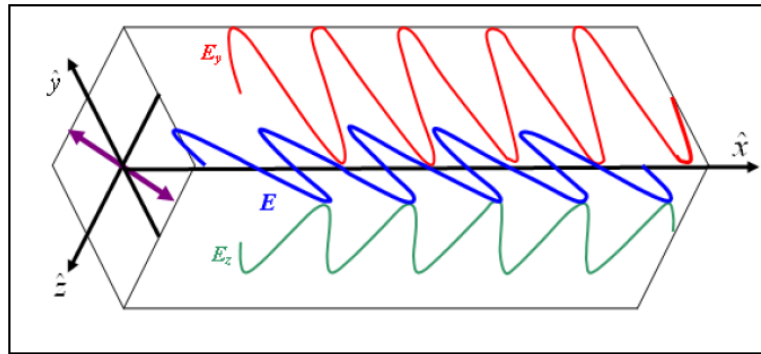


Fig 3-Linear polarization of a plane wave with an angle respect to y

We can see these differences between parallel and perpendicular orientation of the wires respect to the wave polarization from the results obtained using a wired example that we build and comment on chapter 5. Here we can see in plot1 the component S_{21} measured at the UPC for a set of wires placed perpendicular and parallel with respect to the radar radiation:

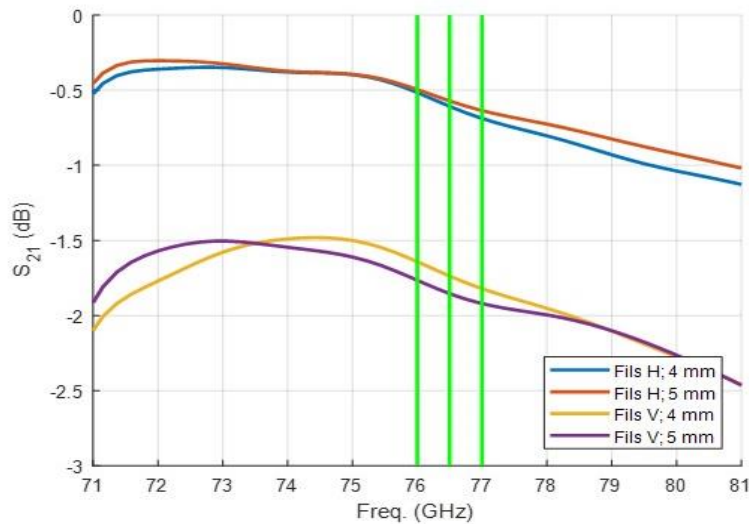


Fig 4 - shows us the S_{21} behaviour of the electromagnetic radiation from 71 to 81 GHz with the set of wires in front.

Fils H refers to the wires oriented perpendicular to the radar polarization and **Fils V** refers to the wires oriented parallel to the radar polarization. Here we have used wires that has a diameter of 0.1 mm in two different samples, one where wires are separated 4 mm and the other one separated 5 mm. the wires were placed parallel between them on the surface of a Polycarbonate (PC) substrate. The attenuation that can be attributed to the substrate have been removed. This example will be further commented in chapter 5.

1.2 Heating systems based on Joule's effect

Here we introduce some basics of the system we want to study. A scheme of the different parts of the Radome is presented and some of the requirements of the system are commented together with some considerations about wires used as a heating system that we need to consider.

1.2.1 View of a common Radome with a heating system based on metallic wires

Here we present a schematic of the system made by the radar and the heated Radome we can find in a car today. The radar that emits and receive the radar signal, an air space between the radar and the Radome controlled and imposed by car's manufactures, the Radome with the cooper wires inside and, finally, air when the signal gets out of the vehicle. Here there are some parameters that can change: distance between the radar and the Radome and the position of the wires inside the Radome. The first parameter is usually determined by the radar manufacturer and the car manufacturer, rarely the Radome manufacturer is involved in the decision. The second parameter: where to place the wires, may be decided by car manufacturers with some consideration of the Radome manufacturers. This second parameter is the origin of many problems since the vehicle's company is most worried on how the Radome looks like than on its electromagnetic performance. The Radome manufacturer can also add some additional limitation since the position of the wires is, of course, affected by the method used to place the wires inside the plastic part that it is not an obvious step.

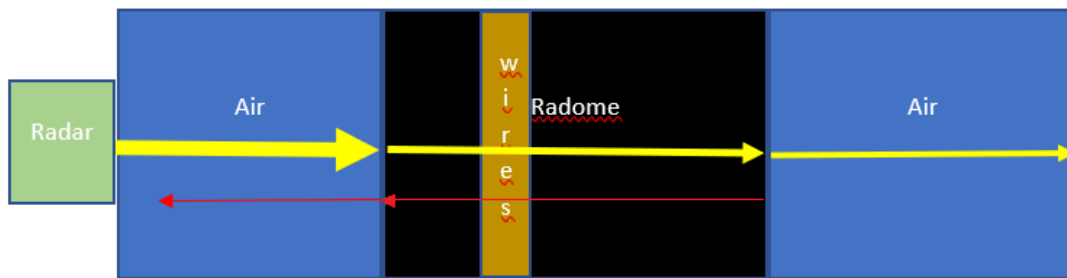


Fig 5 - Scheme of a heated Radome using wires. The wires use to be placed in the mid part of the Radome to hide them

Radar signal coming from the first medium considered air (left air medium), is attenuated in all these mediums but specially in the interfaces of each medium, not only when the radar signal is emitted also when it is received. Automotive companies establish a limit of this attenuation for each project, but the goal is to reduce this attenuation to the minimum. Nowadays the established maximum attenuation is on 3 dB for all the system including Radome and heating, but some companies have started to require for a 2.5 dB heated Radome what makes crucial to find new materials or techniques to achieve the requested requirements.

1.2.2 Radome with a heating system based on TCO

In this thesis we try to change this scheme of metal wired Radome introducing a new medium made by transparent oxide conductors (TCO). This give us the chance of applying them on the surface of the Radome where they are ideally needed for heating. Placing the TCO on the surface is also a necessity due to the difference in electrical conductivity between wires made of materials like cooper which electrical conductivities are of the order of 10^7 in front of conductivities of a TCO [1]. So, the Power produced by joule effect by metallic wires could be higher than the power produced by TCO. However, the position inside the plastic of metallic wires makes the temperature of the surface of the Radome to depend strongly on the thermal conductivity of the plastic material. Thermal conductivity of the plastic materials used are usually very poor. In our case, polycarbonate have a low thermal conductivity of $0.29 \text{ W/m}\cdot\text{K}$ [2] but conversely it has very good dielectric properties and very low em attenuation, with a loss tangent of 0.007, dielectric constant of 2.76 and zero electrical conductivity.

In terms of efficiency, we need also to consider that the surface of the Radome is the outer part of the plastic part but we have also an inner part where a fraction of the heating power is transferred and so it is not used to defrost ice on the surface. So, the position of the heating system is very important. TCO based Radomes have the heating system placed in the outer part of the plastic part and, so, closer to the ice. Since ice have a thermal conductivity between $2.22 - 2.30 \text{ W/m}\cdot\text{K}$ [2] when its temperature is between 0 and -10 degrees, the most important part of the energy dissipated by a heating system will be transferred to ice since it is a better conductor of heat than polycarbonate ($0.29 \text{ W/m}\cdot\text{K}$).



Fig 6 - Scheme of a Radome with the TCO on tis surface

We will present two different Radome schemes where the TCO is placed on the surface of the plastic part using magnetron sputtering deposition but with very different TCO electrical conductivity and thickness:

- **Radome with a uniform heating thin film**

With this system, the surface of the Radome is coated uniformly [REDACTED] [REDACTED] by this way we avoid excessive radar absorption from the conductive film, but [REDACTED]. This method presents some problems to industrialize the system right now as we will see, and the request of [REDACTED] [REDACTED]

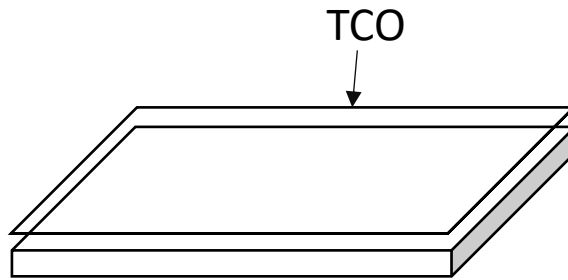


Fig 7 - Scheme of the Radome with a uniform thin film on its surface

- **Radome with a patterned conductive heating thin film**

Another approach consists in two consecutive processes to build the heated Radome, first we deposit the uniform TCO film on the surface of the Radome with [REDACTED] [REDACTED] and then we need to etch the TCO film in order to create the pattern of conducting stripes with optimal width and separation. In our approach, [REDACTED] [REDACTED]. The conducting stripes must be connected between them in series or in parallel in order to have a closed electrical circuit.

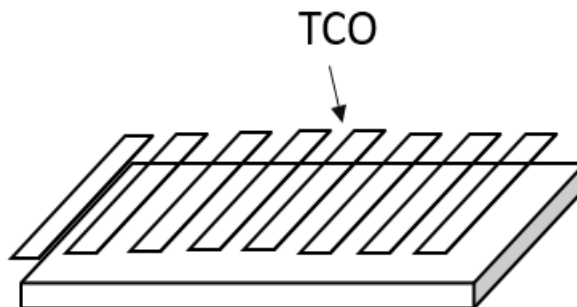


Fig 8 - Scheme of the Radome with etched thin film.

1.3 Substrate Thickness adaptation

Adaptation of the thickness of Radome's plastic substrate material is a key factor to obtain the minimum wave attenuation since a dielectric material absorbs part of the intensity of the signal because of its thickness despite the lack of electrical conductivity. As we can see in plot 1 the trace shows a clear descending trend, which is caused by the increased absorption of the EM wave energy due to the increased dielectric material thickness. This absorption is produced by the interferences occurred inside the material. We can also see local maximums and minimums; these peaks are caused by reflections of the electromagnetic wave on the dielectric-to-free space boundary [5].

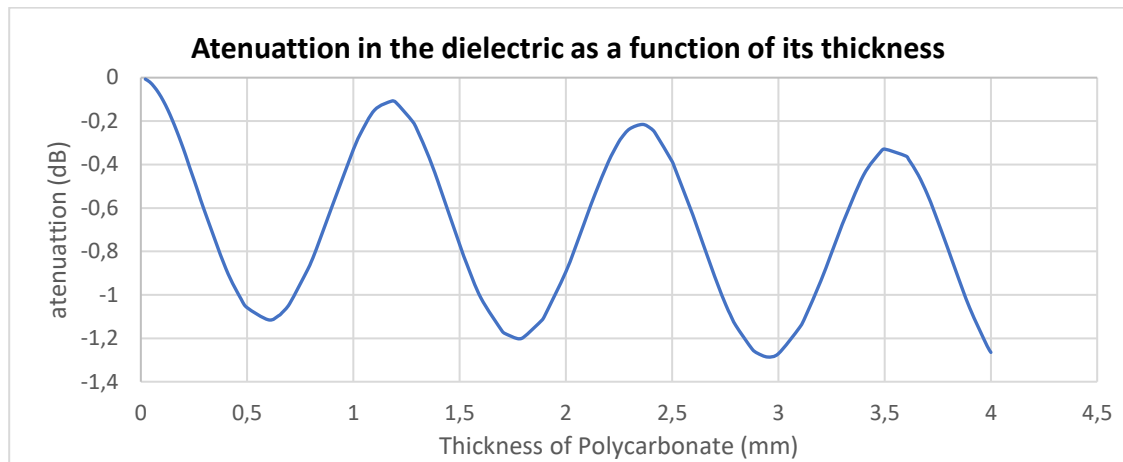


Fig 9 -. Simulation done using CST showing the variation of the attenuation due to the increasing thickness of the Radome material at a frequency of 76.5 GHz

In Fig. 9 we can see clearly how the radar signal is affected by the thickness of the plastic part of the Radome. This is another challenge we have to face to when building a Radome in an industrial process, a slightly mistake in the injection of the plastic can increase the attenuation and then the piece can be useless. So, all the processes must be very precise injection of the plastic, design and construction of molds, control of plastic stress, ... but, at the same time all these techniques must allow small changes in order to correct for small deviation of the right parameters.

As commented on [6] in order to obtain a low loss Radome at the frequencies of interest, we can adapt the thickness of the material to dielectric parameters or adapt the dielectric parameters to the thickness. An example of this is showed in Fig. 10 where we see how attenuation (for em wave with parallel polarization) varies from a minimum to a maximum in a Radome with a heating system based on TCO placed on the surface of the polycarbonate part. the thickness of the plastic part varies from 1.86 mm to 2.86 mm. Comparing Fig. 9 and Fig. 10 we see how a minimum in attenuation of the polycarbonate piece with no heating system (Fig. 9) at 2.36 mm of thickness

becomes a maximum in attenuation when the heating system is placed on the same plastic part and the minimum of attenuation have moved to the left around a thickness of 2.14 mm.

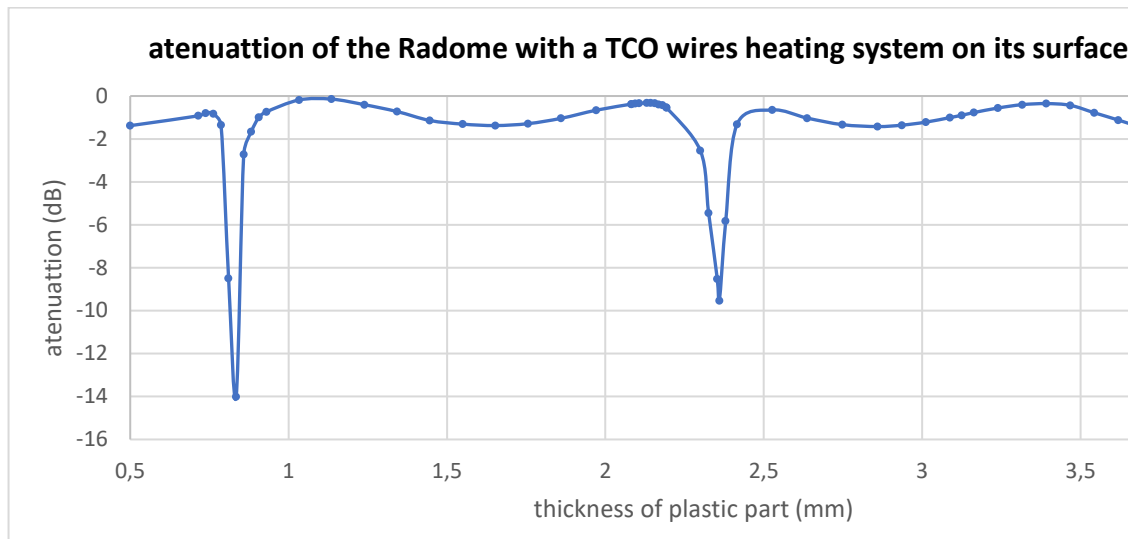


Fig 10 - CST Simulation of the variation of the attenuation due to the increasing thickness of the Radome material with a heating system based on TCO wires

1.4 Materials for Transparent Conductive Oxides (TCO)

Transparent Conductive Oxides (TCO) are known as materials that show both transparent and conducting properties, films of TCO are used in flat panel displays, solar cells and electroluminescent devices as transparent electrodes. The transparent properties mean that TCO show a high optical transmission in the visible range, and this requires an Energy gap larger than 3.3 eV.

Transparent conductive oxides are doped semiconductors used in optoelectronic devices due to its transparency on the visible range more than 80% and its electrical conductivities higher than 10^3 S/cm [3]. Current transparent conducting oxides used in industry are primarily n-type semiconductors, meaning that their conductivity is due to donors of electrons. The choice of a n-type doping is because the mobility of electrons is higher than mobility of holes. T

ABC have the inconvenient that for these reasons other doped compounds such as have been proposed as alternative materials. Also sandwich structures of TCO/thin metal/TCO have been also proposed since their optical and electrical properties can be globally superior to those with of a single-layer TCO and they can also be deposited at low temperatures onto plastic substrates [4].

The first experiments with TCO films were at 1907 when K.Badeker first fabricated Cadmium Oxide (CdO) films by thermal oxidation of Cadmium [5]. Several new materials and manufacturing techniques have been developed to satisfy technological requirements from [3] we sow show a table with the historical development of TCO

Material	Year	Process	Reference
<i>Cd-O</i>			
CdO	1907	Thermally Oxidation	K. Badeker, Ann. Phys. (Leipzig) 22, 749 (1907)
Cd-O	1952	Sputtering	G. Helwig, Z. Physik, 132, 621 (1952)
<i>Sn-O</i>			
SnO ₂ :Cl	1947	Spray pyrolysis	H.A. McMaster, U.S. Patent 2,429,420
SnO ₂ :Sb	1947	Spray pyrolysis	J.M. Mochel, U.S. Patent 2,564,706
SnO ₂ :F	1951	Spray pyrolysis	W.O. Lytle and A.E. Junge
SnO ₂ :Sb	1967	CVD	H.F. Dates and J.K. Davis, USP 3,331,702
<i>Zn-O</i>			
ZnO:Al	1971		T. Hada, Thin Solid Films 7, 135 (1971)
<i>In-O</i>			
In ₂ O ₃ :Sn	1947		M.J. Zunick, U.S. Patent 2,516,663
In ₂ O ₃ :Sn	1951	Spray pyrolysis	J.M. Mochel, U.S. Patent 2,564,707 (1951)
In ₂ O ₃ :Sn	1955	Sputtering	L. Holland and G. Siddall, Vacuum III
In ₂ O ₃ :Sn	1966	Spray	R. Groth, Phys. Stat. Sol. 14, 69 (1969)
<i>Ti-O</i>			
TiO ₂ :Nb	2005	PLD	Furubayashi et al., Appl. Phys. Lett. 86, 252101 (2005)
<i>Zn-Sn-O</i>			
Zn ₂ SnO ₄	1992	Sputtering	Enoki et al., Phys. Stat. Solid A 129, 181 (1992)
ZnSnO ₃	1994	Sputtering	Minami et al., Jap. J. Appl. Phys. 2, 33, L1693 (1994)
a-ZnSnO	2004	Sputtering	Moriga et al., J. Vac. Sci. & Tech. A 22, 1705 (2004)
<i>Cd-Sn-O</i>			
Cd ₂ SnO ₄	1974	Sputtering	A.J. Nozik, Phys. Rev. B, 6, 453 (1972)
a-CdSnO	1981	Sputtering	F.T.J. Smith and S.L. Lyu, J. Electrochem. Soc. 128, 1083 (1981)
<i>In-Zn-O</i>			
Zn ₂ In ₂ O ₅	1995	Sputtering	Minami et al., Jap. J. Appl. Phys. P2 34, L971 (1995)
<i>a-InZnO</i>			
<i>In-Ga-Zn-O</i>			
InGaZnO ₄	1995	Sintering	Orita et al., Jap. J. Appl. Phys. P2. 34, 1550 (1995)
a-InGaZnO	2001	PLD	Orita et al., Phil. Mag. B 81, 501 (2001)

Fig 11 – Historical selected TCO references from [3]

1.4.1 Optical properties of TCO thin films

The optical and electronic properties of semiconductors are governed by their band structure. In semiconducting and insulating materials, the valence and conduction bands do not overlap, leading to a range of energies which cannot be occupied by the charge carriers. Despite this, the presence of defects and/or impurities can lead to conductivity, since they can alter the materials

fermi level, by supplying charge carriers into either the conduction band or the valence band. This is the origin of conductivity in doped semiconductors. At the same time the materials band gap determines which light wavelength will be absorbed and which will transmit through. Visible light has a wavelength range between 390 to 700 nm, corresponding to energies between 3.2 to 1.8 eV. TCO are doped semiconductors which band gap is above 3.2 eV this way the visible light is not absorbed by the material and it looks transparent to us.

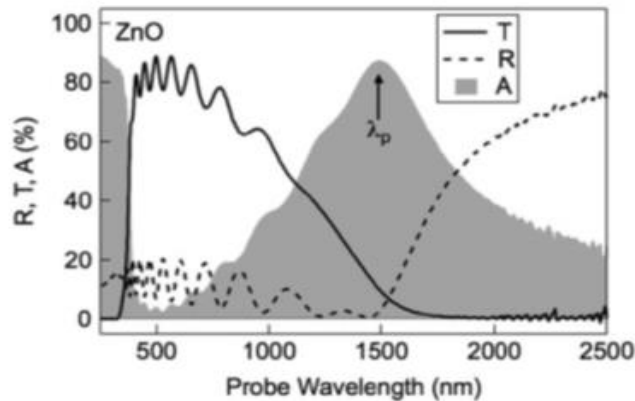


Fig. 11- Optical transmission (T) and reflection (R) spectra of Zinc Oxide

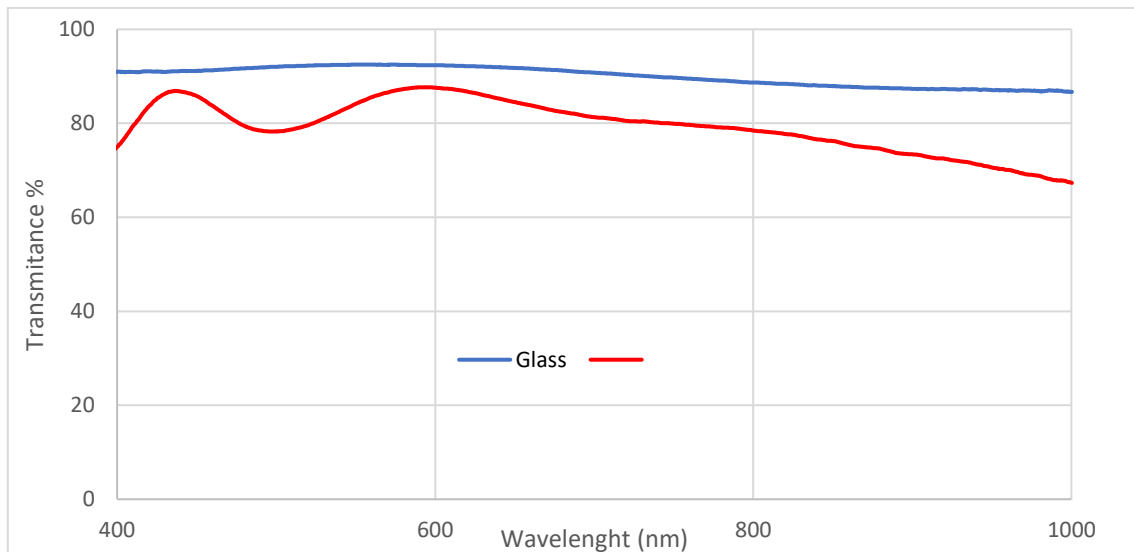


Fig12 - Comparison between transmission of a commercial ABC film of 340 nm on a glass substrate with the absorption of the glass substrate measured at UB

When free electrical carriers are introduced by doping intrinsic semiconductors, optical absorption and reflection by the free carriers appears, this effect adds to the above discussed photon absorption by band-to-band electron excitations. The collective motion of the carriers behaves like the free electron plasma in conductors so, when electromagnetic wave irradiate the conductor the carriers oscillate at the frequency of the light. This plasma oscillation results in the reflection of the light at the surface of the conductors. But, in doped semiconductors, if the

frequency of the light is too high the carriers cannot move at the same frequency as the electric field oscillations then the light is transmitted through the semiconductor without causing any reflection at the surface. The maximum frequency that enables the plasma oscillation, and hence the em absorption, is called the plasma frequency

$$\omega_p = \frac{ne^2}{\epsilon_0 m} \text{ and } \lambda_p = \frac{2\pi c}{\omega_p} = \frac{2\pi c}{e} \sqrt{\frac{\epsilon_0 m}{n}} \quad (37)$$

Where λ_p is the em wavelength corresponding to the plasma frequency. Here m is the electron rest mass and c the speed of light.

In semiconductors, generally λ_p lies in the infrared light range but by doping, λ_p shifts to shorter wavelengths as $\lambda_p \propto 1/\sqrt{n}$ where n is the number of electrons in the conduction band. So, when n grows up such as by substantial doping, the plasma wavelength shifts, this creates a fundamental trade-off between conductivity and the long wavelength transparency limit. At very high electron concentrations, this can even decrease the visible wavelength transparency.

Here electron plasma frequency is commented just as an interesting complement of the optical properties of TCO material but in our case, we are not affected by plasma frequency since our interest in transmittance is on the visible range and plasma frequency is in the infrared range of the spectrum in most of the TCO.

1.4.2 Electrical conductivity of TCO thin films

Electrical current I in materials is expressed by Ohm's law as $I = V/R$, where V and R are applied potential difference and total resistance respectively. At microscopic-local scale Ohm's law can be expressed as $J = \sigma E$ where J, σ, E are current density, conductivity and electric field. The conductivity is generally dependent on the materials and can vary by a factor of 10^{20} . Metals such as Ag, Cu and Al possess high electrical conductivities of the order of 10^7 S m^{-1} . Semiconductors such as Si and Ge have medium conductivities. Although pure semiconductors are rather insulating and it is because of impurity doping that conductivities grows up to the order of 10^5 S m^{-1} .

TCO are doped semiconductors with conductivity in the range of $10^2 - 10^6 \text{ S m}^{-1}$. The TCO conductivity is due to doping either by oxygen vacancies or by extrinsic atoms dopants. In the absence of dopants these oxides are rather good insulators. The electrical conductivity of n-type TCO thin films depends on the electron density in the conduction band and on their mobility $\sigma = \mu n e$ where μ is the electron mobility, n is electron density, σ is conductivity and e the electron charge. The mobility is given by $\mu = e\tau/m^*$ where τ is the mean time between collisions and m^*

is the effective electron mass. However, m^* and τ are negatively correlated so the magnitude of μ is limited.

The electrical conductivity of TCOs is limited since n and μ cannot be independently varied, so, at high electron density carrier transport is limited by ion impurity scattering, then the carrier mobility is reduced to a limit that conductivity cannot be increased. So, with increasing dopant concentration the conductivity gets a higher limit and does not increase beyond it while the optical window could become smaller.

Fig. 11 shows a typical spectrum of a TCO, in this case Zinc Oxide. We can see the transmission (T), reflectivity (R) and absorption (A) in a range of the electromagnetic spectrum, and Fig. 13 shows a schematic electronic structure of the valence band, the band gap and the conduction band as an example of a typical TCO.

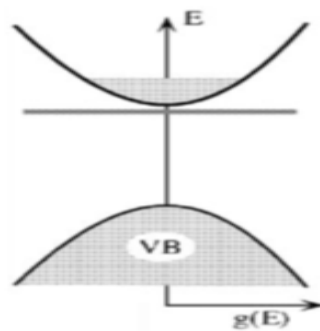


Fig. 13 - the schematic electronic structure of a doped TCO. Image from [3]

1.4.3 ABC

In this thesis we focus our designs of heating systems on ABC. Although other TCO like ABC ABC ABC(ABC) is also used and commented as a possible substituted of ABC for one of the designs.

Our interest in

ABC is widely used in different sectors of the industry so, it is easy to find samples, information and techniques to work with it and characterize it. We can find different examples of use in aircraft windows, antistatic coatings over electronic instrument display panels, heat reflecting mirrors, antireflection coatings and in high temperature gas sensors.

Free carriers are formed in the material by two different electron donor sites: substitutional four-valent Sn ions and oxygen vacancies.

The direct optical bandgap of The high optical transmittance of these films is a direct consequence of their wide bandgap. The most important absorption generally lies in the ultraviolet range. The band structure of the ABC is assumed to be parabolic [9]:

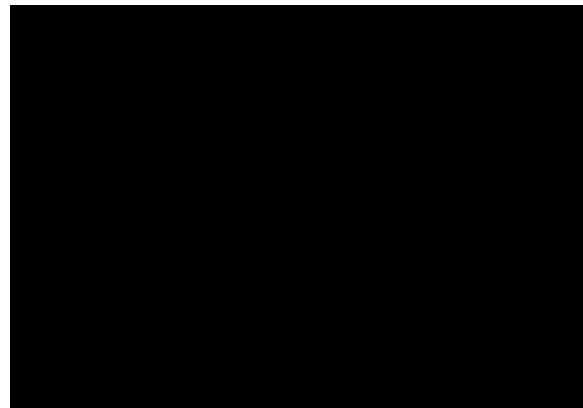


Fig. 14 - comparison between band structure of undoped and the doped from [7]

In Figure 3 we can see the band structures of the doped and undoped .

1.5 EM wave transmission through multiple layer films

Assuming an incident EM plane wave in medium 1 (first air medium) the formulation for the transmission and reflection coefficients can be represented in equations (10) to (16) in Salazar et al (2014) [12], [13]. From these equations in a multilayer Radome model the EM wave incident angle is represented by θ_i and transmitted and reflected angles by θ_t and θ_r respectively. The transmitted EM wave in a multilayer Radome of n layers can be estimated using eq (x), the impedance characteristic of each layer can be estimated by using eq (x). In this expression t_n represents the thickness of each layer. The reflections (Γ_H and Γ_V) and transmission coefficients for H and V polarization in each layer can be obtained by the expressions (x) and (x):

$$\theta_{t(n+1)} = \cos^{-1} \left(\sqrt{1 - \frac{\epsilon_{rt(n)}}{\epsilon_{rt(n+1)}} \sin(\theta_{i_{t(n)}})^2} \right) \quad (38)$$

$$\eta_{t(n)} = \eta_{t(n+1)} \left[\frac{\eta_{t(n)} + j\eta_{t(n+1)} \tan(\beta_{t(n+1)} t_n)}{\eta_{t(n+1)} + j\eta_{t(n)} \tan(\beta_{t(n+1)} t_n)} \right] \quad (39)$$

$$\Gamma_{Ht(n)} = \frac{\eta_{t(n+1)} \cos \theta_{t(n+1)} - \eta_{t(n)} \cos \theta_{i_{t(n)}}}{\eta_{t(n+1)} \cos \theta_{t(n+1)} + \eta_{t(n)} \cos \theta_{i_{t(n)}}} \quad (40)$$

$$\Gamma_{Vt(n)} = \frac{\eta_{t(n+1)} \cos \theta_{i_{t(n)}} - \eta_{t(n)} \cos \theta_{t(n+1)}}{\eta_{t(n+1)} \cos \theta_{i_{t(n)}} + \eta_{t(n)} \cos \theta_{t(n+1)}} \quad (41)$$

$$T_{Ht(n)} = \frac{2\eta_{t(n+1)} \cos \theta_{i_{t(n)}}}{\eta_{t(n+1)} \cos \theta_{t(n+1)} + \eta_{t(n)} \cos \theta_{i_{t(n)}}} \quad (42)$$

$$T_{Vt(n)} = \frac{2\eta_{t(n+1)} \cos \theta_{i_{t(n)}}}{\eta_{t(n+1)} \cos \theta_{i_{t(n)}} + \eta_{t(n)} \cos \theta_{t(n+1)}} \quad (43)$$

These equations are for a n layer Radome model like that of Fig 15

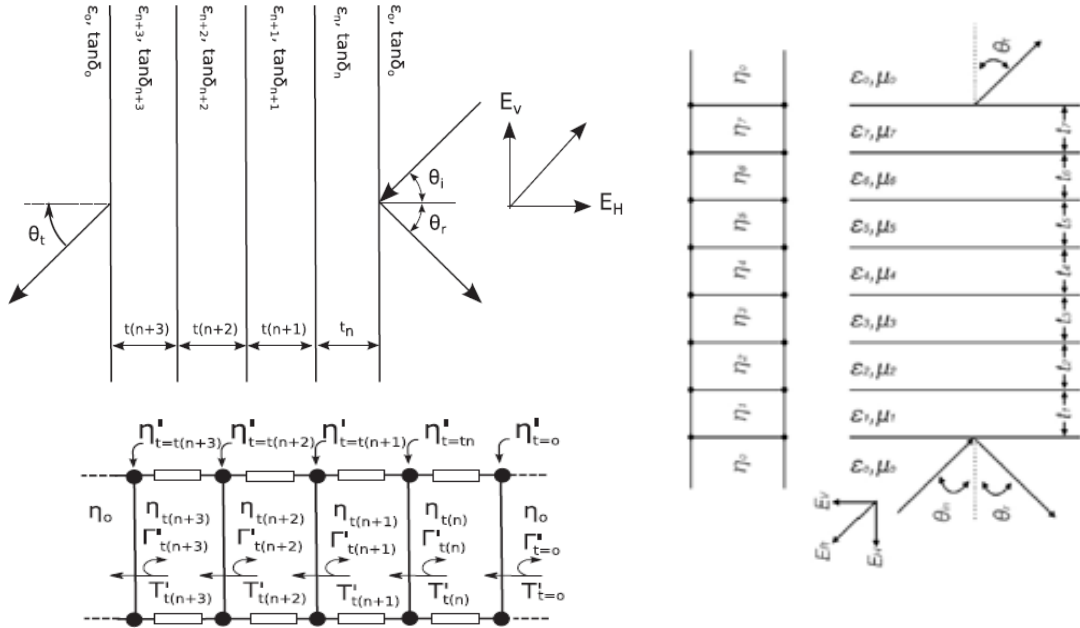


Fig 15. Model of n layers Radome from [3] (left) model for a Radome of seven layers from [13]

We only will consider normal incidence, $\theta_i = 0$ and $\theta_t = 0$ and so all the equations are simplified, and we have just only one reflection coefficient and one transmission coefficient, and so:

$$\Gamma_{t(n)} = \frac{\eta_{t(n+1)} - \eta_{t(n)}}{\eta_{t(n+1)} + \eta_{t(n)}} \quad (44)$$

$$T_{t(n)} = \frac{2\eta_{t(n+1)}}{\eta_{t(n+1)} + \eta_{t(n)}} \quad (x)$$

In the case of the TCO wire Radome the heating medium is a layer with a combination of two different materials air and the TCO wires also from [3] we can find the equivalent dielectric properties using the Maxwell-Garnet mixing formulation and use then the equation (9) from Salazar et al (2014) estimates the effective dielectric constant based on a fraction volume (f) of the TCO wires and the air in the specified volume:

$$\varepsilon_{eff} = \varepsilon_2 + \frac{3f\varepsilon_2(\varepsilon_1 - \varepsilon_2)}{\varepsilon_1 + 2\varepsilon_2 - f(\varepsilon_1 - \varepsilon_2)} \quad (45)$$

Then the outer layer of the Radome could be considered a mix of air and conductive material with an ε_{eff} .

On the same way we can also consider the Radome and the heating system as a whole system and reduce all the radar scheme to a three-medium system. Furthermore, we must do this when we treat the problem of adaptation of the thickness of the Radome as we will see later.

The thickness of our TCO films (50 to 360 nm) and the etched design of some of our heating systems make the analytical treatment complicated so, as a theoretical study of the attenuation and the dielectric properties of the different Radome design we use simulations made by CST Studio Suite 2019 software.

1.6 About the simulation software – CST Studio Suite

CST Studio Suite is a software package for Electromagnetic and Multiphysics simulation. CST studio Suite offers a wide range of tools for designing, analyzing and optimizing products. This software offers a powerful parametric CAD interface for editing our own models and to transfer our designs from other design applications. This helps us to simulate the samples we want to study in order to have an idea of how electromagnetic radiation behaves. We also have the option to define the properties of our own materials so we can use the data from the UPC measurements to define our materials on the software and study its electromagnetic behavior.

In the following we will work using a unitary cell mode so, we will just need to design a small unitary part of the sample that the software will reproduce on the space to get results valid for a full sample.

1.7 Minimum energy requested to melt ice on a Radome surface

It is necessary to have an idea of the energy process that take place when a film of ice is heated to melt on a flat plastic part. These numbers are very important since they can give us an idea of

how difficult could be to melt a film of ice with a heating system either embedded or located on the surface of the plastic part.

In our case the heating systems studied are all placed on the surface of the plastic part, so, what we have is a plastic part of 3.6 mm of thickness and a film of water ice of 1 mm on the surface.

First, we are going to compute the energy needed to melt an iced water film of 1 mm of thickness. The initial conditions of the system would be the same conditions we use in the laboratory tests so the starting temperature of ice would be -10° . The size of the water ice film is the same of the plastic part let's say 10 cm x 15 cm, typical dimensions of rectangle car Radome as we can see in the picture.

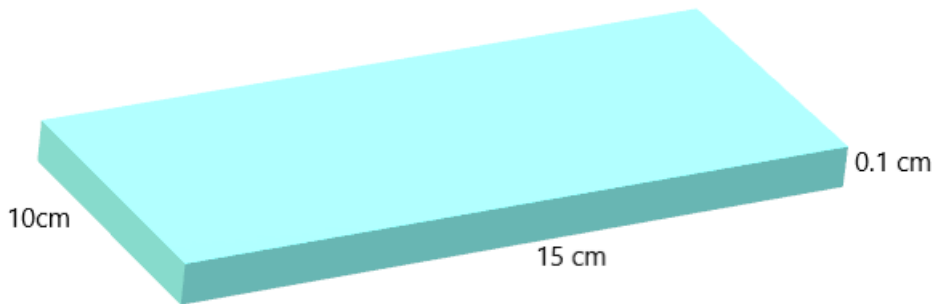


Fig. 16.- Ice film geometry

First, we need to know the mass of ice we have in the film. Knowing that the density of ice is 0.9167 g/cm^3 it is easy to compute

$$m_i = v_i \rho_i = 10 \cdot 15 \cdot 0.1 \cdot \rho_i = 13.75g$$

Now we can compute the heat needed to change the temperature of the ice from -10°C to 0°C and the phase transition heat needed change the phase of water from solid to liquid. To do this we will need the heat capacity of ice $c_i = 2.00 \text{ J/g}\cdot\text{K}$ at -10°C [1] and the phase transition heat $Q_t = 334 \text{ J/g}$

$$Q_1 = m_i c_i \Delta T = 13.75 \cdot 2.00 \cdot (10) = 275 \text{ J}$$

$$Q_2 = m_i Q_t = 13.75 \cdot 334 = 4592.5 \text{ J}$$

Where Q_1 is the heat related to the rise of temperature of the ice from -10°C to 0°C and Q_2 is the transition heat from ice to water. So, the total amount of heat needed is:

$$Q_T = Q_1 + Q_2 = 4867.5 \text{ J}$$

Generally, companies request that the heating system needs to do all this process in 5 minutes (300 seconds), so this means a power of

$$P = Q_T/t \approx 16.275 \frac{J}{s} = 16.275W$$

So, we need a minimum heating power introduction of 16.28W since this value have been calculated for and ideal situation where all the dissipated power of the heating system is transferred to water. In a real case the power dissipated is also transferred to the plastic part, so not all power is used for the melting of the ice film.

We can calculate the full system considering that the heat capacity of the polycarbonate is 1.1 J/g·K [16]. Considering the polycarbonate part, 3mm thick, we can deduce that the amount of heat:

$$Q_p = m_p c_p \Delta T = 39 \cdot 1.1 \cdot (10) = 429 J$$

And the total heat: $429 + 4867 = 5296 J$

So, the minimum power needed to melt a 1mm ice film on the part will be: $(429 + 4867)/300 =$
18 W.



Fig. 17 - Scheme of the polycarbonate plastic part (black) with the ice film on its surface (blue)

Chapter 2

Instruments and methods

2.1 Magnetron Sputtering

There are several deposition methods to produce coatings of ABC thin films: thermal evaporation and electron beam evaporation (in a vacuum environment), or others without vacuum: Spray pyrolysis technique, Screen printing technique [1] But in this work, we will focus on Physical Vapor Deposition (PVD) by Magnetron Sputtering. The reason is because as an Industrial PhD we need to adapt our research conditions to that of the company interests, and PVD magnetron sputtering is a technique widely used in Zanini production plants, in fact Zanini already designs and produce Radomes using this technique but just as a PVD decorative coating. Also, PVD magnetron sputtering allows to deposit ABC at room temperature with the final characteristics of the film that are good enough for our objectives.

Magnetron sputtering is a vacuum deposition method involving a gaseous plasma that attacks the material to be deposited called target material. The material is evaporated from the target by the high-energy ions within the plasma (generally Ar⁺) and the target free atoms travel through the vacuum environment and deposit onto a substrate to form a thin film. To initiate the plasma, a high voltage is applied between sputtering target material (cathode -) and the reactor steel walls (anode +). Electrons in the sputtering plasma gas are accelerated away from the negatively charged cathode causing collisions with nearby atoms of the sputtering gas (Ar), these collisions ionize the sputtering gas atoms. Conversely, the positive charged ions (Ar⁺) are accelerated towards the negatively charged cathode causing high energy collisions with the surface of the target material. Each of these collisions can cause the ejection of several atoms of the surface of the material into the vacuum environment with enough kinetic energy to reach the surface of the substrate to be coated. During this process, the coated substrate can get hot but generally not above of 50 or 60 Celsius degrees. The sputtering process acts as a cool sublimation-condensation process, because neither the target material nor the deposited material has high temperatures, but as compared to the vacuum thermal evaporation or sublimation process, the deposition atoms flux benefit of a higher kinetic energy and a higher fraction of ionized atoms.

Magnetron sputtering uses very strong magnets to confine the electrons of the plasma near the surface of the target, this way we get a higher density plasma and increase deposition rates.

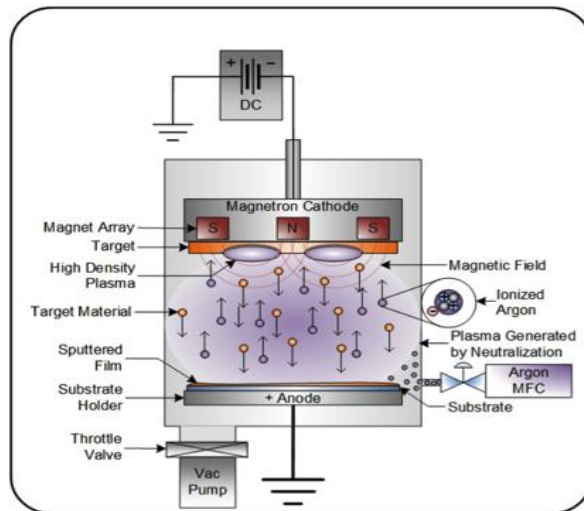


Fig 1. Diagram of DC magnetron sputtering from SEMICORE

In this thesis we used two different machines of magnetron sputtering one from University of Barcelona and the other from University of Zaragoza. The company's sputtering machines were during that period fully occupied for the industrial production.

2.1.1 Sputtering system at the University of Zaragoza (UZag)

At the university of Zaragoza, we found an industrial PVD sputtering system similar to those of Zanini company also with the capability of depositing films on large substrates of 350x600 cm for this reason we collaborated with them. Here we show a scheme of that PVD sputtering system.

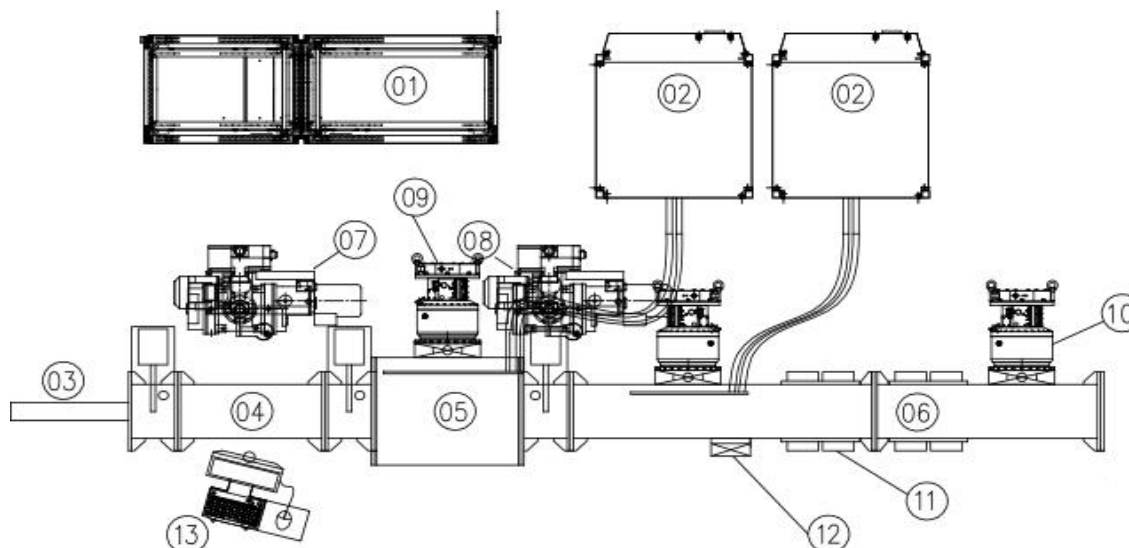


Fig 2. Scheme of the PVD sputtering system at the university of Zaragoza [2]

The system consists of three chambers: charge (04), transference (05) and process (06). The sample is placed at atmospheric pressure on the entrance of the system (03) and then transferred

to the charge chamber where pressure is reduced to 10^{-2} mbars in 2-3 minutes. Then the sample is moved to the transference chamber held permanently at a pressure of 10^{-7} mbar. In the same way the sample is transferred to the process chamber where the pressure is kept at 10^{-3} mbar of Ar + O₂ gas during all the process with no contamination thanks to this process of transfer of the sample.



Fig 3. Image of the PVD sputtering system at the university of Zaragoza [2]

2.1.2 Sputtering system at the University of Barcelona (UB)

The sputtering system of the UB is an AJA international Inc model ATC-Orion 8 HV. This sputtering system can be fitted with up to 5 targets of 3" or 8 targets of 2" in our case at the University of Barcelona 3 targets of 3" are enable to use. The characteristics of this system can be found at [3]. The ATC Orion Sputtering Systems feature a con-focal sputter source flange oriented at specific angles; these angles are determined by the AJA company. Its design allows a high degree of uniformity over more than twice the target diameter. We can find an example of this uniformity at [3] that we show here in fig 4:

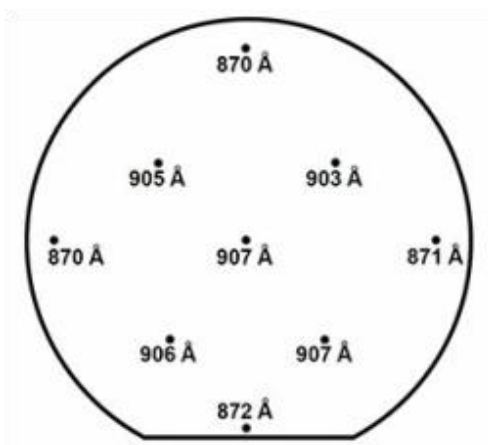


Fig 4. Shows a typical distripotion of thickness of a SiO₂ film of deposited from a 2" target onto a 10 cm diameter Si substrate. The conditions used for this sample samples are 150 W, 3 mTorr and 140 mm of distance between the target and the susbstrate that give us a uniformity of +/- 2 %

The confocal ATC Orion system utilizes motorized, rotating substrate holders to achieve good uniformity, allow the co-deposition of alloy films and facilitate the deposition of pristine, ultra-

thin film multilayers since the substrate is always in the plasma. feature reactive gas injection rings, RF/DC bias capability, in situ manual or motorized Z motion for working distance adjustment and load-lock transfer.

The sputtering system is controlled by the AJA Labview based Phase II-J computer control system. This control system uses a large screen laptop connected to a single 4U rack mount hardware module. The back panel of the hardware module is populated with connectors to interface to all aspects of the sputtering system.



Fig 5 (left). Labview based computer control. Large screen laptop for labview based ATC system computer control.



Fig 6 Sputtering system at the clean room at the University of Barcleona

2.2 Thickness Measurements

To characterize the different samples of ABC coatings we needed to know the thickness of the layers and we have measured it by using three different techniques. Some of these techniques are also used in other instances of the research for checking some other characteristics and properties of the samples and the designs.

The measurement of the thickness is very important in order to calculate the conductivity of the samples from the sheet resistance values measured directly with the four-point probe method.

2.2.1 Profilometer

A Profilometer is an instrument used to measure the profile of a surface to quantify its roughness. In our case we use a contact profilometer where a diamond stylus is moved vertically until it gets contact with the sample. Then its lateral motion in contact with the sample follows the profile of its surface, by this way, small surface height variations can be measured.

The profilometer from UB has a height accuracy of few Amstrongs. We use the profilometer to measure the thickness of the samples made at the UZag studied on chapter 3 and the purchased samples studied in chapter 4 and 5. We also use the profilometer to analyse the profile of ABC stripes of the etched circuit studied in chapter 5. Then these measurements can be compared with those obtained by using the confocal microscope as we will see later.

The thickness of UZag samples were also measured right after its deposition at UZag using the same stylus profilometer we use at the UB, by this way we have two different measurements of the thickness to compare.



Fig 7 (left) .Image of the Profilometer used at the UB. (down) results of a measurement of a profile of ABC stripes from a etched in a purchased ABC sample.



2.2.2 Focused ion beam (FIB)

The profilometer is a good way to measure the thickness of the thin films that we have made by our own at the UB and at the UZag, because we could prepare in these films a line-step in the coating, before the film deposition; but commercial samples need to be manipulated using etching techniques in order to produce the step, necessary to measure the thickness of the coating using the profilometer. To improve the thickness measurement of commercial samples we have also employed Focused Ion Beam (FIB). In the FIB, the ion beam produces a cut deep into the coating until it reaches the substrate and then it is also possible to analyse the internal structure of the thin film, through the cut, using a Scanning Electron Microscopy (SEM). This allows us to have a more accurate measurement of the thickness of each layer in the sample and even its composition.

In a FIB instrument, a focused beam of heavy ions, typically Ga⁺, is used to hit a sample and causing local sputtering, removing material on a controlled way. The Ga⁺ are generated by a liquid metal ion source (LMIS), which is a small Ga reservoir connected to a tungsten needle. When the reservoir is heated Ga flows to the tip of the needle forming a small point source. A strong electric field applied to the needle tip extracts ions from this source. The FIB can be used for, site specific milling, metal deposition and patterning.

FIB usually is used combined with a scanning electron microscope (SEM) into a combined FIB-SEM workstation allowing easy site-specific in-depth analysis of the material. In our case deposition of a platinum thin film is needed before ion beam local etching to protect the samples and avoiding damages on the surface of the sample we want to study. In the image that we will comment deeply in chapter 5 we can see the damage caused by the ion beam deposition of Pt on the surface of the electron beam deposition of Pt. These two layers of Pt ensures the protection of the sample we are interested to.

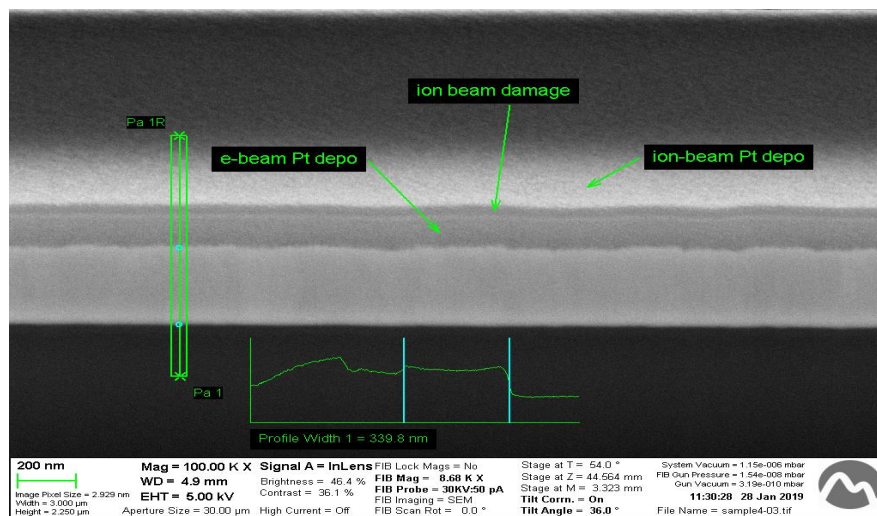
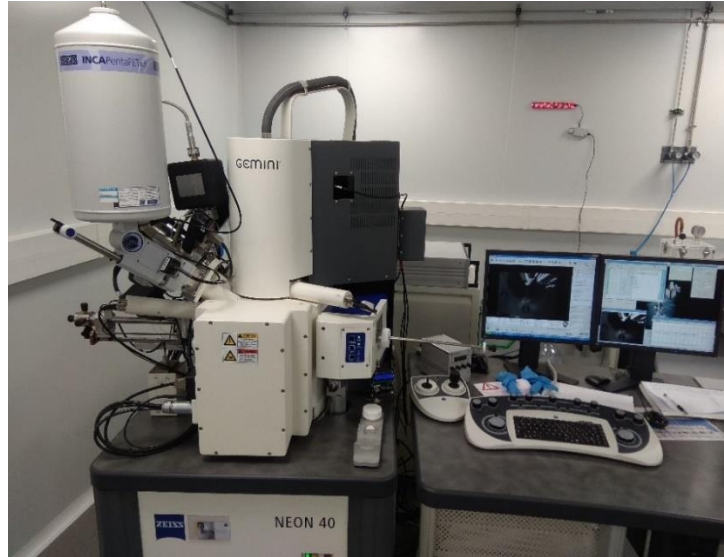


Fig 8. Image of the FIB with the differencet layers we need to do on the sample to avoid damaging the surface.

FIB measurements have been done at the Campus Besòs Laboratory of the Universitat Politècnica de Catalunya. There, we prepared the samples and made the analysis with the help of the FIB expert technician. As we commented, the FIB we used was combined to a SEM for images and we also used the SEM-EDX composition analysis of the different layers in order to see the different materials that make up these commercial transparent conductive films.



Fig 9.- (Up) Images of the transparent conductive samples analysed on (right) FIB-SEM-EDX instrument.



2.3 Resistance Measurements

2.3.1 Four-point probe with Jandel RM3

Four-point probe is a technique that measures the Sheet resistance of a thin film, this measure is used to characterize the electrical resistivity of the sample if we have a film with uniform thickness. Knowing the sheet resistance and the thickness of the sample we can compute the resistivity of the film or its conductivity. Sheet resistance (R_{\square}) is measured in square Ohms Ω_{\square} and it is invariable under sample surface size scaling, for this reason we can compare electrical properties of films that are significantly different in size. From (1) R_{\square} is related to the thickness of the sample and the bulk resistance of the material.

$$R = \rho \frac{L}{Wt} = \frac{\rho}{t} \frac{L}{W} = R_{\square} \frac{L}{W} \rightarrow \text{if: } \frac{L}{W} = 1 \rightarrow R_{\square} = \frac{\rho}{t} \quad (1)$$

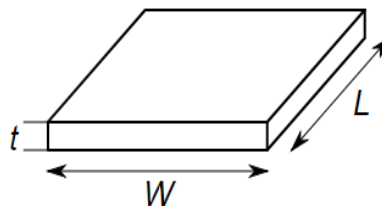


Fig 10. Scheme of sheet resistance R_{\square} calculus referred to eq 1 we can see parameters L, W and t geometrically defined

Four-point probe measurement procedure is useful to measure low resistance since the system eliminates the connection leads and contact resistances from the measurement. The electrical contacts are done by pressing 4 sharp tungsten probes on the conducting film surface.

The Jandel Four-point Probe System with RM3 Test Unit has a combined constant current source and digital voltmeter. The unit supplies a constant current and displays either the resultant voltage or the sheet resistance of the sample in ohms/square, depending which function has been chosen. Voltage and sheet resistance can be measured on samples ranging from 5mm x 5mm to 5” diameter wafers.

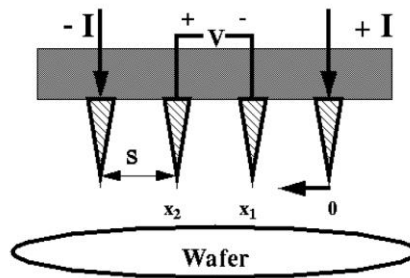


Fig 11. Scheme of four-point probe function

If we want to compute the bulk resistivity for wafers where $t/s < 0.5$ where t is the thickness in cm and s the separations between probes, simply it is: $\rho = R_{\square} \cdot s \cdot t$ where R_{\square} is the sheet resistance from the Jandel instrument. For a wafer thickness t that exceed 0.625 times the probe spacing s we need to add to the equation a correction factor from table 1. And if we are measuring a small surface sample geometry, we need to use a correction factor from table 2 where d is the diameter of the sample surface:

FPP Correction Factors for Sample Thickness t	
t/s	$C1(t/s)$
0.3	1.0000
0.4	0.9995
0.5	0.9974
0.6	0.9919
0.7	0.9816
0.8	0.9662
0.9	0.9459
1.0	0.9215
1.2	0.8643
1.4	0.8026
1.6	0.7419
1.8	0.6852
2.0	0.6337

Table 1 correction factors for sample thickness

FPP Correction Factors for Sample Diameter d	
d/s	$C2(d/s)$
10	4.1712
20	4.4364
30	4.4892
40	4.5080
50	4.5167
60	4.5215
70	4.5244
80	4.5262
90	4.5275
100	4.5284
200	4.5314
∞	4.5320

Table 2 correction factors for sample diameter

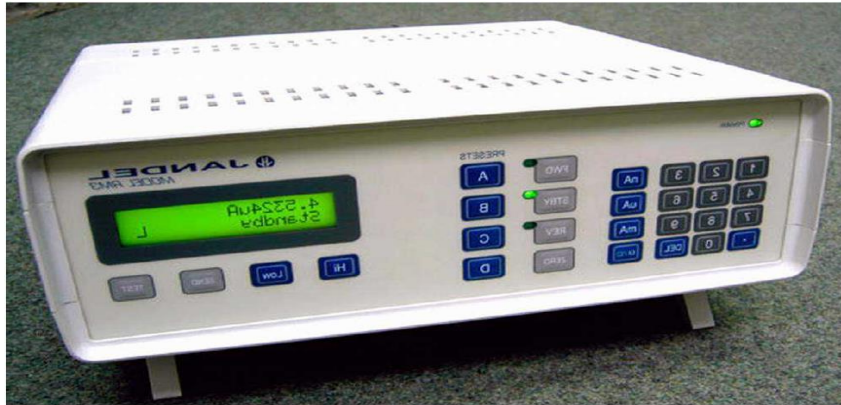


Fig 12. Image of Jandel RM3 instrument

2.3.2 Hand-made system for measuring square Resistance of samples

Because we were working with big samples (12 cm x 10 cm or 10 cm x 10 cm) we decided to make a support structure to measure the resistance R of the whole sample between two parallel long contacts on the conductive layer. Then, after measuring the size of the sample and the shape and the size of the contacts, we compute easily, from $R = V / I$, the square resistance R_{\square} of the samples. We did this because some of the results we obtained from Jandel RM3 for the high resistive films were suspiciously strange and, in some cases, they vary very randomly. The hand-made support structure was made of polycarbonate and was adapted to the size of the samples we were measuring. The two contact bars were made of aluminum and the wires from the power source were connected directly to the aluminum bars. To get a good contact between the aluminum bars and the films we used cooper adhesive tape of 5 mm of width. We apply different measured currents between the 2 contacts and simultaneously we measure the voltage drop between both contacts. This way we easily compute the sheet resistance R_{\square} of the films. The same structure was later used to perform the heating test inside the climatic chamber.

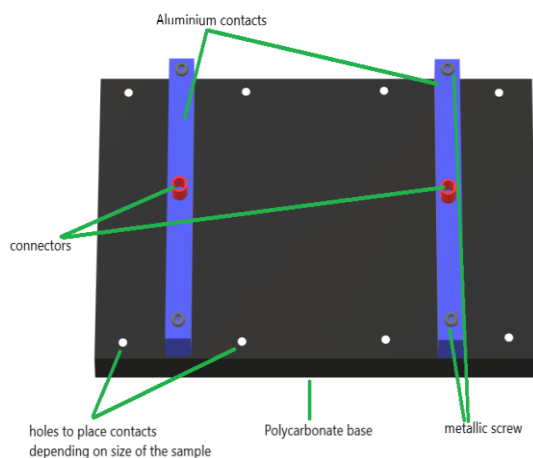


Fig 13. 3D Design of the Hand hand-made system



Fig 14. Image of the hand made system

2.3.3 Confocal Microscope - Sensofar PL μ 2300

It is a powerful tool that combines two techniques: confocal microscope and interferometer. Sensofar PL μ 2300 is the confocal microscope used for the dimensional analysis of ABC wires and ABC films. Confocal profilometers have been developed to measure the surface topography of smooth to very rough surfaces. The samples are optically scanned vertically in steps so that every point on the sample surfaces passes once through the microscope focus. So, during the a full measure, the distance of the microscope's focal plane changes continuously by a prefixed step and the detector keeps information from each step, then all the information is send to a computer the that joins the light received at each step to create a 3D image of the sample.

And different principle has in an interferometric microscope: a light beam passes through a beam splitter, which directs the light to both the of the sample surface and a built-in reference flat mirror. The light reflected from both surfaces recombines and a fringe interference pattern is formed over the plain image of the sample surface, and from the fringes it is possible to calculate the height topography of the sample surface.

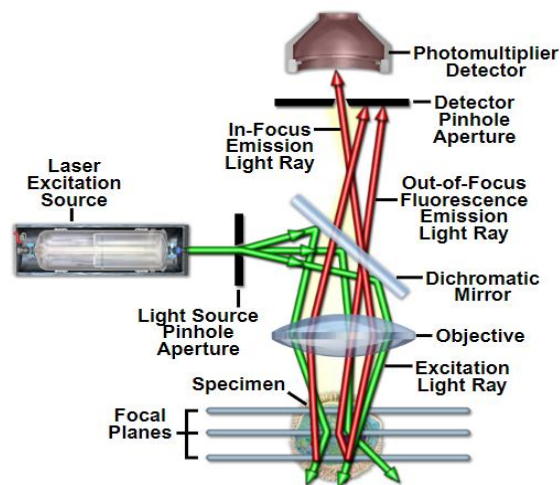


Fig15. Light pathway in a basic confocal microscope configuration from Nikon Microscopy

A confocal microscope creates sharp images of a sample that would otherwise appear blurred when viewed with a conventional microscope. We can get this by excluding most of the light that comes reflected from the sample and that does not come from the microscope's focal plane. The image has better contrast than that of a conventional microscope and represents a thin cross-section of the Sample. This way of working apart from allowing better observation of the details makes possible to build three-dimensional (3D) reconstructions of a volume of the Sample by assembling a series of thin slices taken along the vertical axis.

From confocal images we can measure the width of the ABC stripes of chapter 5 and simultaneously the thickness of these ABC stripes made by using laser etching of the ABC coating. We also will use these measurements to compare results with those obtained with the stylus Profilometer.



Fig16. Image of the confocal microscope at the U.B. Laboratory

2.4 Attenuation and Reflectivity microwave measurements (UPC)

Attenuation and Reflectivity set ups were placed at the UPC and controlled by PhD Santiago Buitrago from the CommSenseLab, Signal Theory and Communications Department, who was also enrolled in an Industrial *PhD* at Zanini. Here we describe the measurement systems used in this thesis for all the attenuation and the reflectivity measurements.

2.4.1 Scattering parameters (S-parameters)

The elements of the scattering matrix describe the electrical behavior of linear electrical networks when undergoing various steady state stimuli by electrical signals.

As we will see in the next section our system consists of a two-port network where an emitter and a receiver are involved. Two-port measurements provide explicit characterization of linear system blocks with a single input and a single output, by far the most common type of element. A two-port network could be as simple as a section of cable, or as complex as a complete transmitter-

receiver link. In its simplest format, a reference excitation is applied to one port, and the response from the other port is recorded as a function of the sweep frequency. A two-port network can be represented as:



Fig 17. Representation of a two-port network. The blue box represents the system that electromagnetic wave passes through.

In this case the relationship between the reflected, incident waves and the S-parameters matrix is given by:

$$\begin{pmatrix} b_1 \\ b_2 \end{pmatrix} = \begin{pmatrix} S_{11} & S_{12} \\ S_{21} & S_{22} \end{pmatrix} \begin{pmatrix} a_1 \\ a_2 \end{pmatrix} \quad (1)$$

Therefore, defining the incident voltage wave as $a_1 = V_1^+$ and $a_2 = V_2^+$ with the reflected voltage waves being $b_1 = V_1^-$ and $b_2 = V_2^-$. Expanding the equations, we find:

$$S_{11} = \frac{b_1}{a_1} = \frac{V_1^-}{V_1^+} \text{ and } S_{21} = \frac{b_2}{a_1} = \frac{V_2^-}{V_1^+} \quad (2)$$

$$S_{12} = \frac{b_1}{a_2} = \frac{V_1^-}{V_2^+} \text{ and } S_{22} = \frac{b_2}{a_2} = \frac{V_2^-}{V_2^+} \quad (3)$$

S_{11} is the input port voltage reflection coefficient

S_{12} is the reverse voltage gain (attenuation)

S_{21} is the forward voltage gain (attenuation)

S_{22} is the output port voltage reflection coefficient

This way we can define the reflectivity (Input Return Loss) in dB as:

$$IRL = -20 \log_{10} |S_{11}| \text{ dB} \quad (4)$$

the reflection coefficient as:

$$\Gamma = |S_{11}| \quad (5)$$

And the attenuation or gain is defined in dB as:

$$g = -20 \log_{10} |S_{21}| \text{ dB} \quad (6)$$

For a lossless network and so, if the system has no absorption some conditions must be met.

$$S_{mn} = S_{nm} \quad (7)$$

And

$$|S_{nm}| + |S_{pm}| = 1 \quad (8)$$

2.4.2 Attenuation system

The system consists in an emitter and a receiver of electromagnetic radiation in a similar way that a radar does. The lenses focus the radiation on the surface of the sample like if the wave was emitted from the infinity with a spot of a diameter of approximately 16 mm. The system is connected to a controller and an analyzer which allow us to compute and see the behavior of S parameters.

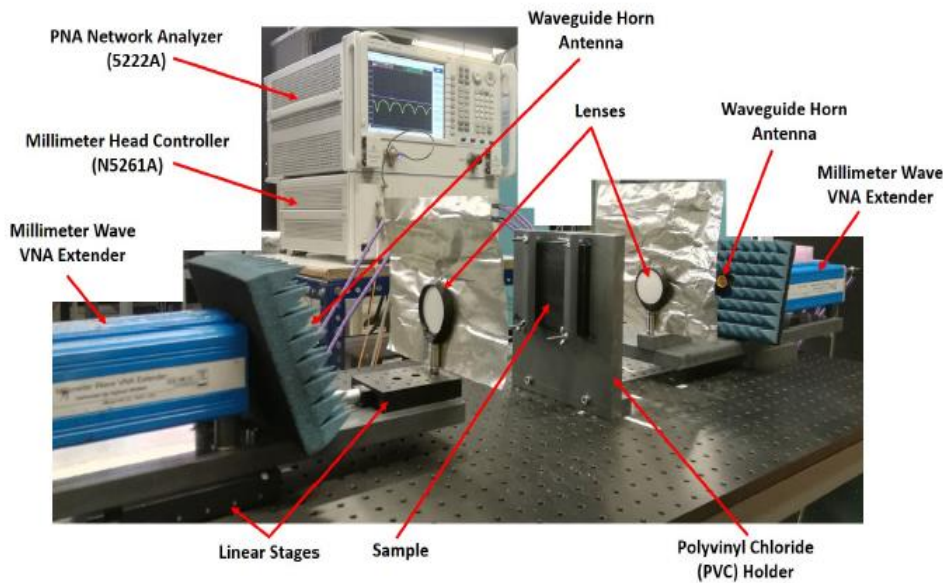


Fig 18. Attenuation and Dielectric characterization set-up. This image is extracted from [1]

The waveguide and the antennas were chosen in order to have a signal as similar as possible to the radar signal. With this set-up we could measure all the S parameters for each sample we analyzed in this thesis so we can obtain the attenuation and the reflectivity for each sample. Also, from the S-parameters we can obtain the dielectric parameters of the substrate materials used for the ABC coatings and after use these values to perform our simulations.

Before measurements are done, the system needs to be calibrated. To calibrate the set-up we make two measurements, the first one is a measurement of a metallic sample we already know and the second one is a measurement with no sample, that will be used to remove the system noise. Each

time we change the sample we need to move emitter the same shift as the thickness of the sample, in order to focus the electromagnetic radiation on the surface of the sample.

2.4.3 Reflectivity set-up

To obtain a map of reflectivity of the full surface of a sample we used a different set-up to measure attenuation to have more precision, since the spot of this system is 2 mm instead of 16 mm. This system allows us to see if there are regions in the surfaces of the samples that are significantly different of the rest of the surface.

This system is tough to operate with a moving array of antennas (Fig 19), in our case we can only use one antenna and the sample moves to generate a virtual matrix array of antennas (Fig 20). The result is the same than using an array of antennas, but it takes more time to have a complete image of the sample. The system is show in Fig 21.

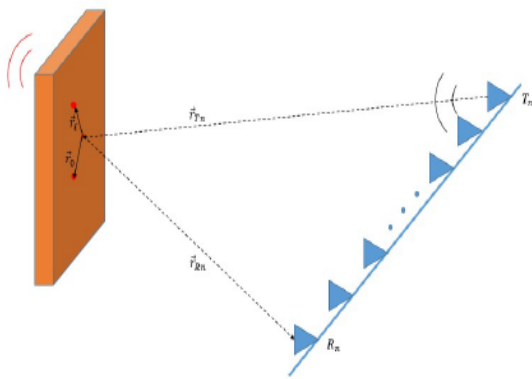


Fig 19. System using an array of antennas. From [1]

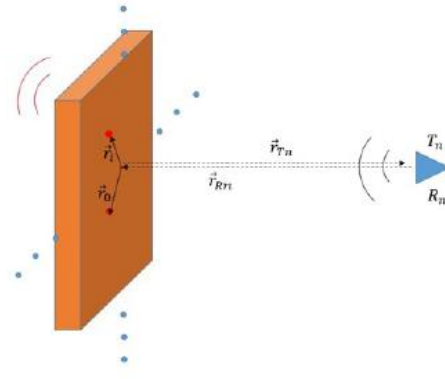


Fig 20. System using one antenna and moving on a y or x axis. From [1]

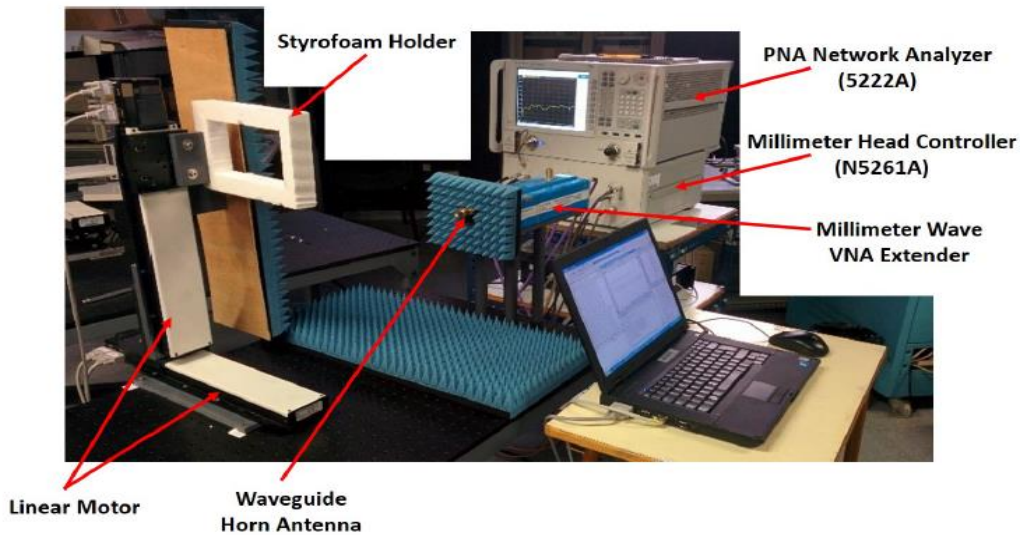


Fig 21. Reflectivity characterization set-up. From [1]

2.5 Climate Chamber - Weiss WKL 100

Weiss WKL 100 is the Climate Chamber at the Laboratory at the Department of Applied Physics of the U.B. This climatic chamber is used for the heating tests. The room temperature for a correct work of the chamber must be between 10°C and 27°C that is a normal temperature in our Laboratories during all the year.



The test Chamber has a volume of 100 l so it is big enough for our test that use parts of plastic with a maximum size of 15 cm x 15 cm. The Chamber is provided with a 3.5" TFT screen panel from this panel we can control all the parameters inside the Chamber and program tests with different conditions. The chamber rear wall incorporates a recirculated-air duct with built-in humidification/dehumidification system, built-in heat exchanger, electric heaters and a recirculated air fan. The special air flow via baffle plates in the test chamber floor and ceiling produces homogeneous ambient air and temperature distribution. Test space illumination is provided. The test chamber is completely sealed by a door with a double glass observation window.

An access port is on the lateral of the chamber of approx. 5 cm of diameter, it allows us to introduce the electrical connections from the power source, different thermocouples, thermal camera connexions and all measurement tools. The rubber plug covers the hole to isolate the chamber but allowing the pass of the wires of the different measurement tools.

The recirculating air passes a fin-type heat exchanger, which cools the air, if necessary. The refrigerating system avoids unintended condensation at the heat exchanger during climatic operation and guarantees highest temperature and humidity constancies in time. An electrical heater, installed in front of the heat exchanger in air direction, is heating-up the recirculating air. The humidification is made via a temperature conditioning humidification bath, which enables an aerosol-free humidification. This recirculating system needs to be stopped in some test.

The humidity of the space air is measured with two resistance thermometers fitted with a dry and a wet bulb respectively. These sensors are arranged next to each other in the recirculating air flow. Depending on the climate the material of the wet bulb sensor is humidified.

The maximum temperature the chamber can get is 180°C and the minimum is -40°C and the temperature changing rates are 5.0 K/min and 3.4 K/min for cooling and heating respectively with a constancy in time of ± 0.3 to ± 0.5 K and homogeneity in space of ± 0.5 to ± 1.5 K. The humidity range is between 10 to 98 %r.h. with a maximum heat compensation of 1100 W and a constancy in time of ± 0.5 to ± 2.0 K %r.h.

2.6 Optical measurements of Transmission Spectra

On chapter 4 we will analyze the transmission spectra of commercial ABC films to characterize them and obtain optical and electrical data of the films. Here we present the experimental set up to measure the transmission spectra of the samples and how the electrical and optical parameters are obtained. The set-up used is shown in the Fig. 23. The set up includes a Computer with the corresponding software to process and save the data, an RS232-interface to translate the light signal, a detector, and a light source in the visible and near infrared range.

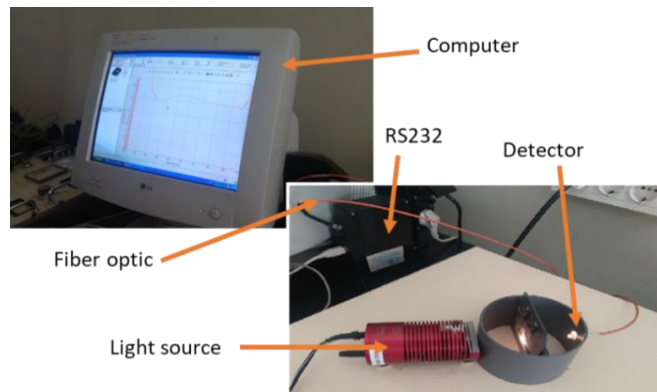


Fig 23. Transmission spectra measurement set-up

The transmission spectra of each sample are measured in the range from 400 nm to 1100 nm. The transmission spectra of the substrate with no film is also measured and stored in order to subtract it during the data process to obtain just the thin film spectra. The ray diagram according to our experiment would be like the one shown in Fig 24 where each medium is characterized by its refractive index n_i . n_0 is always considered to be air for this reason no k appears in its expression.

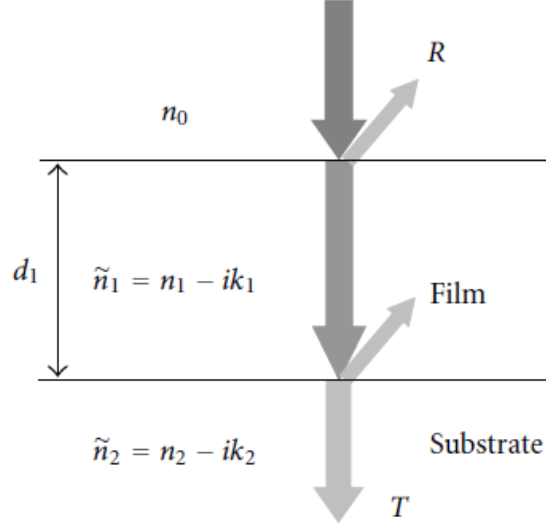


Fig 24. Light ray diagram [18]

To obtain the optical and electrical properties of the different commercial thin films we try to fit a curve on the measured data using Swanepoel notation for an infinite substrate [12], [13], [18], given by:

$$T = \frac{16n_0n_2(n_1^2 + k_1^2)}{b_1e^\alpha + b_2e^{-\alpha} + b_3 \cos v + b_4 \sin v} \quad (6)$$

where

$$b_1 = [(n_0 + n_1)^2 + k_1^2][(n_1 + n_2)^2 + (k_1 + k_2)^2]$$

$$b_2 = [(n_0 - n_1)^2 + k_1^2][(n_1 - n_2)^2 + (k_1 - k_2)^2]$$

$$b_3 = 2\{[n_0^2 - (n_1^2 + k_1^2)][(n_1^2 + k_1^2) - (n_2^2 + k_2^2)] - 4n_0k_1(n_1k_2 - n_2k_1)\}$$

$$b_4 = 4\{[n_0^2 - (n_1^2 + k_1^2)][n_1k_2 - n_2k_2] + n_0k_1[(n_1^2 + k_1^2) - (n_2^2 + k_2^2)]\}$$

And

$$\alpha = \frac{4\pi k_1 d_1}{\lambda}, \lambda = \frac{c}{f}, v = \frac{4\pi n_1 d_1}{\lambda} \quad (7)$$

Where c is the speed of light and so λ is the wavelength in the vacuum. The expression of transmittance depends only on refractive indexes of each medium, the thickness of the film d_1 and the measured wavelength, this last is known at each step. The thickness d_1 and the real and imaginary part of the refractive index can be related with the electrical parameters of the film using the following expressions for real and imaginary parts of the electrical permittivity from the Drude model of electrical conduction [15],[16]:

$$\varepsilon_1 = n^2 - k^2 \quad (3)$$

And

$$\varepsilon_2 = 2nk \quad (4)$$

These expressions allow us to get a relation between optical parameters n and k with the electrical parameters of the film. And to obtain:

$$k = \sqrt{\frac{-\varepsilon_1 + \sqrt{(\varepsilon_1^2 + \varepsilon_2^2)}}{2}} \quad (5)$$

$$n = \sqrt{\frac{\varepsilon_2 + \sqrt{(\varepsilon_1^2 + \varepsilon_2^2)}}{2}} \quad (6)$$

Where ε_1 represents the real part of ε and ε_2 is the imaginary part of ε . Then from the Drude model we have:

$$\varepsilon_1 = \varepsilon_s - \frac{Ne^2}{\varepsilon_0 m_e^* [v_c^2 + (2\pi\varepsilon_s)^2]} \quad (7)$$

$$\varepsilon_2 = \frac{Ne^2 v_c}{2\pi f \varepsilon_0 m_e^* [v_c^2 + (2\pi\varepsilon_s)^2]} \quad (8)$$

Where ε_s is the static dielectric constant and it is defined as:

$$\varepsilon_s = 1 + \frac{(\varepsilon_\infty - 1)}{\left[1 - \left(\frac{\lambda_0}{\lambda}\right)^2\right]} \quad (9)$$

And N is the conduction band free carrier concentration, e is the electron charge, ε_0 is the free space permittivity, m_e^* is the effective mass of the charge carrier, v_c is the frequency of collision of the charge carriers, f is the light frequency, ε_∞ is the high frequency dielectric constant and λ_0 is the oscillator wavelength. To adjust the experimental data, we use μ , the mobility of the free charge carriers, instead of v_c . μ is a more relevant parameters to us and it is related to v_c through the equation [20]:

$$\mu = \frac{e}{m_e^* v_c} \quad (10)$$

Giving values to ε_∞ , λ_0 , d_1 , m_e^* , N and μ we can find the parameters that adjust better to the experimental data. To do this we use the solver application of Excel that use initial conditions given by us to find the parameters that minimize the difference between the experimental data and the fitting plot.

The fitting plot obtained using this procedure considers that the substrate is infinite. To have a more accurate result we need to adapt our results to a finite substrate. To do it we need to take also into account the reflectivity of the film that that can be calculated in the same way as transmission and use a relation between the refractive index of the different media:

$$R = \frac{a_1 e^\alpha + a_2 e^{-\alpha} + a_3 \cos v + a_4 \sin v}{b_1 e^\alpha + b_2 e^{-\alpha} + b_3 \cos v + b_4 \sin v} \quad (11)$$

where

$$a_1 = [(n_0 - n_1)^2 + k_1^2][(n_1 + n_2)^2 + (k_1 + k_2)^2]$$

$$a_2 = [(n_0 + n_1)^2 + k_1^2][(n_1 - n_2)^2 + (k_1 - k_2)^2]$$

$$a_3 = 2\{[n_0^2 - (n_1^2 + k_1^2)][(n_1^2 + k_1^2) - (n_2^2 + k_2^2)] + 4n_0 k_1 (n_1 k_2 - n_2 k_1)\}$$

$$a_4 = 4\{[n_0^2 - (n_1^2 + k_1^2)][n_1 k_2 - n_2 k_1] - n_0 k_1 [(n_1^2 + k_1^2) - (n_2^2 + k_2^2)]\}$$

α and v have the same expression as in (2). Finally, we obtain the transmission spectra value for our sample with a finite substrate from the relation:

$$T_f = T_i \frac{(1 - R_s)}{(1 - R_s R_i)} \quad (12)$$

where

$$R_s = \left(\frac{n_2 - n_0}{n_2 + n_0}\right)^2 \quad (13)$$

T_f is the Transmission spectra of the sample with a finite substrate, T_i is the Transmission spectra of the sample with an infinite substrate that we have already computed and n_2 and n_0 are the refractive indexes for the substrate (medium 2) and the air (medium 0).

This procedure will be used in chapter 4 to characterize ABC commercial samples.

Chapter 3

TCO films

3.1 Introduction

Electrical conductivity depends on many parameters of the material, the number of free charges existing in the material, the material geometry, the atomic structure of the material, the number of impurities, ... The atomic structure primarily affects the chemical, physical, thermal, electrical, magnetic, and optical properties. The microstructure and macrostructure can also affect these properties, but they generally have a larger effect on mechanical properties and on the rate of chemical reaction.

In this chapter we will use TCO because its atomic structure and its impurities (doping) allow these materials to have good optical properties for our purpose and

We will present the different films produced at the UB and at the UZag, the parameters of deposition, its optical and electrical characterizations, their radar attenuation behavior, and the heating tests that we have carried out with them.

3.1.1 Background

From chapter 1

We saw in the chapter 1, in the polycarbonate substrate thickness adaptation section, that the phase parameter β is the main responsible of the substrate attenuation for the micro-waves

We have performed a computer simulation with a piece of polycarbonate, coated with TCO film, and, with a constant TCO

conductivity and the result showed that the attenuation of the radar signal was invariable, the same for all different thickness. To perform the simulation, we used the same dielectric properties of the polycarbonate used to make the Radomes: $\epsilon=2.76$ and a loss tangent $\text{tg}\delta=0.007$, these are the commercial Makrolon 2207 characteristics. The thickness of the polycarbonate piece is 2.36 mm, which is the optimal thickness of polycarbonate for a Radome working at 76.5 GHz. In Image 1 we can see the design of the simulated sample.

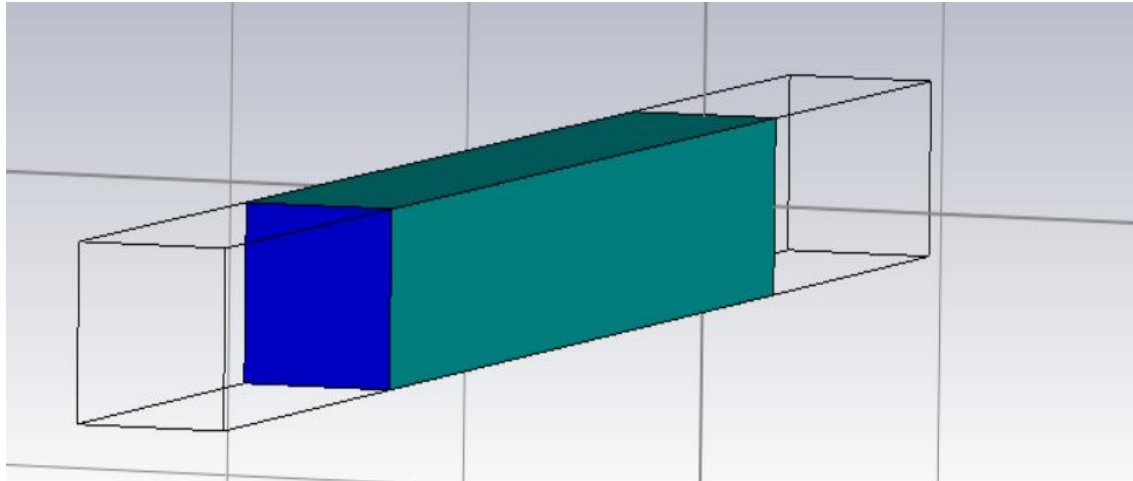


Fig 1 - Scheme of the samples. In blue the thin film, the greenish block is the polycarbonate substrate of 2.36 mm

We saw in chapter 1 that a variation on the polycarbonate thickness of the Radome can cause a big change in attenuation. In addition, the attenuation added to the polycarbonate piece will come from the conductivity of the TCO thin film. To calculate the attenuation due to the thin film we just subtract the value of the attenuation of the polycarbonate piece to the value of attenuation of the polycarbonate and the thin film together.

This simple method to compute the attenuation of the heating system will be also further used in this thesis but just to have an idea of how the attenuation of the Radome is affected.

Experimentally, different depositions of thin films with different thickness were done on the surface of a polycarbonate Radome using a good conductive TCO material. In that case, the substrate used was a plate of polycarbonate of the same polycarbonate used to make the Radomes at Zanini. The radar measurements are made at the UPC using the system commented in chapter 2. This system is used to test different Radomes, so the measurement facility is adapted to test them in real working conditions. The value of the attenuation of the TCO thin film is obtained by subtracting the value of the attenuation of the Radome without film and the value of the same Radome with the deposited film.

To study the behavior of the TCO films, we deposited ABC at the University of Zaragoza and ABC (ABC ABC ABC) at the university of Barcelona on Polycarbonate Radomes, using the two different deposition machines described in chapter 2.

3.2 Properties of ABC thin films deposited at the University of Zaragoza (UZag)

Zanini Company have a wide experience in collaborating with different research centers, this gives us the opportunity to collaborate with external experienced research teams and to have access to well-equipped installations. So, some of the films deposited in this section of the thesis were obtained at the University of Zaragoza in collaboration with the thin film research team of the UZag Physics Department. We already introduced its sputtering installations on chapter 2.

The local research on TCO at UZag focus its objective to find the best deposition conditions for high electrical conductivity TCO thin films, since most of their research is oriented to solar energy panels. [REDACTED]

3.2.1 Thin film parameters

The substrate used is the plate of polycarbonate with a size of 10 cm x 10 cm and 2.36 mm thick. In order to coat these substrates with ABC films with the right characteristics, we did different deposition tests to find the adequate depositions parameters. At the end, 8 samples were prepared by using the unique optimal deposition conditions, [REDACTED]

[REDACTED] The power of the sputtering machine was set at 1000 W, the Ar flux into the chamber was fixed at 286 sccm and the Oxygen flux was fixed at 14 sccm with a precision on fluxes for both gases of +/- 1 sccm. [REDACTED]

To measure the thickness of each film a small glass plate was placed side by side to the polycarbonate substrate at the same time that each deposition was done, the glass has some ink marks easy to remove after the deposition in order to define a clear step at the film coating that could be further analyzed with the profilometer at the University of Zaragoza and afterwards the same measurements were done at the University of Barcelona

The film's sheet resistance was measured at the university of Zaragoza using Jandel RM3 instrument, commented in chapter 2, with an auto positioning accessory that helps to reproduce the measurement at the same places in all the samples. We did afterwards these measurements at the University of Barcelona, using a similar instrument, but we do not have the auto positioning accessory, so we have to locate the position manually, so, we cannot ensure that measurements were done exactly at the same place in each sample. The sheet resistance result is an average of different measurements done in different points of the sample; these points were chosen at the University of Zaragoza and they are shown in the figure 2:

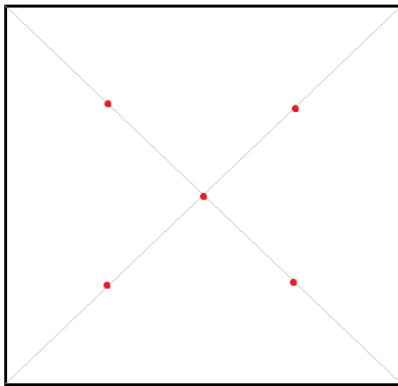


Fig 2 - The measurements of sheet resistance were done at the centre of the sample and on the halfway of the diagonals from the centre to the vertex of the square sample.

The Jandel RM3 measurements were quite repetitive, but being a local measurement in a point, the results were different at each point. We wanted to know the global resistance of the thin film if it is applied on a circuit like it should be in a car Radome system. So, the pieces were after measured on the handmade system ensuring we were measuring the global sheet resistance of the full square sample, and results can be seen at table 1

Electrical conductivity of the TCO films, σ , were computed from:

$$R_{\square} = \rho/t \rightarrow \sigma = 1/\rho \rightarrow \sigma = 1/(t \cdot R_{\square}) \quad (1)$$

Where R_{\square} is the sheet resistance measurement result and t is the thickness of the thin film from the profilometer measurement result

3.2.2 MW transmission, reflection, and absorption measurements

The microwave transmission, reflection and absorption parameters of these square samples were measured at UPC, using different techniques commented in the chapter 2. With these measurement results we could relate the thickness and conductivity of the different TCO films with the absorption of the radar radiation figure 3. We can also observe the linear relationship between the attenuation of the radar radiation and the inverse of sheet resistance figure 4 of the TCO film.

We can see ABC film deposition parameters used for each sample at UZag and the corresponding measurement results obtained at the UB and at the UPC.

Sample name	Deposition Conditions			Measurements			Computed
	Power (W)	Ar Flux (sccm)	O2 Flux (sccm)				
ABC21	1000	286	14				
ABC19	1000	286	14				
ABC20	1000	286	14				
ABC16	1000	286	14				
ABC15	1000	286	14				
ABC14	1000	286	14				
ABC08	1000	286	14				

Table 1. Deposition conditions of ABC samples obtained at the UZag and measurement results from UB and UPC.

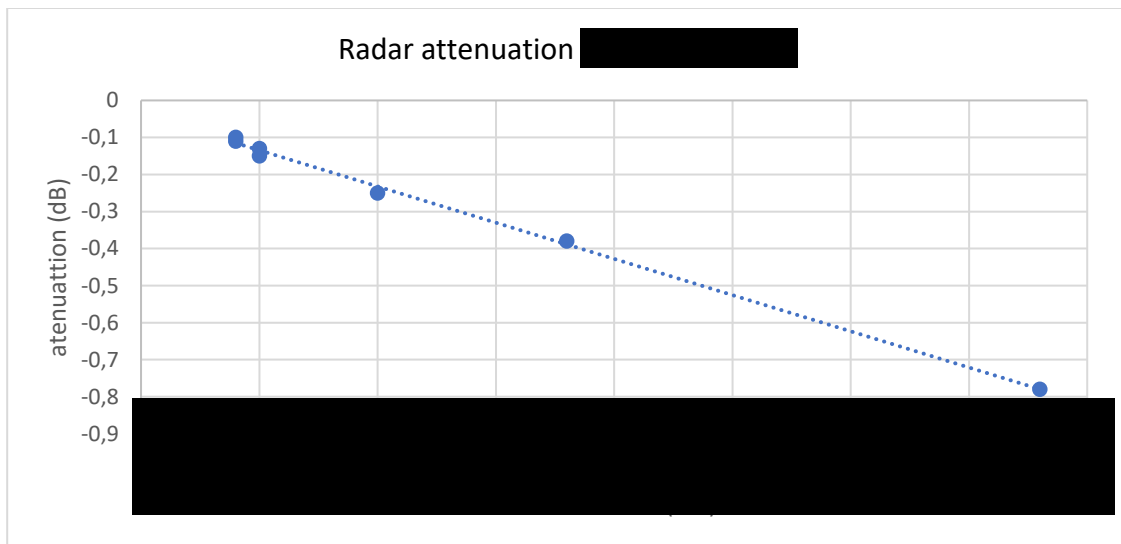


Fig 3 - We can see how the attenuation due to the absorption and reflection of the thin film

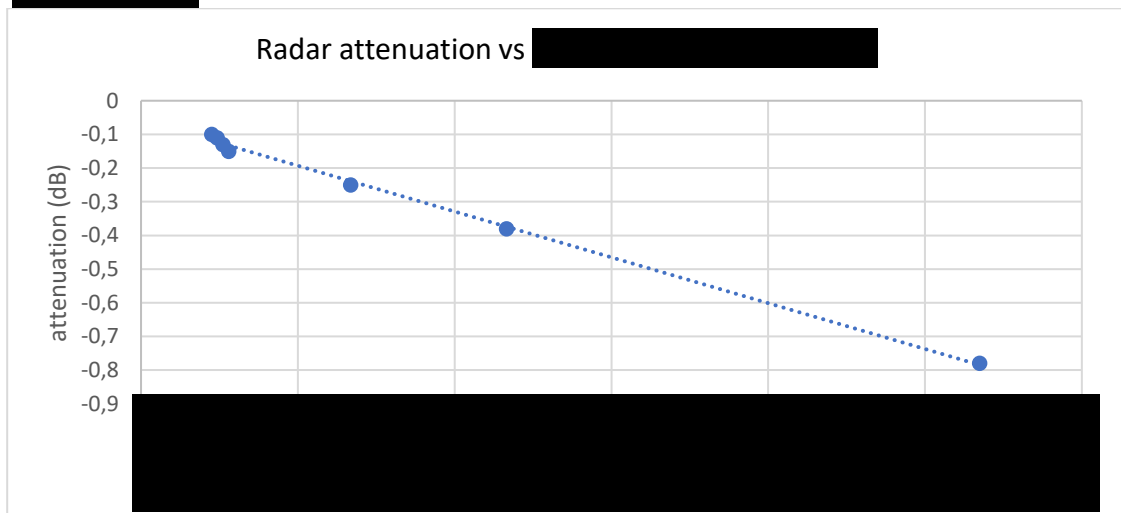


Fig 4 - We can see how the attenuation of the electromagnetic wave is

When looking at plot 1 and 2 we must consider different things:

- The attenuation measured includes absorption due to conductivity and the reflections when radiation changes of medium from air to PC and from PC to ABC.
- The attenuation represented is just the attenuation due to the thin film since we have subtracted the attenuation due to the Polycarbonate substrate.

Figs.3 and 4 show the two parameters related with attenuation in which we are interested on.

We can also see this behavior if we analyze the variation of the modules of S11 and S21 parameters in terms of relative power since they are normalized to 1 we have that

$$|S_{11}|^2 + |S_{21}|^2 = 1 \quad (2)$$

But if there is absorption the relation is no correct since some of the radar radiation is absorbed by free electrons inside the film, then

$$|S_{11}|^2 + |S_{21}|^2 + |\alpha|^2 = 1 \quad (3)$$

Here α represents the absorption of the free electrons inside the film, if we plot the modules of the three parameters, we can see that the square module of the reflectivity keeps almost constant, but the square module of attenuation gets down when the square module of absorption grows.

Here S_{11} and S_{21} are measured at the UPC as commented in chapter 2, α is computed using the previous equation.

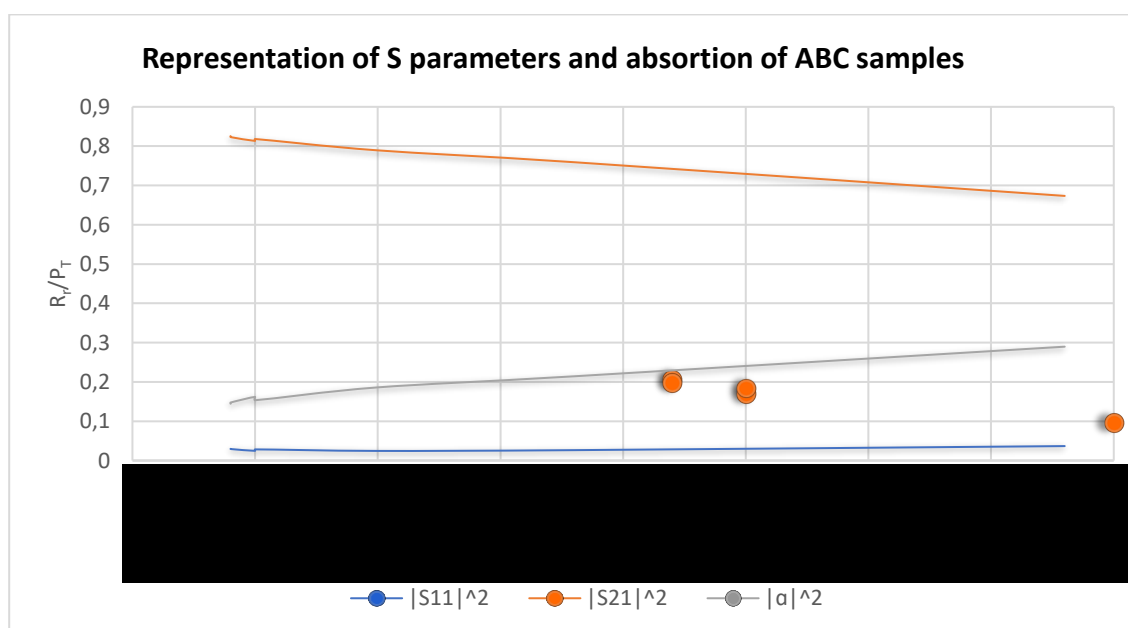


Fig 5 - Representation of the square modules of S11, S21 and absorption of

3.3 Properties of ABC thin films deposited at the University of Barcelona (UB)

We used the PVD sputtering machine of UB introduced in chapter 2. The depositions were done at the same time of those of the university of Zaragoza. As we saw in chapter 2 the machines are completely different but the access to the UB machine was easier and we could control completely the thin film deposition process.

In the UB deposition experiments we changed the deposited material to ABC (ABC ABC ABC) instead of ABC in UZag. We used the same substrates as those used at UZag: a square of polycarbonate squares of 10 cm x 10 cm and 3mm thick.

3.3.1 [REDACTED] (ABC)

[REDACTED] a transparent and conductive film material because it exhibits a wide band gap, high UV and VIS light transparency and low electrical resistivity. [REDACTED]

[REDACTED] Appropriate dopants of [REDACTED] can make it an effective n- or p-type semiconductor by incorporating electrons or holes that easily flow across the lattice.

3.3.2 Deposition of ABC

The same deposition conditions were used for all the samples, the deposition time was set at 25 minutes and we did the depositions at room temperature, the distance between the substrates and the [REDACTED] target was 30mm, the total vacuum pressure was set at $5 \cdot 10^{-6}$ Torr by introducing Ar/O₂ with a flow of 9 sccm. To increase the film homogeneity, we did a rotation of substrate stage of 50 rpm. [REDACTED]

[REDACTED] [12], [13].

The measurements of film thickness and sheet resistance and electromagnetic transmittance were made with the same procedures as we applied for the samples obtained at UZag.

sample name	Deposition Conditions			Film Measurements			Computed
	Dep Pw (W)	Bias V (V)	Dep rate (nm/min)	[Redacted]	[Redacted]	[Redacted]	[Redacted]
Zanini3	150	93-94	3,2	[Redacted]	[Redacted]	[Redacted]	[Redacted]
Zanini4	180	106-107	5,6	[Redacted]	[Redacted]	[Redacted]	[Redacted]
Zanini5	200	110-111	9,2	[Redacted]	[Redacted]	[Redacted]	[Redacted]
Zanini6	250	125-127	15,2	[Redacted]	[Redacted]	[Redacted]	[Redacted]

Table 2. Deposition conditions of ABC samples obtained at the UB and measurement results from UB and UPC.

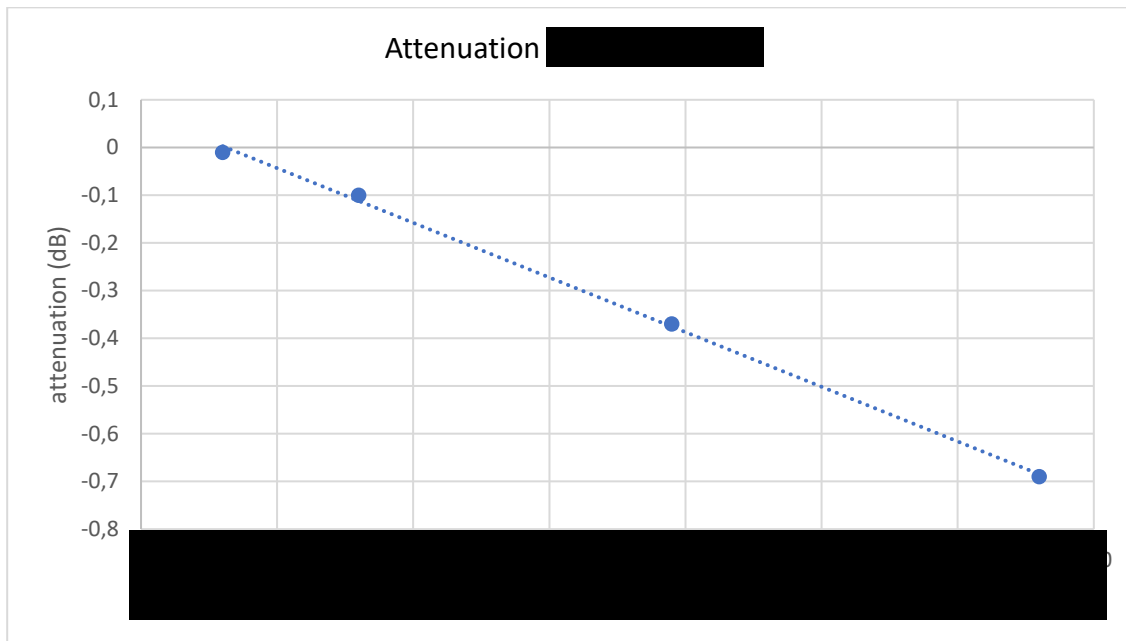


Fig 6 - We can see how the attenuation due to the MW absorption and reflection of the thin film is increased when the thickness of the film is also increased.

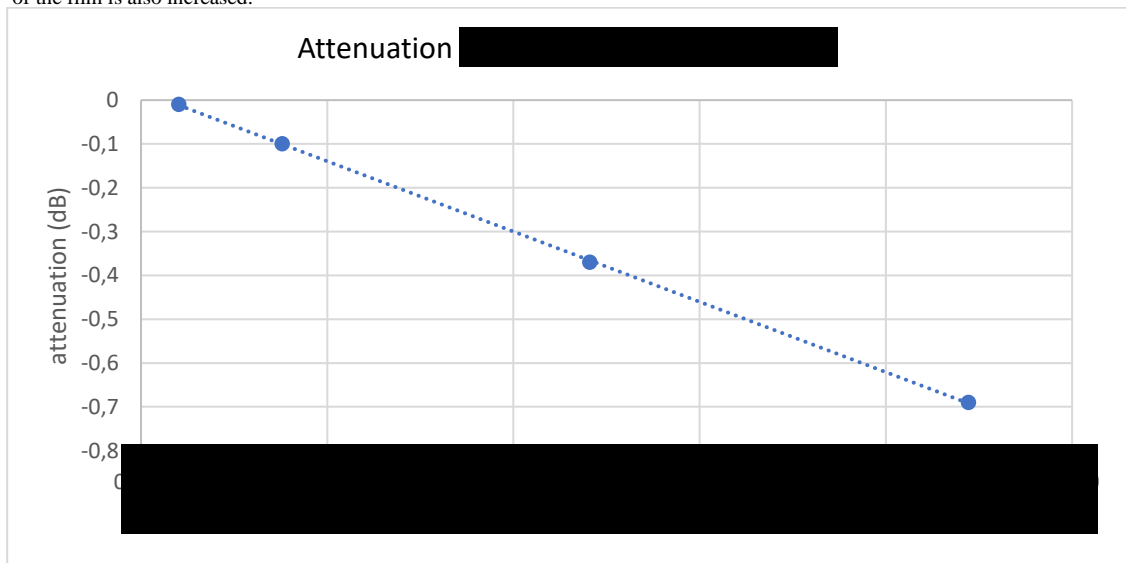


Fig 7 - We can see how the attenuation of the electromagnetic [Redacted]

We can see, in figure 6 and figure 7, how the attenuation is related [REDACTED]
 [REDACTED] As we commented for figure 3 and 4, when looking at figure 6 and 7 we must consider different things:

- The attenuation measured includes MW absorption due to conductivity and the MW reflections when radiation changes of medium from air to PC and from PC to ABC.
- The attenuation represented is just the attenuation due to the thin film since we have subtracted the attenuation due to the polycarbonate substrate.
- In this case we also must consider that the samples [REDACTED]
 [REDACTED]

As expected, the attenuation of the samples made at the UB behaves in the same way that the ABC samples made at UZag. [REDACTED]
 [REDACTED]
 [REDACTED]
 [REDACTED]

Here we can also plot the square modules of S11, S21 parameters and the square module of the absorption (plot6) and we see a similar plot like plot 3. In this plot 6 we can also observe some interesting effects when absorption tends to zero, in this situation reflectivity becomes a more important source of attenuation than absorption.

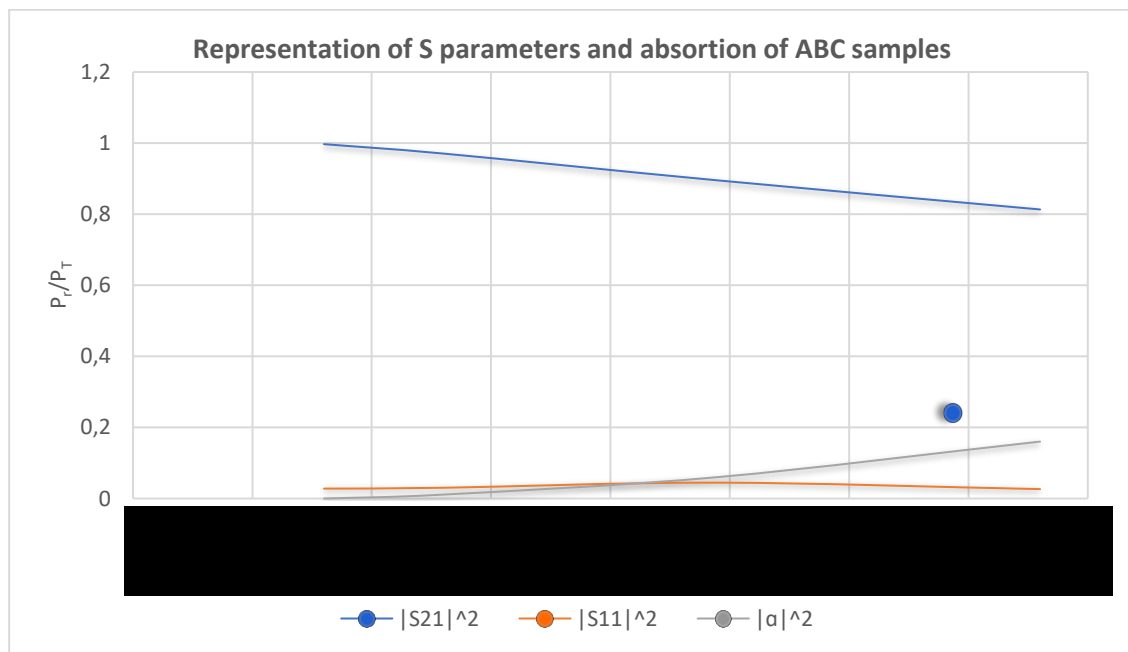


Fig 8 - Representation of the square modules of S11, S21 and absorption of the samples [REDACTED].

3.4 Thin film homogeneity

Before starting the heating tests, we decided to check if the ABC and ABC films deposited on the PC plates had a homogeneous distribution since the size of the samples is quite big (10 cm x 10 cm) and this could bring some inhomogeneities at the edges of the sample. We did this at the UPC, measuring the reflectivity of the samples we are going to use to perform the heating tests samples ABC14 and Zanini6. The only reason we choose these samples was because they are similar in Sheet Resistance besides ABC14 is made with ABC and Zanini6 is made with ABC so, we will be able to compare material performance. The measurement was done sequentially in regions of 2 mm of diameter one next to the other to have an image of all the surface of the sample. We also did this measurement with a PC part with no deposition on it as a reference. Measuring the reflectivity of a complete surface takes more than 2 hours due to the number of small measurements that must be done.

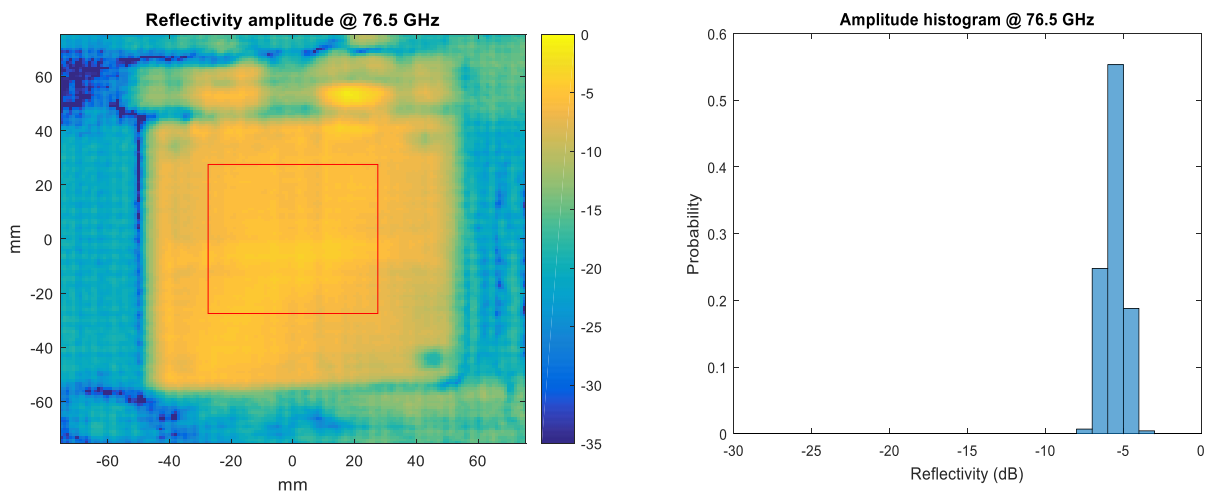


Fig 9 - The Polycarbonate substrate with no deposition on the left and the average reflectivity of all the surface on the right

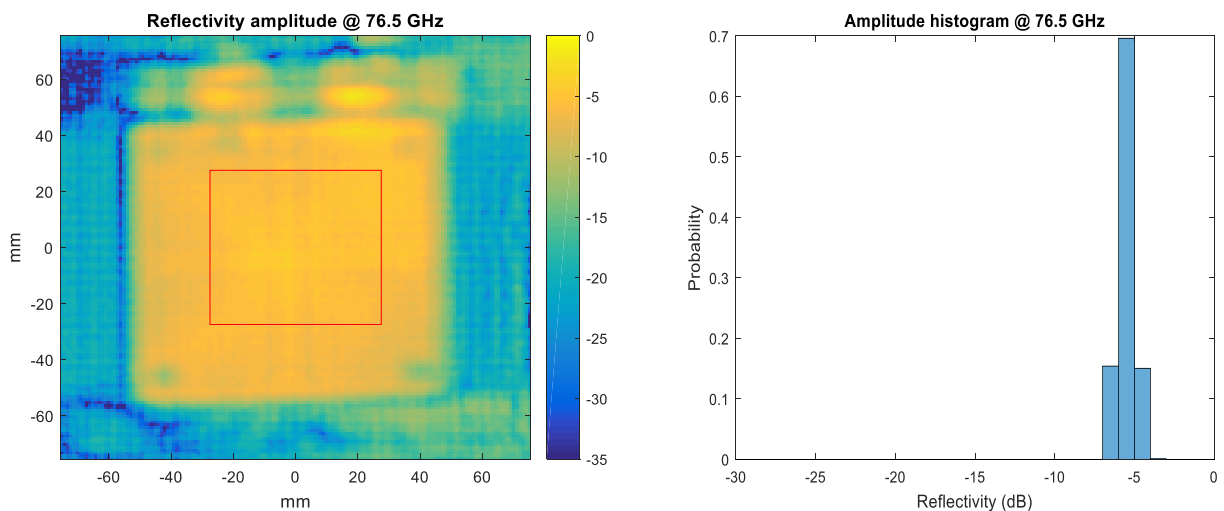


Fig 10 - ABC14 sample [redacted] on the left and the average reflectivity of all the surface on the right

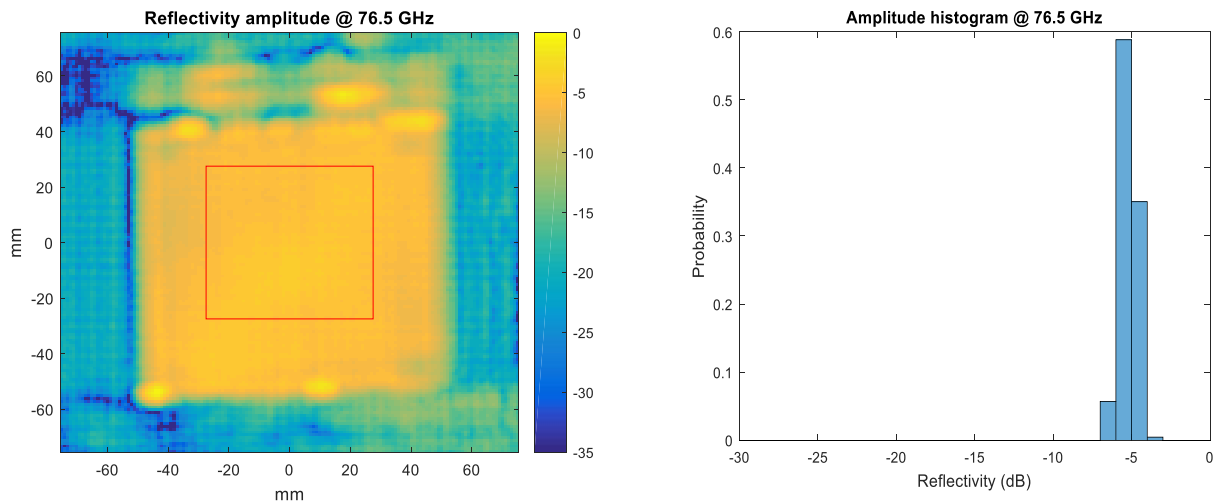


Fig 11 - Zanini6 sample [redacted] on the left and the average reflectivity of all the surface on the right

In figure 9 we can see the reflectivity of the sample of Polycarbonate with no coating on its surfaces, on the left we see the map done during the measurement and the red square is the region where the histogram (on the right of each map) is applied. The histogram gives an idea of the average reflectivity in dB of the sample. The histogram represents the probability to find a value of the Reflectivity on the region limited by the red square.


If we focus on the samples of interest ABC14 (figure 10) and zanini6 (figure 11) we can consider that they are homogeneous in all its surface with some small variations at the edges of the samples. This is not surprising since the local sheet resistance behave in the same way when approaching the edges of the surfaces. Regarding at the histogram of ABC14 and Zanini6 we can consider that ABC14 is more homogeneous than zanini6 since the main value have the biggest probability to appear at the red region than the main value of zanini6. Also, the probability for values different from the main value in ABC14 is smaller than in zanini6. These two last considerations can give us information about the process of deposition, since the machines (the one from UB and the one from UZag) are completely different, so we can consider that the sample done at the UZag is more homogeneous than the sample done at the UB as we could expect from the information of the two sputtering machines commented on chapter 2.

3.5 Heating test

The two samples Zanini 6 and ABC 14 used for the heating test have a sheet resistance in the range that we considered acceptable for the final application. [redacted]

- These are the voltages necessary to heat the samples and get a power between 10 and 40 Watts



The heating test were performed in the climatic chamber at 0 °C, the samples were placed at the center of the chamber pressed in the handmade (HM) tool commented on chapter 2. The HM tool was connected to a power source able to supply a maximum , placed out of the climatic chamber. To control the temperature a thermocouple was used, but we did the measurement on the opposite face of the thin film (figure2), so we had to take into account a thickness of 2.6 mm of polycarbonate between the heating and the thermocouple that we computed after the tests.

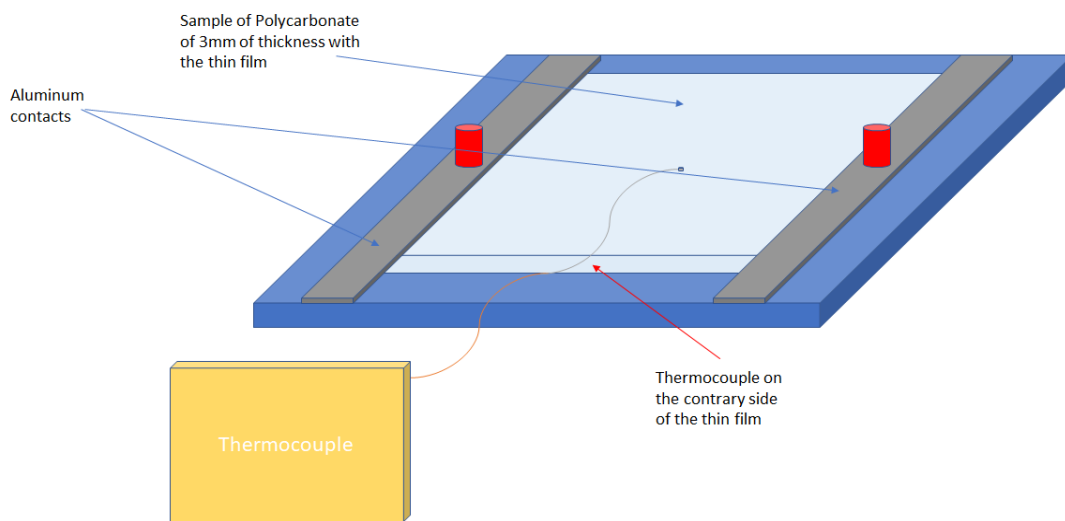




Fig 12 - Scheme of how the measurement of temperature was done. The thermocouple had to be placed between the Polycarbonate sample and the HM tool in order that the current going through the thin film do not disturb the measurement

To compute the temperature difference between the measured surface and the heated surface of the polycarbonate we used:

$$\Delta T = \frac{Pt}{\kappa S} \quad (4)$$

Where P is the Power, t is the thickness of the sample, κ is the thermal conductivity of the material and S the area of the sample, for our polycarbonate 0.29W/mK the κ given by the supplier.

Heating test were done at the climatic chamber at 0°C and 0% of humidity (0% humidity was a requirement of the university department to ensure a good function of the chamber  , these voltages imply a power dissipation between 10 W to 37 W depending on the sample and the applied voltage. The tests were 10 minutes long as required by general client specifications.

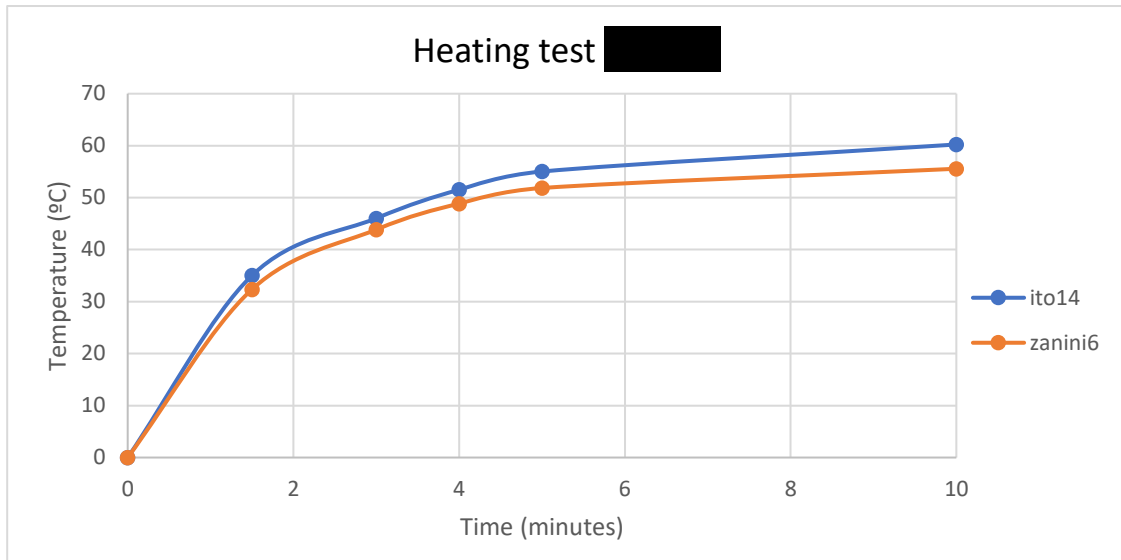


Fig 13 - Variation of the temperature computed from the measurements of the thin film faces

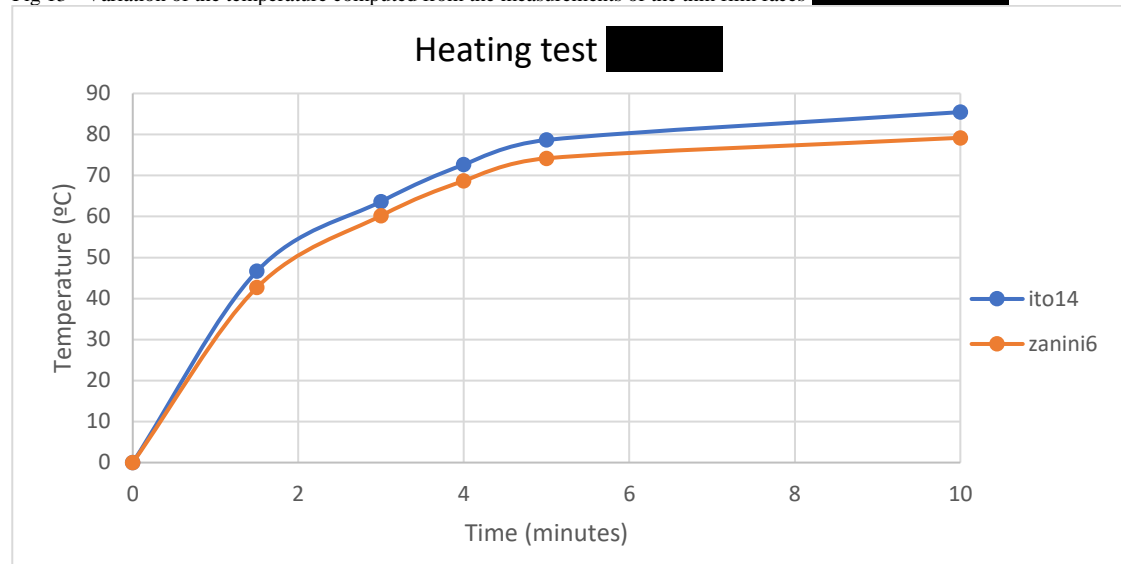


Fig 14 - Variation of the temperature computed from the measurements of the thin film faces

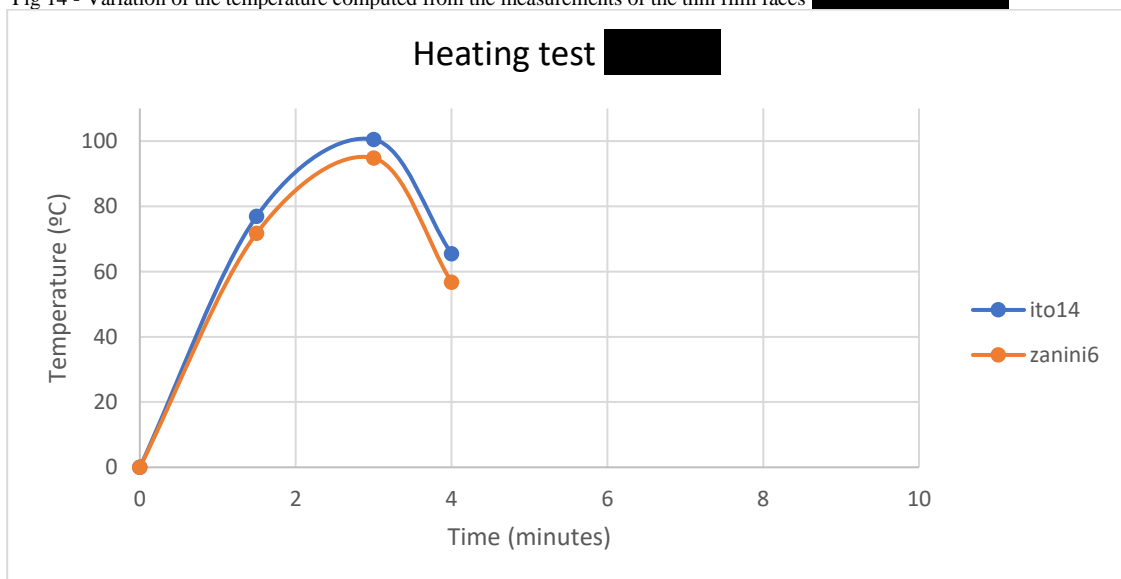


Fig 15 - Variation of the temperature computed from the measurements of the thin film faces

A piece of copper foil tape had to be added between the aluminum contacts and the thin film to ensure the current contact between the power supply and the thin film. We tried this copper foil tape with other samples, and we considered that it was the easiest and most efficient solution to make the heating measurement works properly.

In figure 13 and figure 14 we can see the evolution of the temperature of the thin film computed from the data taken on the opposite face of the polycarbonate sample. The shape of the plots corresponds to a fast increase of temperature during the first 5 minutes and the initial saturation situation between the minute 5 and 10 as we could expect. But the saturation limit was not achieved as we can see in the plot that the temperature is still growing very slowly at the end of the test. In each case, the voltage applied to the samples are the same, but the power dissipated is slightly different since sheet resistances of the sample have a small difference.

Figure 15 have and interesting shape since it indicates that the rising of temperature is interrupted at some point during the test around 100°C. We considered many options to explain this phenomena and we think that a mechanical problem occurred during the heating of ABC and Polycarbonate since the coefficients of thermal expansion (CTE) are very different between them, for ABC [redacted] and for Polycarbonate $66-70 \times 10^{-6} K^{-1}$ [14], so, polycarbonate expands by the effect of heat 8 times faster than ABC and 18 time faster than ABC. Even if thermal conductivity of PC is very bad and the transport of the heat is slow, the expansion of the material could break the ABC and ABC thin film on its surface. This rupture of the ABC and ABC thin film can be observed by naked eye, although it is very subtle, we can observe like a fissure from the top to the bottom of the sample breaking the thin film in two parts, so the current is not able to continue going through. This could explain the drop of the temperature.

3.6 Summary and comments

In this chapter we saw how a heating system with no preferred direction or orientation can be done using sputtering and thin film technology. We did it using ABC and ABC on a Polycarbonate substrate using different methods: increasing time deposition and increasing the applied voltage; and different deposition machines. [redacted]

[redacted] So, we can use a conductive and transparent material as a heater of a plastic surface [redacted] in order to match the attenuation requirements.

Some problems occurred and that we would need to be further investigated deeply. The thermal expansion of the substrate produces fissures on the thin films when heated at high temperatures very rapidly. We have two options to solve this problem, first: to change the Radome plastic material, but polycarbonate is the most common material used to make Radomes and, so, it is almost mandatory to use it in the process of fabrication. The other possible solution is to add a film between the polycarbonate with a thermal expansion coefficient compatible with both materials, the polycarbonate and the material used as a thin film. This last option could be tricky since we would be adding another film in our Radome that could add some new attenuation effects.

Also, the electrical contacts with the thin films needs to be improved since a copper foil tape cannot be used in the final product and it also showed some problems with some samples that we did no commented because they were not of our interest. A good solution would be to replace the foil tape by a sputtering deposition of copper along the two parallel edges of the sample. Also, the aluminum bars would then be replaced by two contact points welded on the copper deposition. Of course, all this new contact system would need to be studied and tested.

Furthermore, Radomes are not completely flat so, these thin films we studied here will need to be transferred to slightly curved pieces. Then homogeneity could be a new threat of this heating system to be studied again deeper.

Finally [REDACTED]
[REDACTED]
[REDACTED]
[REDACTED]

Chapter 4

Characterization of commercial samples

4.1 Introduction

In chapter 5 commercial conductive ABC samples will be used to develop a conductive heater with transparent wires. So, in this chapter 4 we will characterize the samples that we will use in chapter 5.

The commercial conductive ABC samples have a nominal sheet resistance of $4 \Omega_{\square}$, $10 \Omega_{\square}$, $20 \Omega_{\square}$ and the substrate is Soda Lime Float Glass of 1.1 mm of thickness. The size of the samples was chosen to be 10 cm x 11 cm, similar to the size of a standard Radome. The supplier company reported us specifications for the thin film, its configuration is: Glass substrate / Passivation layer / ABC (Fig. 1). The passivation layer is a film of Silicon Oxide (SiO_2) of 25 nm of thickness, the ABC film was deposited at a temperature of 300°C by magnetron sputtering, the surface roughness (RMS) is 1nm and the transmittance of the sample is 83% at a wavelength of 550 nm.

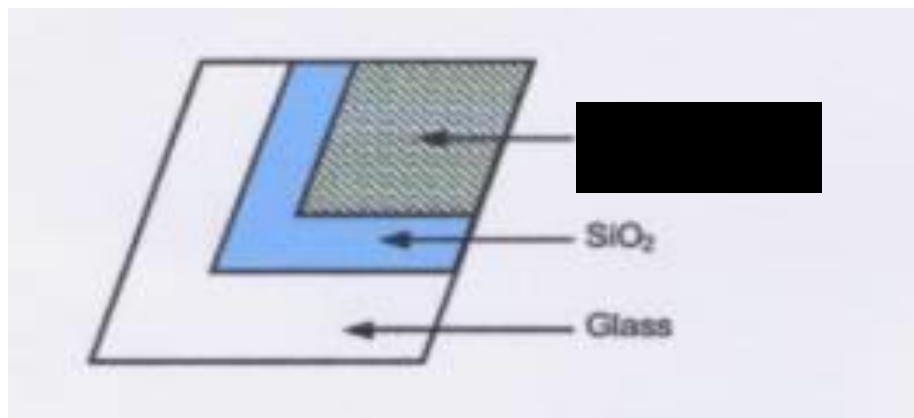


Fig 1 - Scheme of the ABC samples issued by [redacted]

4.2 Characterization of the samples

To characterize these samples, we did measurements of sheet resistance, thickness, transmission spectra, and attenuation and transmission of the radar radiation. To measure the thickness, we used two different techniques: Focused Ion Beam (FIB) and Profilometer measurements. From these measurements we could compute the ABC layer conductivity since we know the sheet

resistance of the film. After that, transmission spectra gave us more accurate values of electrical parameters and thickness. With the obtained data we can simulate a structure that mimics our samples on our simulation program. We will use the MW attenuation and transmission measurements to adjust the permittivity and the loss tangent of our virtual structure. Then, in the next chapter, we will be able to predict the optimal designs for our heater.

4.2.1 Sheet Resistances

As a first point of the characterization, we measured the sheet resistance of the samples to ensure the values given by the supplier. The measurements were made using the four-point probe equipment commented in chapter 2. The results obtained are shown in the following table:

Sample	Sheet Resistance (Ω/\square)
Sample4	3,9
Sample10	7,9
Sample20	16,6

Table 1 - Results of sheet resistance of the commercial samples

So, first we see that the sheet resistances are quite lower than the value that the supplier gave us. In the following steps we will use these values that we have measured to make our calculations but, for simplicity, we will keep the name of the samples as Sample4, Sample10 and Sample20.

4.2.2 Profilometer measurements

We need to create a step where we can measure the thickness of the ABC films since the films are commercial and they are not made by ourselves. We protect a region of the samples with a drop of regular engine oil and we attack the ABC film by immersion in hydrochloric acid for 24 hours, see figure 2. After this time, the ABC film has been removed from the surface of the substrate except on the oil protected region. We clean the oil and use the step created between the left ABC film region and the clean substrate to measure the thickness of the ABC film.

From the thickness measurements and the nominal sample Sheet Resistances we computed the ABC conductivity (table2):

Sample	Thickness (nm)	Sheet Resistance (Ω/\square)	conductivity (S/m)
Sample 4	340	3,9	7,54E+05
Sample 10	182	7,9	6.96E+05
Sample 20	90	16,6	6.96E+05

Table 2 - Results of ABC conductivities (thickness measured with profilometer)

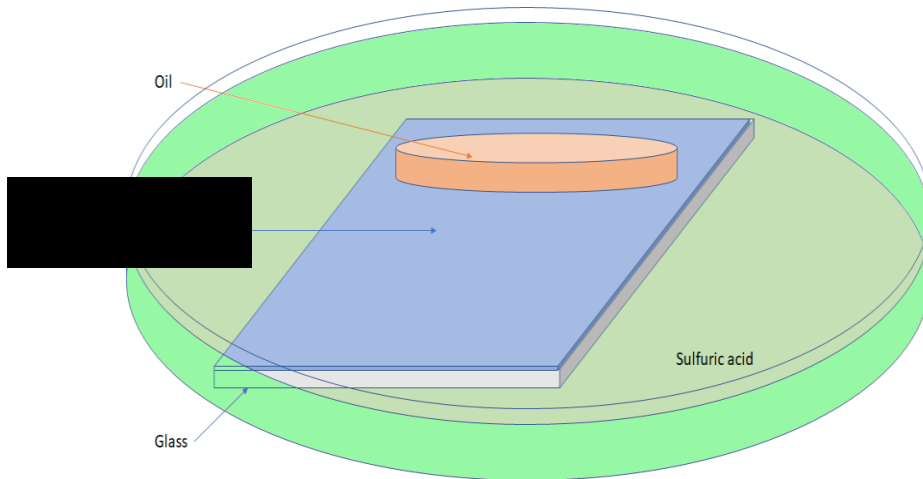


Fig 2 - Scheme of the etching method used to measure the thickness of the commercial thin films using hydrochloric acid

4.2.3 FIB and SEM measurements

FIB (Focused Ion Beam) and SEM (Scanning Electron Microscope) measurements were done to measure more precisely the thickness of the commercial samples. We have already described about the FIB and SEM system used at the UPC in chapter 2 so, in this part we will go directly to the obtained results. The position of the cursors delimiting the thickness of the film is placed by hand, to define the limits of the film we used the Full Width at Half Maximum criteria. So, for the different samples we obtain the following thickness:

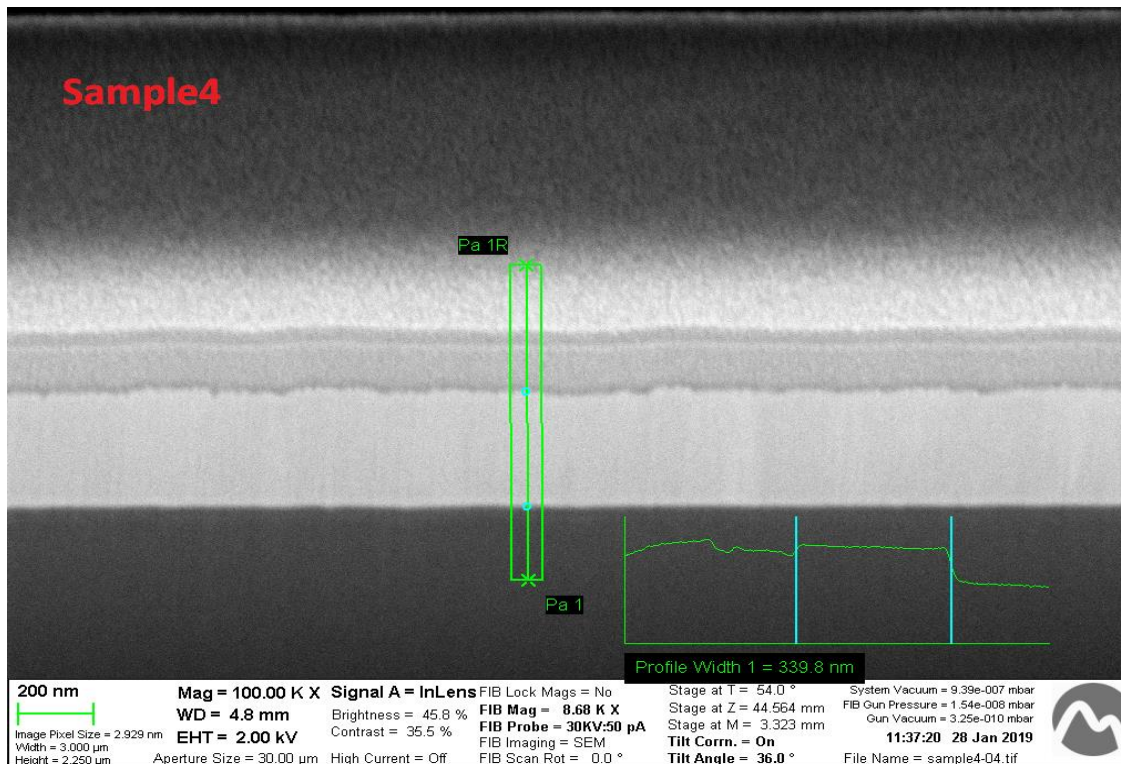


Fig 3 - FIB measurements of Sample 4.

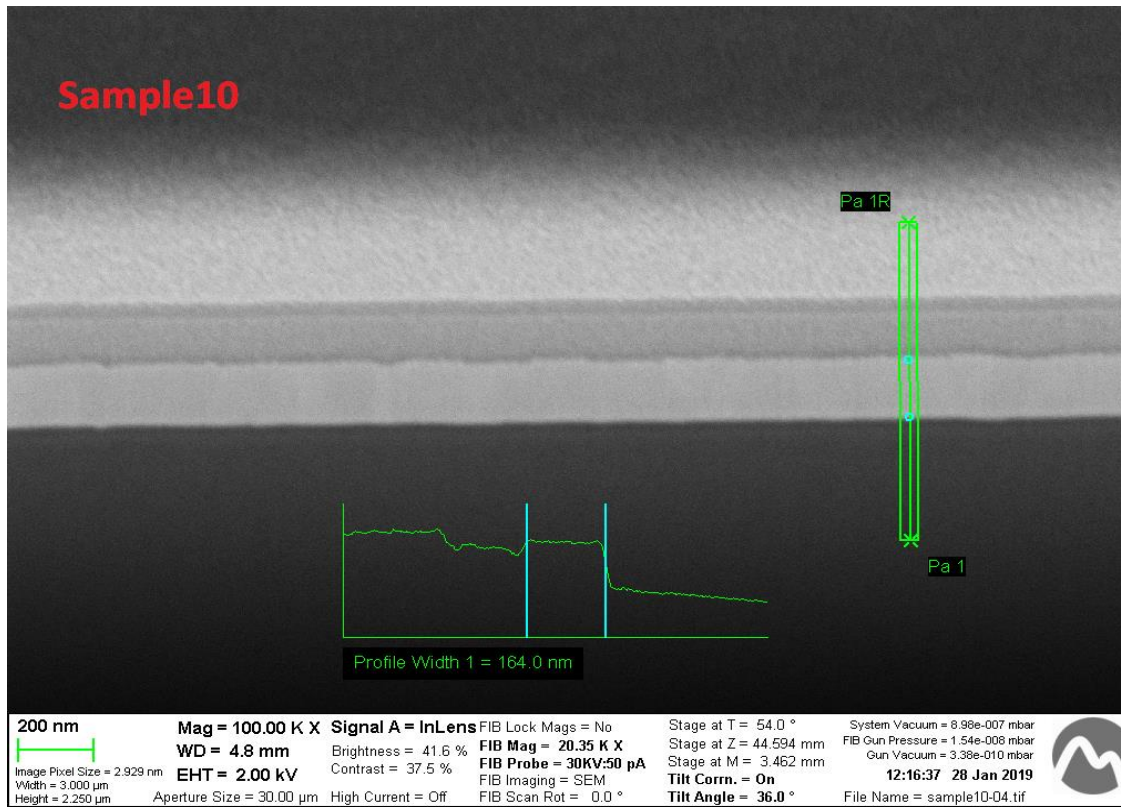


Fig 4 - FIB measurements of Sample10.

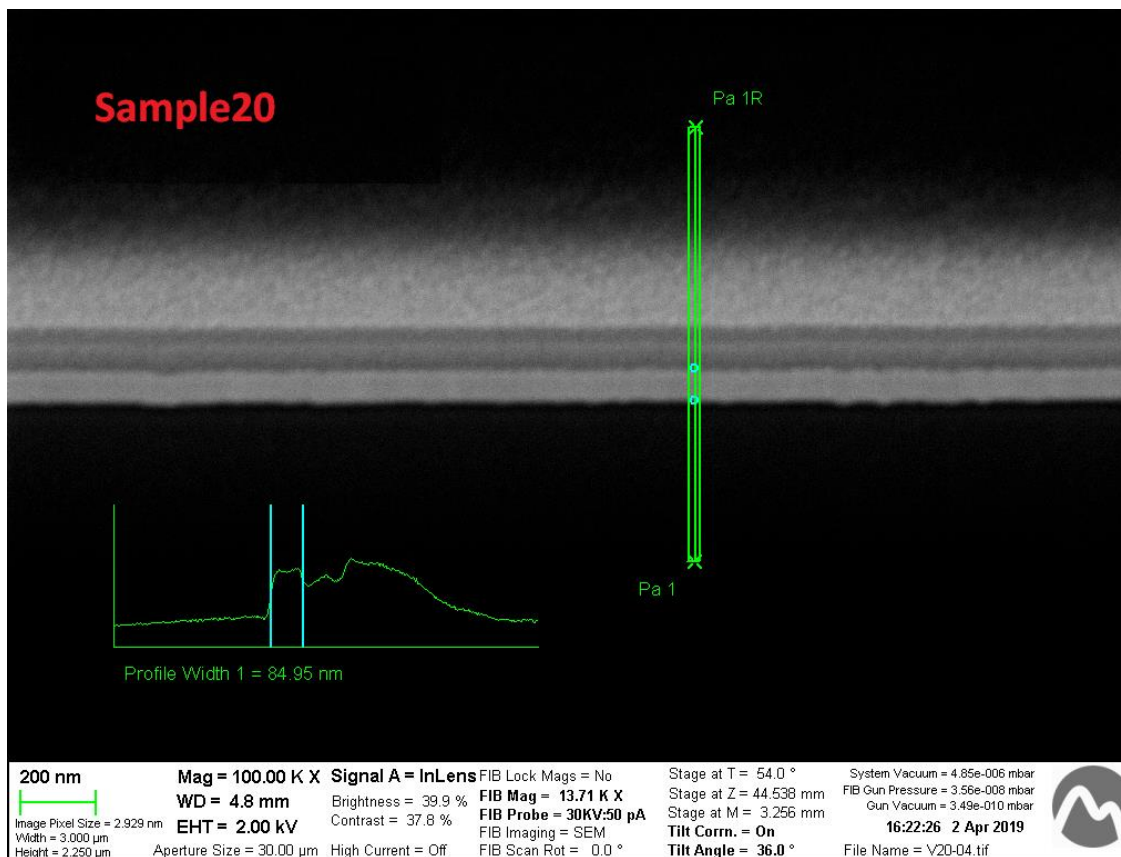


Fig 5 - FIB measurements of Sample20.

We obtain the results show in table 3 that we can compare with the results in table 1:

Sample	Sheet Resistance ($\Omega\Box$)	Thickness (nm)	conductivity \Box (S/m)
Sample 4	3,9	340	$7,54 \cdot 10^5$
Sample 10	7,9	164	$7,72 \cdot 10^5$
Sample 20	16,6	85	$7,09 \cdot 10^5$

Table 3. Results of ABC conductivities (thickness measured with FIB)

We consider that the differences between the two measurements of the thickness could be consequence of some oil remains on the ABC surface, in the profilometer measurements, especially on sample 10. Also, some mistakes due to the manual positioning on the FIB measurements can bring to some mistakes in the measurements. However, we can consider that both measurements are in good agreement since the values are similar. Conductivity also gives us a warning that perhaps the thickness measurements are not quite accurate since we consider that differences between the layers are not big enough to introduce changes in the conductivity of the material. Transmission Spectra measurements can give us more accurate values of the conductivity since this kind of measurements can also inform us of the electrical parameters of the thin films.

4.2.4 Transmission Spectra

In this section we will use Optical measurements of the transmission spectra of the three samples to extract optical and electrical parameters of the thin films. The measurements were made at the University of Barcelona with the procedure described in chapter 2.

The following plots are representations of the spectral data measured (in red) and the fitted function calculated from supposed film parameters (in blue). The fitted function is obtained by varying the film thickness and the optical and electrical ABC parameters. To find the most appropriated values we have used the solver tool from Excel which is able to adjust the function between some minimum and maximum values we impose, considering the initial parameter values introduced by us. These initial values are extracted from the data we already known from the films. The optimal fit parameters are deduced by minimizing the differences between the function obtained from the measured data and the fitted function at each point.

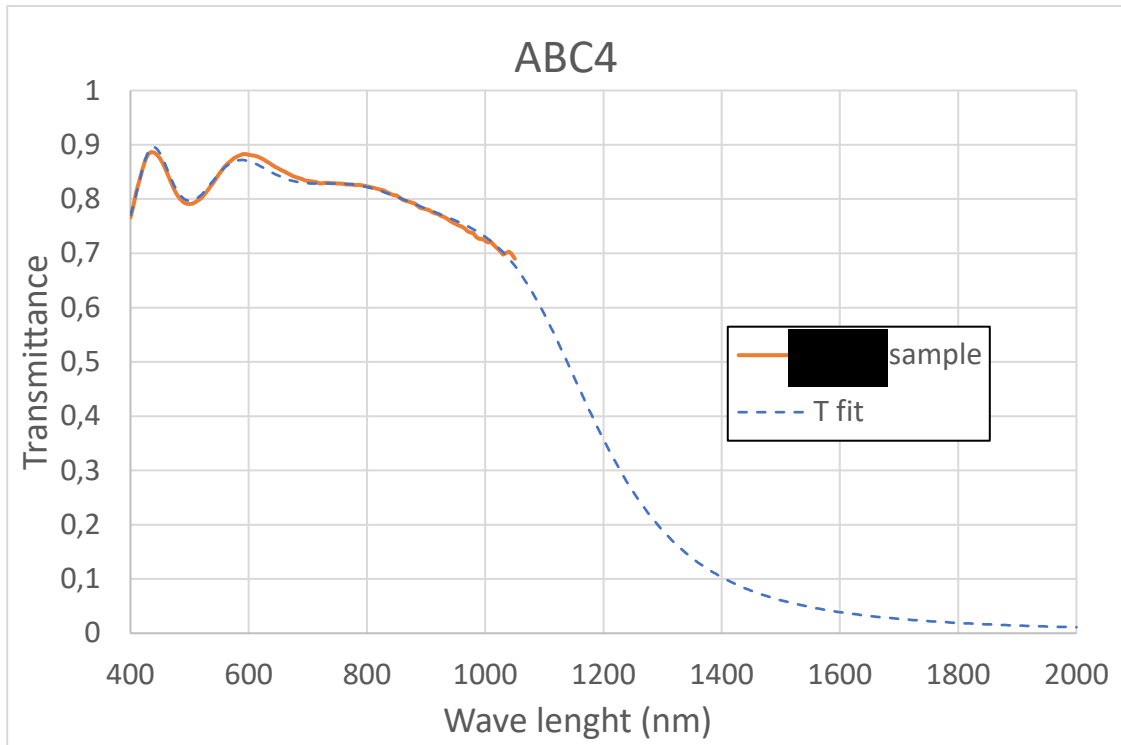


Fig 6 - In red the spectra measured and in blue the adjust we get from equations fitting for sample4 measured spectrum

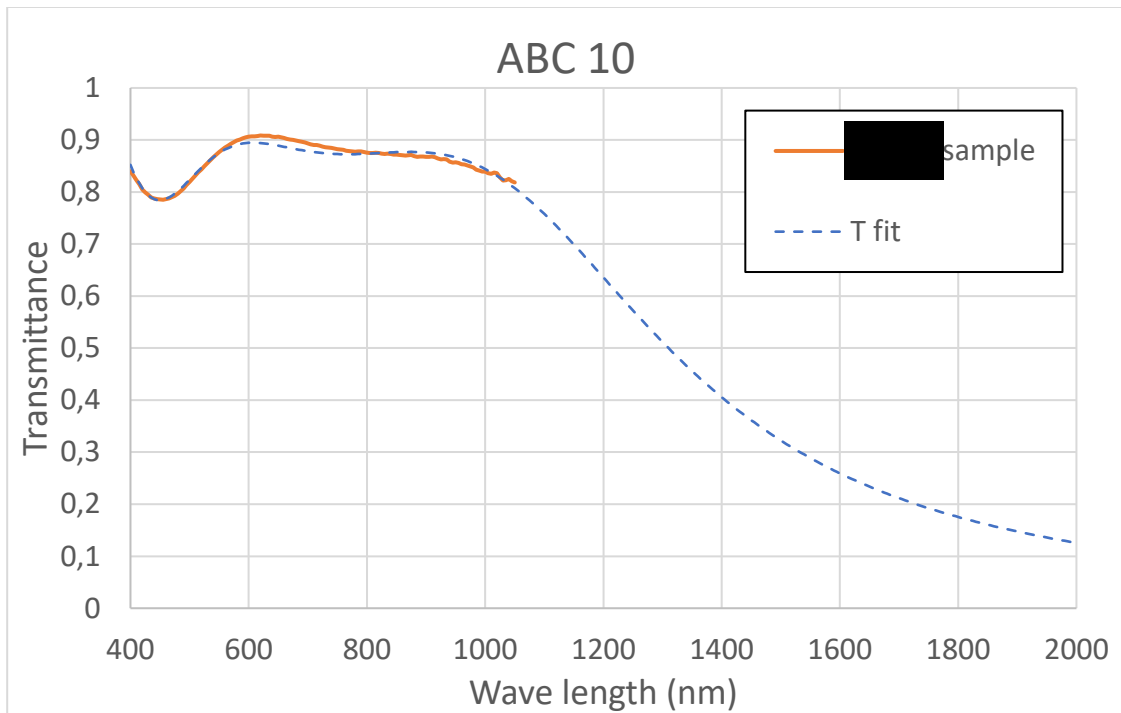


Fig 7 - In red the spectra measured and in blue the adjust we get from equations for sample10

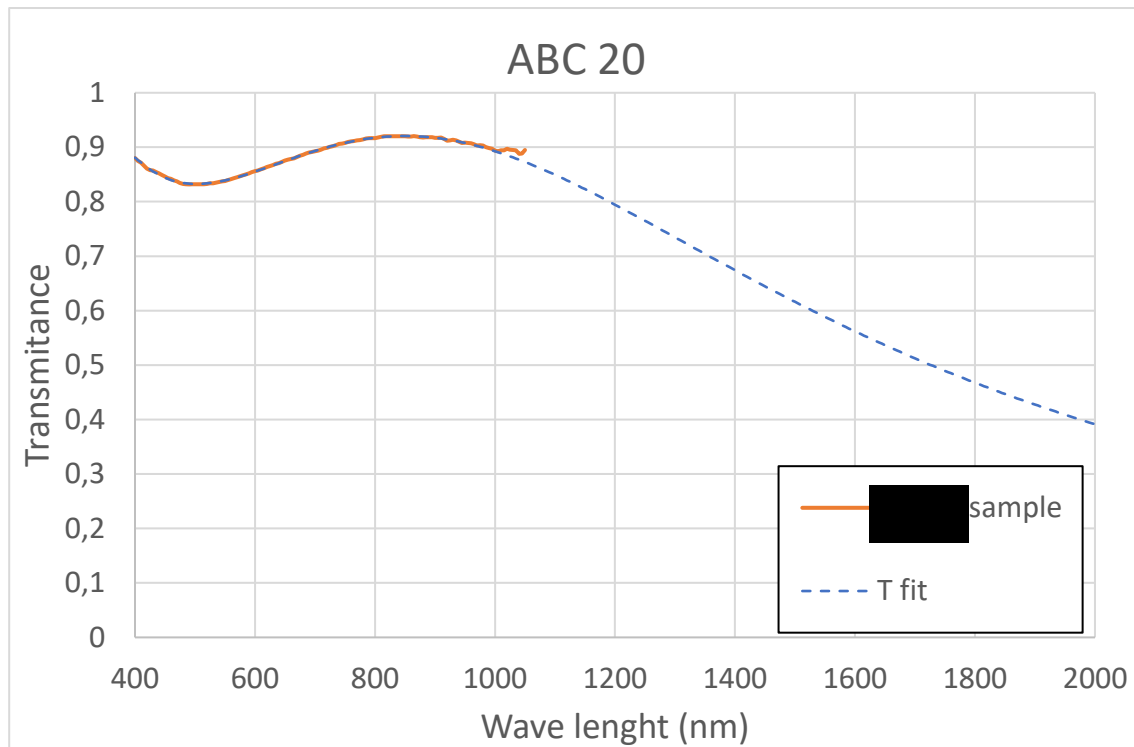


Fig 8 - In red the spectra measured and in blue the adjust we get from equations for sample20

These measurements are markedly valuable since we obtain almost all the information we need of the films just from the optical measurement.

From the data measured we obtain another value for the thickness that approaches the value obtained using the FIB technique. We also obtain the charge carrier density (N) and the mobility (μ); these two parameters determine the conductivity of the films. We collect all the parameters obtained from the optical data fitting in the following table:

sample	ϵ_{∞}	λ_0 (nm)	t (nm)	m^*e/m_e	N (cm^{-3})	μ ($\text{cm}^2/\text{V}\cdot\text{s}$)	σ (S/m)	ΣX^2
sample4	█	█	344	0,22	█	█	$7,54 \cdot 10^5$	0,0062
sample10	█	█	180	0,22	█	█	$7,53 \cdot 10^5$	0,0105
sample20	█	█	80	0,20	█	█	$7,57 \cdot 10^5$	0,0027

Table 4. parameters obtained from the fit we get from the data of each sample. ϵ_{∞} (high frequency dielectric constant), λ_0 (plasma wavelength), t (thickness), N (free carrier concentration), μ (mobility), σ (conductivity), ΣX^2 (chi square)

Chi square (ΣX^2) showed on the table is the square of the difference between measured data and computed data, this parameter gives us an idea of how accurate the fitted data to the measured data is. Here we can see that conductivity values are almost the same for the three samples, as we already thought. From this we can think that the measurements of the thickness by profilometer

are not as accurate as the transmission spectra measurements and the differences in thickness bring us errors when computing the conductivity.

4.2.5 Radar measurements

We are also interested in the behavior of the radar radiation in front of the commercial homogeneous film of conductive ABC. These measurements were done at the UPC as commented in chapter 2. In Both plot 1 and plot 2 we can see the three samples and a sample of the glass substrate with no ABC film on its surface named: ref. sample.

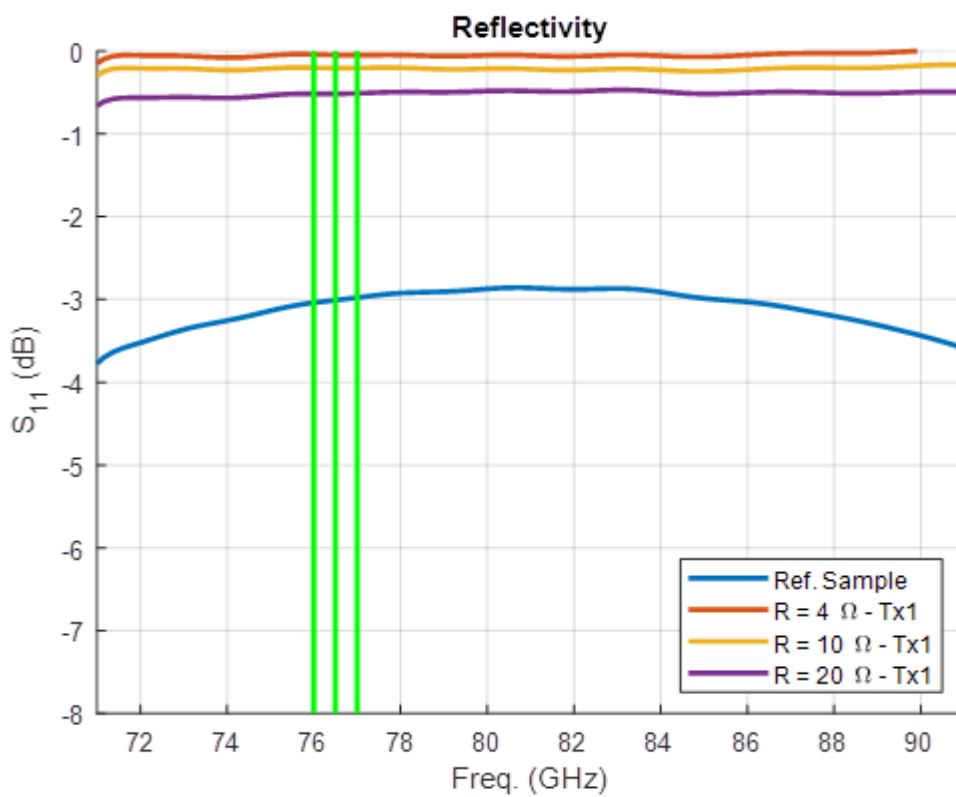


Fig 9. Shows us the Reflectivity of the samples 4, 10 and 20 and the reflectivity of a reference glass with no ABC film on its surface. Plot from UPC measurements

The first plot shows us the parameter S_{11} on the range of frequency from 71 GHz to 91 GHz. The parameter S_{11} measures the reflectivity of the sample, that means that S_{11} is how the electromagnetic radiation received by the receiver 1 has diminished with respect to the electromagnetic radiation emitted by the emitter 1, receiver 1 and emitter 1 are the same. S_{11} tells us how the signal has diminished when goes back to the emitter after being reflected by the sample. The blue line represents the reflectivity of the glass substrate with no ABC coated. From this plot we can see that all the radiation from the Radar is going back to the radar when a sample

with a homogeneous conductive film of ABC is in front. The differences between ABC coated samples are very small in terms of dB as we can see in the following table 5:

S11 measured in dB			
Sample	76,0 GHz	76,5 GHz	77,0 GHz
Ref	-3,03	-3,00	-2,98
Sample4	-0,04	-0,05	-0,05
Sample10	-0,20	-0,21	-0,20
SAmple20	-0,51	-0,52	-0,51

Table 5. Values of Reflectivity for samples with a homogeneous ABC thin film on its surfaces

The values of 76,0 GHz, 76,5 GHz and 77,0 GHz are shown and choose as a reference since are the working frequencies of a common car radar.

In the following plot we can see the values for S_{21} . S_{21} give us information about what the receiver2 gets from the emitter1 and so represents the attenuation produced on the radar signal due to the presence of our samples. Attenuation indicates us that practically no radiation gets the receptor as we can deduct from reflectivity results since all radiation is reflected.

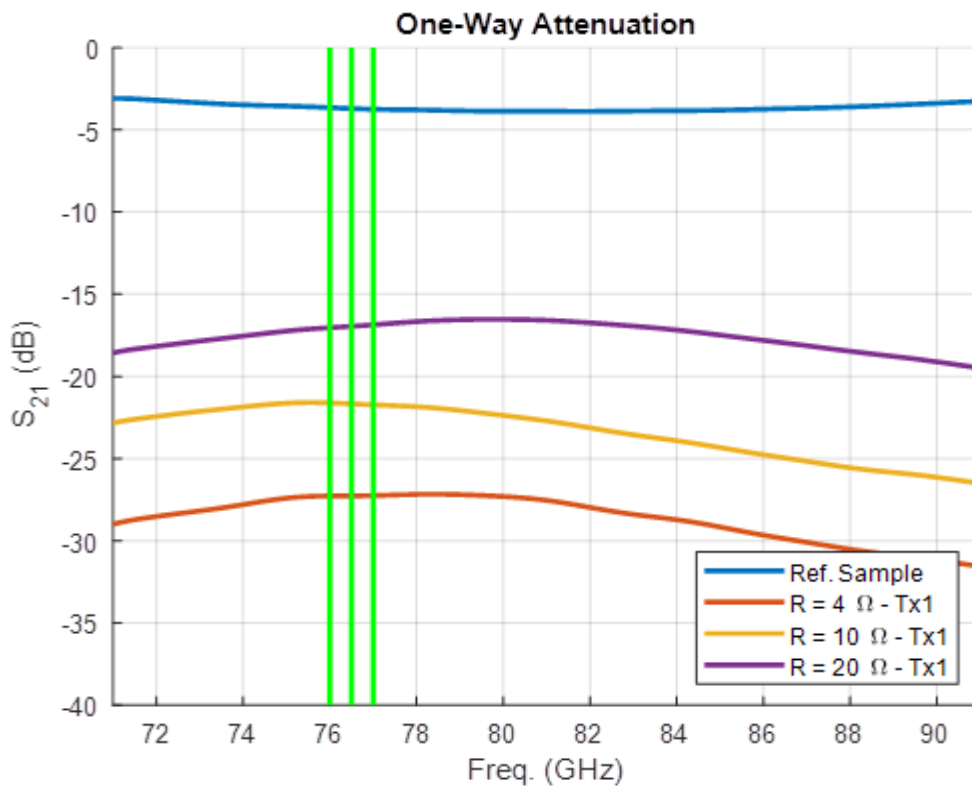


Fig 10 - Shows us the one way attenuation of the samples 4, 10 and 20 and the attenuation of a reference glass with no ABC film on its surface. Plots from UPC measurements

S21 measured in dB			
Sample	76,0 GHz	76,5 GHz	77,0 GHz
Ref	-3,75	-3,81	-3.89
Sample4	-27.17	-27.21	-27.25
Sample10	-21.55	-21.59	-21.61
Sample20	-17.19	-17.15	-17.11

Table 6. Values of Reflectivity for samples with a homogeneous ABC thin film on its surfaces

These values of attenuation give us the idea that we can consider that almost no radiation is arriving to the reciver2.

4.3 Simulations

In this section we use the electromagnetic simulation program to obtain information about our samples by comparing the results obtained from reflectivity and attenuation measurements to the results we will find with simulations.

To start we need to characterize the glass substrate in our simulation program. To do this, we design in our software a 3D rectangle of 1.1 mm thick and 10 cm x 11 cm of size, and we also define its electromagnetic properties. In the case of soda lime glass there exist some properties in a software library that we will use as initial conditions. Despite the software library data, we will need to adjust the electromagnetic parameters to adapt the results of our simulation to the measurements done at the UPC.

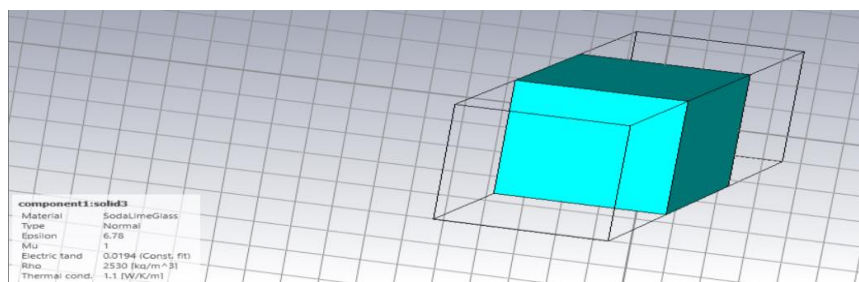


Fig 11 - Image of the substrate from the simulator software with the final electromagnetic parameters

On figure 11 we can see the design of the substrate in the simulation software. The electromagnetic parameters *permittivity* (ϵ) and *loss tangent* ($\tan d$) have been successively changed until the values of attenuation and reflection fits to the measurements done at the UPC. Finally, the parameters obtained were:

ϵ	$\tan d$
6.78	0.0194

Now we need to add the ABC homogeneous films of $3.9 \Omega\mu$, $7.9 \Omega\mu$ and $16.6 \Omega\mu$. So, we add a new 3D rectangle on the surface of the substrate. Here we need to use the electrical parameters measured in this chapter. Basically, we just need the conductivity and the thickness values to adjust the simulated structure. To do this we scan these two parameters between the values obtained previously in this chapter. As a result, the best values to adjust the simulation structure to the UPC attenuation measurement data are for the conductivities and thickness of those obtained from the transmission spectra measurements. So, taken the conductivity of Sample4 and just changing the value of the thickness of the film by the values obtained in transmission spectra we obtain a good matching between simulations and the attenuation and reflectivity measurements done at the UPC. We can see the film used at the simulation in red in the following image.

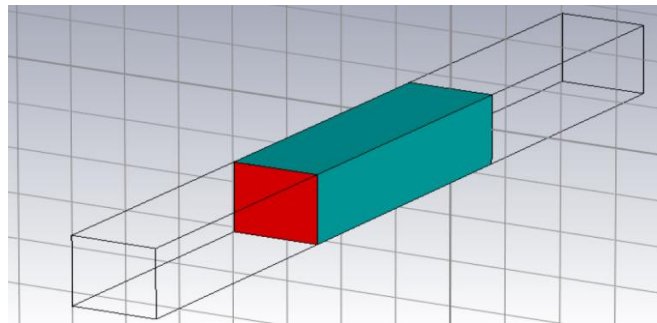


Fig 12 - Image of the substrate (turquoise) with a homogeneous film of ABC (red) on its surface

Results of the simulations are plotted in figure 13 and figure 14. figures 13 and 14 shows the Reflectivity and Attenuation of our simulated samples compared with the measurements made at the UPC in the range of frequency between 71 GHz to 81 GHz, the region we are interested on.

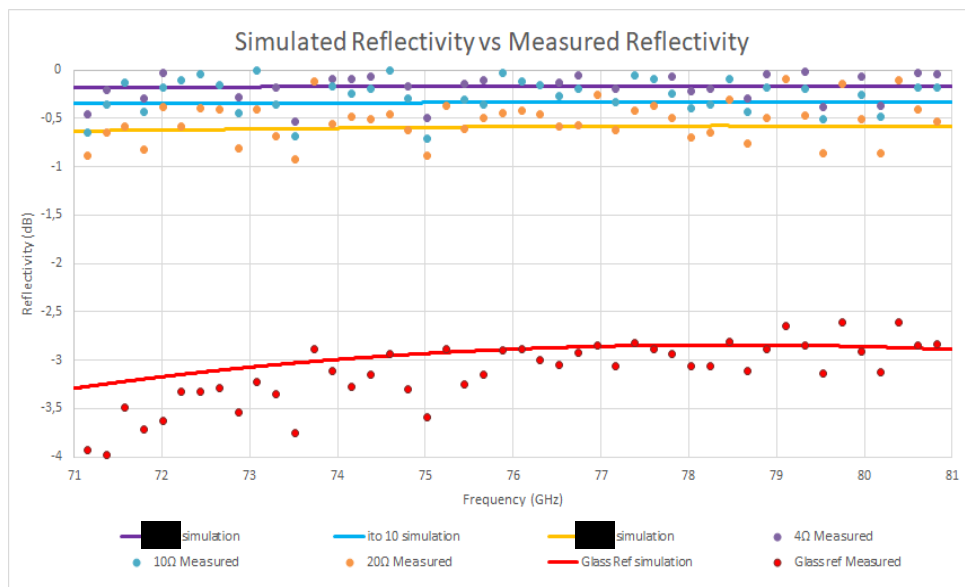


Fig 13 - Comparison between the data obtained from simulation and the data obtained by measurement. The points represent each measurement done in the range of 71 GHz and 81 GHz. Solid lines are the data obtained from the simulation.

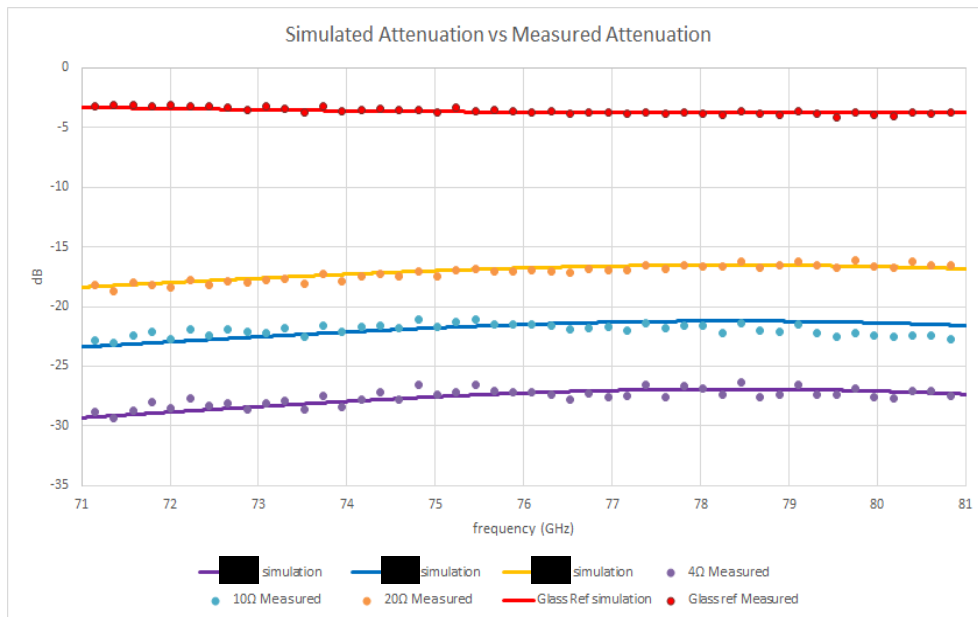


Fig 14 - Comparison between the data obtained from simulation and the data obtained by measurement. The points represent each measurement done in the range of 71 GHz and 81 GHz. Solid lines are the data obtained from the simulation.

We can see from figure 14 that simulations are in very good agreement with measurements. In figure 13 we can see that measurements are slightly dispersed, but they have a clear behavior for each of the samples. In this case simulation results show a behavior that approaches the average of these dispersions. This dispersion in Reflectivity results are consequences of our proximity to a total reflection situation and this makes small changes to have an important effect to the measurements. Despite this we can accept the results from simulations since it gives us a very good idea of the Attenuation and Reflectivity of the samples.

4.4 Summary and comments

In this chapter we have studied and characterized our basic commercial sample of 3.9Ω that we will use in the next chapter to develop the wires printed circuit as a heating system. We also have also studied the commercial samples of 7.9Ω and 16.6Ω to compare and have a clearer idea of how radar radiation is affected by a homogeneous thin film of a Transparent Conductive Oxide. We have seen different techniques to extract information of thin films and we introduced the electromagnetic simulations that will help us in the next chapter.

We also have seen, in contrast with chapter 3, [REDACTED]
[REDACTED]
[REDACTED]
[REDACTED]

Chapter 5

ABC etched circuit

In this chapter we study the possibility to create an ABC etched circuit as a heater. [REDACTED]

[REDACTED]

[REDACTED]

[REDACTED]

[REDACTED]

We will adapt the ABC coating to the common idea of the twisted wire as a heater for our Radome. So, improving two important characteristics: the aesthetics, since ABC is not visible, and its efficiency since heat will be produced just about 20 microns of distance from ice and water surface, instead of several tens of millimeters, in this way less heat will be lost during its way to the surface. The design of the ABC twisted circuit and how to develop these wires will be the two main points of this chapter.

In this chapter we decided to use glass as a substrate to avoid the compatibility problems between ABC and PC, this way we would not have samples fissured during heating tests. So, in this chapter we will see the development of an ABC etched circuit on glass substrate, the development of this technology on PC substrate will be later done in the company after we have the results on glass.

5.1 Introduction

When regarding the patents of other Radomes (state of the art, chapter 1), we see that all heating systems are circuits of one, two or three long wires twisted and embedded on a plastic part describing a circuit with many turns. The separation between two consecutive wires use to be between 4 and 5 mm and this is for some reasons:

- Aesthetics, more separation implies less density of wires in front of the logo of the company.
- Attenuation, less density of wires implies less perturbation of the electromagnetic waves from the radar. Furthermore, this 4 or 5 mm are distances larger than the wavelength of the radar radiation that is 3.92 mm, which implies less perturbation too.
- Homogeneity, we would like a homogeneous distribution of the heat over the entire of the surface of the Radome, but a high separation between the wires will bring to higher

temperature differences between different points of the surface of the Radome. This point is clearly on the contrary to the previous mentioned points.

So, 4 or 5 mm are distances that OEMs consider that keeps an equilibrium between these three commented points.

To have an idea of how these separations and polarization can affect to the attenuation of the heating system we performed a test using a simple design of metal wires. We can see in table 1 the attenuation of a set of wires placed in parallel with a separation of 4 and 5 mm glued on a standard polycarbonate substrate. The values of the frequency are the common values used in car radars. The attenuation showed is just the attenuation of the set of wires, because the attenuation produced by the substrate has been subtracted. The measurements are made, at the UPC, by placing the wires parallel and perpendicular to the radiation of a simulated radar. We can see that there is not much difference between 4 and 5 mm of wires separation, but it does exist a clear difference between the orientation of the wires with respect to the polarization of the radar radiation. In the table 1 and figure 1 the H means that the set of wires is placed perpendicular with respect of the radar polarization of the and V that the orientation is parallel to the radar polarization. Fig.1 shows us the behavior of the attenuation of the radar radiation in the range of frequencies that we are interested to. (fils is the Catalan word for wires that we used on the table since it was used when doing the plot and measurements)

	76.0 GHz	76.5 GHz	77.0 GHz
Fils H; 4 mm	-0.53 dB	-0.61 dB	-0.68 dB
Fils H; 5 mm	-0.51 dB	-0.57 dB	-0.63 dB
Fils V; 4 mm	-1.66 dB	-1.74 dB	-1.81 dB
Fils V; 5 mm	-1.78 dB	-1.85 dB	-1.91 dB

Table 1. different values of attenuation of the wire set for 4mm and 5mm distance between them in parallel and perpendicular polarization.

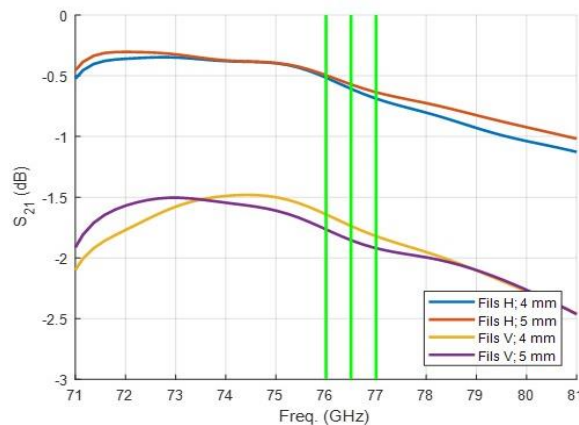


Fig. 1. behaviour of the electromagnetic radiation from 71 to 81 GHz through the set of wires in front.

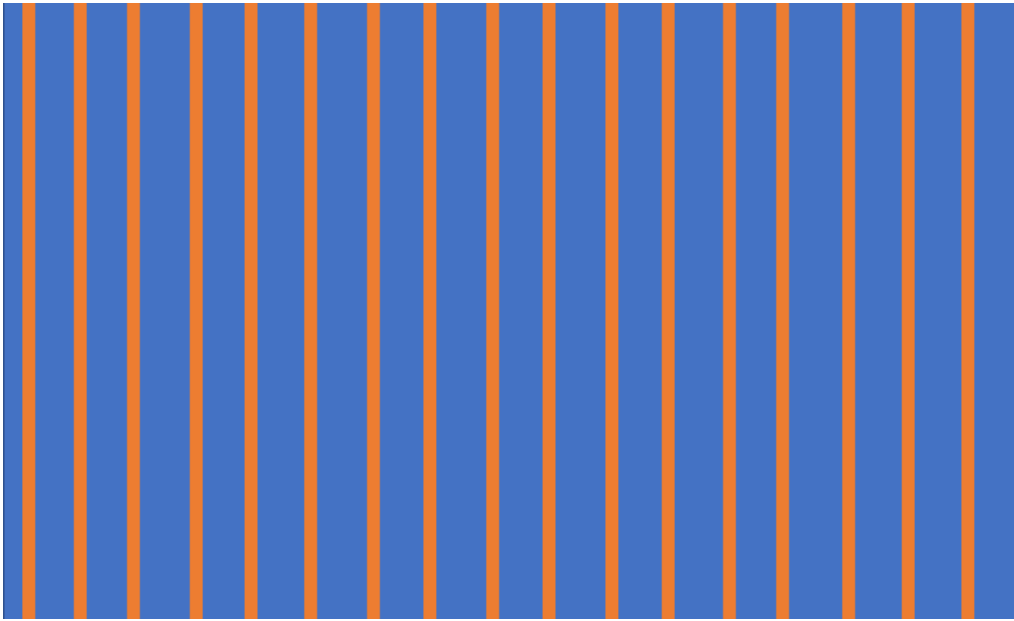


Fig. 2 distribution of the wires grid in this test and the distribution we will use along this chapter

Fig 2 shows the simple design we have used in this test. The wires used here had a diameter of 0.1 mm, in contrast, the copper wires used in a heating system of a Radome have a diameter around 0.05 mm, they are half diameter than the used in this test, attenuation will be slightly smaller, but the behavior related to polarization will be the same. This test gives us an idea of the difference in attenuation produced by a set of copper of wires depending on the orientation with respect of the radar polarization.

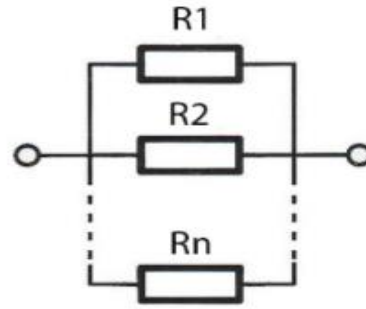
5.1.1 Designed circuit

Figure 2 is a scheme of the distribution of wires used in this preliminary test to see the effect of the polarization, but it will be also the main circuit we will use in this chapter to distribute ABC wires since it is the distribution that minimize the resistance of the circuit and guarantees a homogeneous distribution of heating.

Along the next pages, we will write “wires” for the linear conducting stripes etched on the ABC coating

For our trials, the wires of the heating systems will be also connected each other using a copper foil on upper and bottom sides of the samples that will ensure a good distribution of the electricity in the heating system. As the conductivity for copper foil is 100 times higher than the conductivity of the ABC wires, the current will be homogeneously distributed to all wires. The resistance of the set of wires can be easily written using:

$$\sum_{i=1}^n \frac{1}{R_i} = \frac{1}{R_s}$$



Scheme of n resistances Connected in parallel

Where R_i is the resistance of each i wire and R_s is the resistance of all the set of parallel wires. This way as many wires we connect less resistance will have the full set of wires. This is a difference from other heating systems with just one, two or three thin metal long wires twisted over all the surface of the Radome. Here, with a set of parallel ABC wires, the resistance of the heating system will reduce, as it is necessary because the resistivity of ABC is 100 times higher than metals like copper used in common Radomes. This will be also convenient, since if a wire is broken, the heating system continues to work with all the other wires, and it is an advantage compared with common metal wired Radomes.

5.2 Preliminary test

To have an idea of the behavior of the ABC wires and the attenuation of the system, we made many samples with different width of wires and separation between them. [REDACTED]

5.2.1 Samples

To proceed, we need to choose appropriate samples for our purpose and an appropriate method to develop the wires. The samples need to have some predefined characteristics:

- Minimum ABC sheet resistance, between 2- and 5-Ohms square, since the resistance of the circuit will be always higher than the sheet resistance of the non-etched coating. We need to avoid that the resistance of the circuit overpasses the limit of 23.6 Ω since it is the resistance that produces the power computed in chapter 1 for an applied voltage of 24 V. And we need to approach as much as we can to the value of 5.9 Ω since it is the

resistance that produces the right power computed in chapter 1 for an applied voltage of 12 V.

- The samples must be on glass substrate to avoid the ABC cracking problems we found in chapter 3.
- We need to be able to choose the size of the samples.

The ABC foil samples from [REDACTED] analyzed and characterized in Chapter 4, will allow us to choose a size of the ABC area similar to that of a standard Radome and they have a sheet resistance of 4Ω that is smaller than 5.9Ω that will allow us to make a realistic sample with the right low circuit resistance.

5.2.2 ABC etching

As a method to build the wires we decided to use etching by laser since it gives us the chance to prepare many different samples in a short period of time. Photolithography was also considered but this technique needs a mask for each different sample we want to do, and this takes a lot of time and it is not a versatile system at this stage. Laser etching gives us the chance to modify the parameters for each sample at any moment and the sample can be done easily in some minutes or seconds. This system is versatile, but it introduces some factors that could damage the sample and would slightly change the results we could obtain as we will comment later.

The laser used was from Laser Marking System SL (LMS) a company which already collaborates with Zanini and it is located in Vic so, we can etch the samples by ourselves in its facilities. The laser used is a diode pumped Nd:YAG from Rofin. We will not get into details about the laser, but we will do some comments about it. This kind of lasers are IR solid-state lasers that pump a solid gain medium, in our case a neodymium doped YAG crystal (neodymium-doped yttrium aluminum garnet $\text{Nd:Y}_3\text{Al}_5\text{O}_{12}$), with a laser diode. DPSSLs (Diode Pumped Solid State Lasers) have advantages in compactness and efficiency over other older types of Nd:YAG lasers which are optically pumped by using a flashtube or laser diodes. These are one of the most common types of and are etching lasers used for many different Zanini applications. Nd:YAG lasers typically emit light with a wavelength of 1064 nm, in the infrared.[5] However, there are also transitions near 946, 1120, 1320, and 1440 nm. Nd:YAG lasers can operate in both pulsed and continuous mode. In our case the laser operates in pulsed mode since we must specify the frequency of the pulses and the speed of the movement of the laser and adjust both to have a clear and defined etching of the wire.



Fig 3 the laser used at the Laser Marking Systems facilities

5.2.3 Tests

We have to define two variables for each sample: the width of wire stripe (WW) and the separation between wires (WS [REDACTED])

[REDACTED] In this preliminary test 23 samples were laser etched at the Facilities of LMS. The characterization of the samples was done at the UB and at the UPC. At the UB we checked if the sizes of the wires were what we planned to be, by using the confocal microscopy and the profilometer. We found that the separations used to be bigger than we planned, and we considered that this was because of the expansion caused by the heat produced by the laser when [REDACTED]. The resistance of each sample was measured using the HandMade tool used in chapter 3 and commented in chapter 2. The attenuation at 76.5 GHz was measured at the UPC facilities as commented in chapter 2. The wires were placed in perpendicular orientation with respect of the radar polarization for all the attenuation measurements. The results are shown in fig 4 and 5.

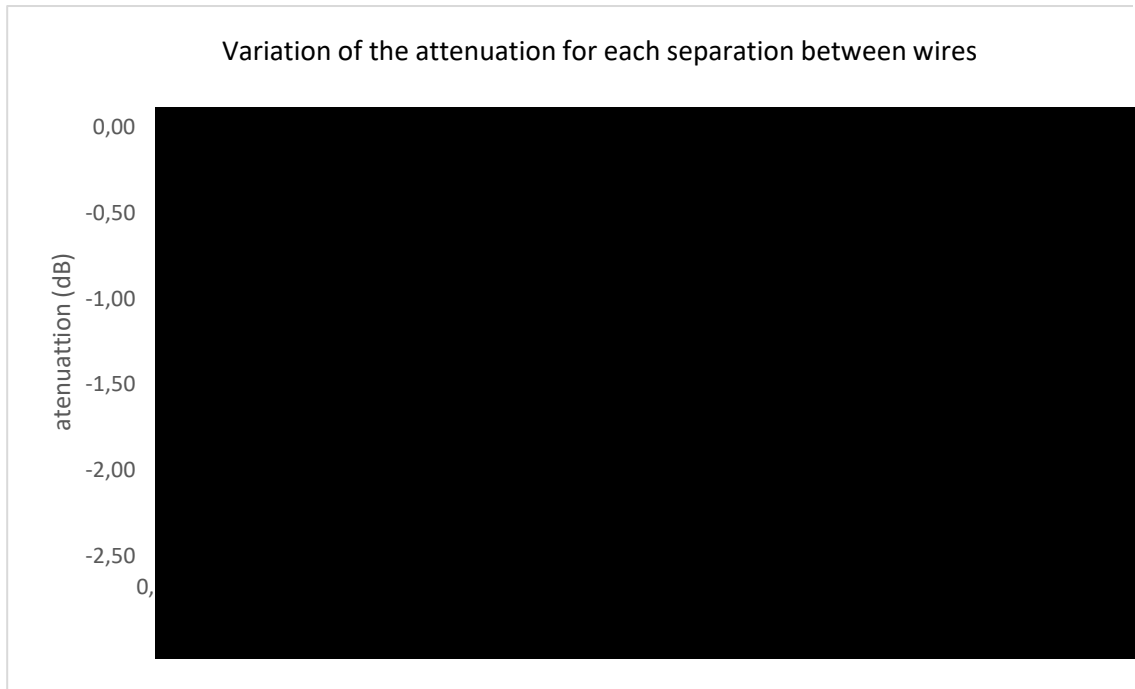


Fig 4 atenuation of 12 samples. The samples were classified by the separation between wires

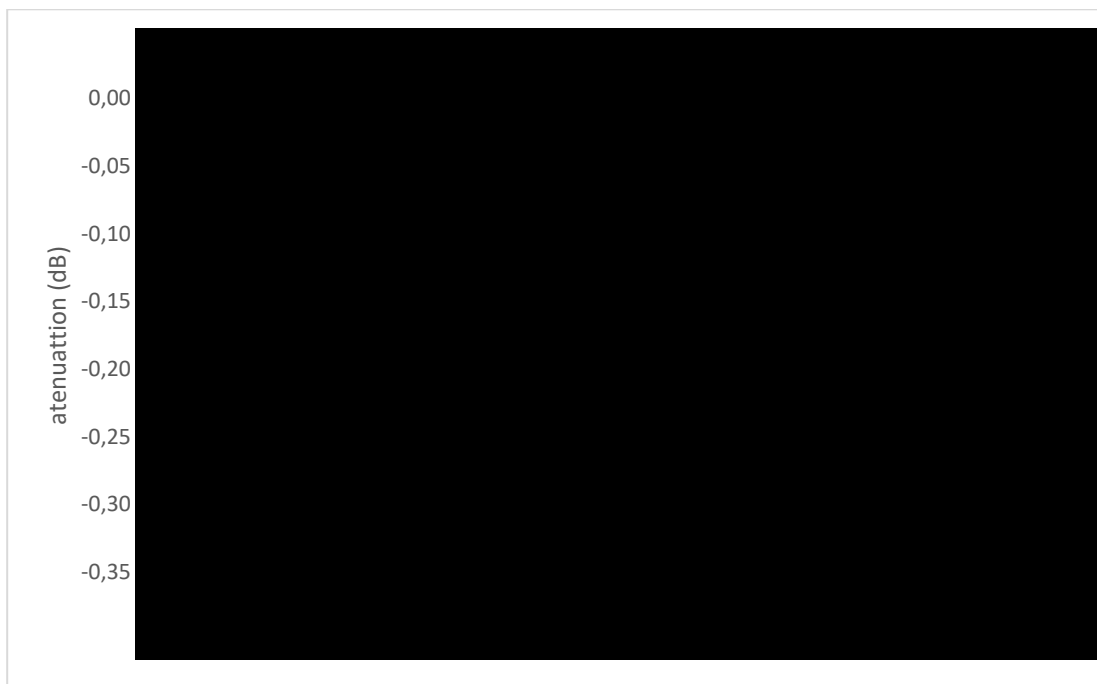


Fig 5. atenuation of the 9 samples

In fig 4 the atenuation of samples with different wire separations (WS) is represented in different colors. We can see that the tendency of the atenuation is the same independently of the WS. The atenuation of the samples tends to diminish as the width of the wires (WW) is reduced. So, we could say that as the whole surface of ABC is reduced the atenuation is also reduced, which is something we could expect.

[REDACTED]

5.3 Optimization of samples and results

[REDACTED]. To do this we need to study the expansion of the wire respect to the planned width produced by the laser heating during the etching process. We will also use computer simulations to design the best configuration of wires to reduce the attenuation but considering the limitations of WS imposed by the laser that we will comment later in this section.

5.3.1 Laser expansion

To make the ABC wires we started etching parallel lines across the film surface that separates parallel stripes of ABC surface, these regions play the role of ABC wires. The trace of the laser etching it is always a straight line made by laser spots, so to etch a rectangle the laser etches a straight line next to the other since it gets the width of WS. This implies that the laser spends a lot of time on the same region of the thin film, this heats the region of the surface causing a burr on the edges of the etched lines that produces a rectangle bigger than we expected. We can see the rectangles and the burr caused by the laser in images 2, 3, 4 and 5, these images correspond to the sample Y32 that we will see in detail later in this chapter.

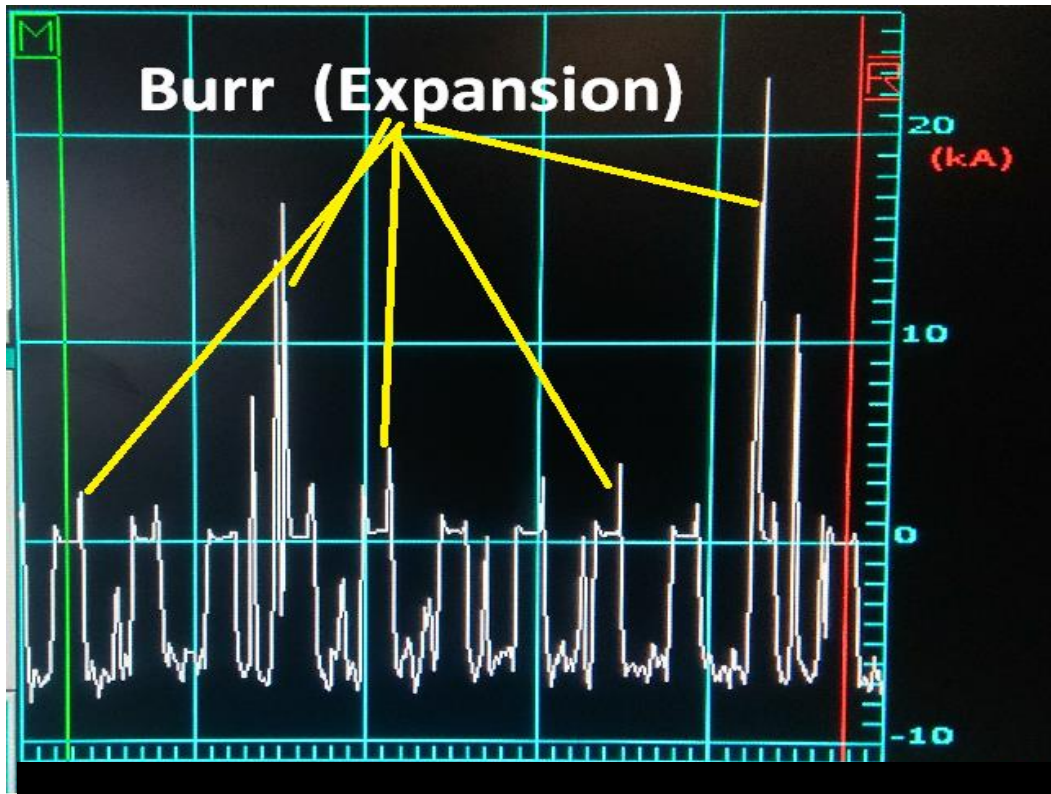


Fig 6 shows a profilometer measurement of the ABC wires done by laser etching

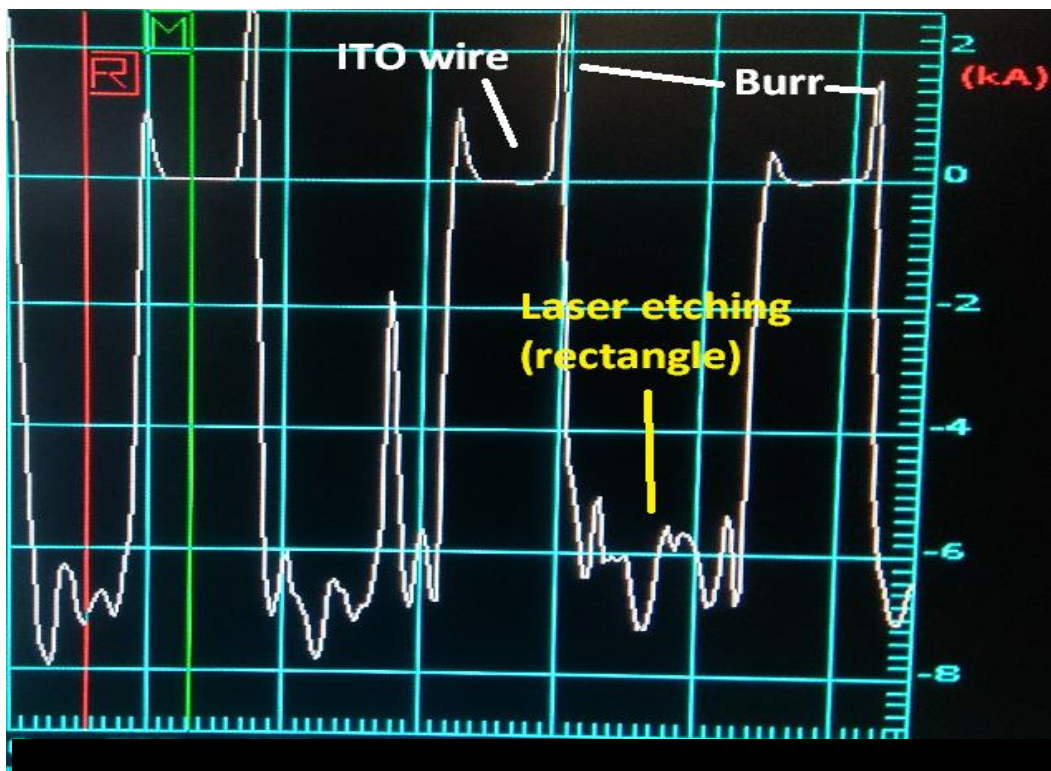


Fig 7 is a zoom of a region of ABC wires of Img2. We can also see the valleys produced by the laser on the ABC film. The scale of the Y axes is not correct by a factor of 2.26 in this case, this is a problem we solve later during the thesis, but we need to consider at this point.

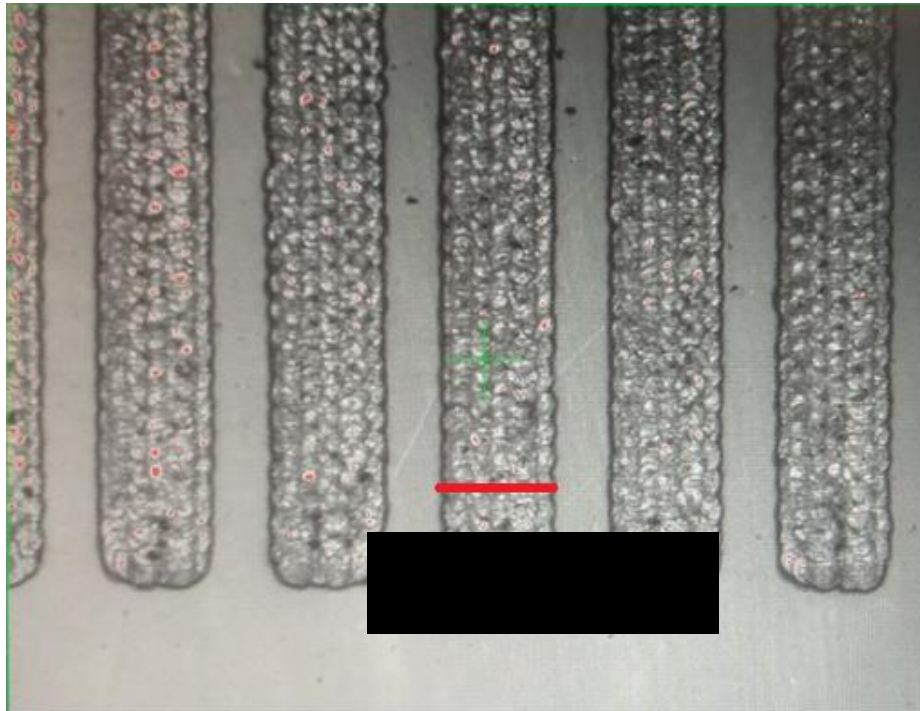


Fig 8 shows the rectangles produced by laser etching.

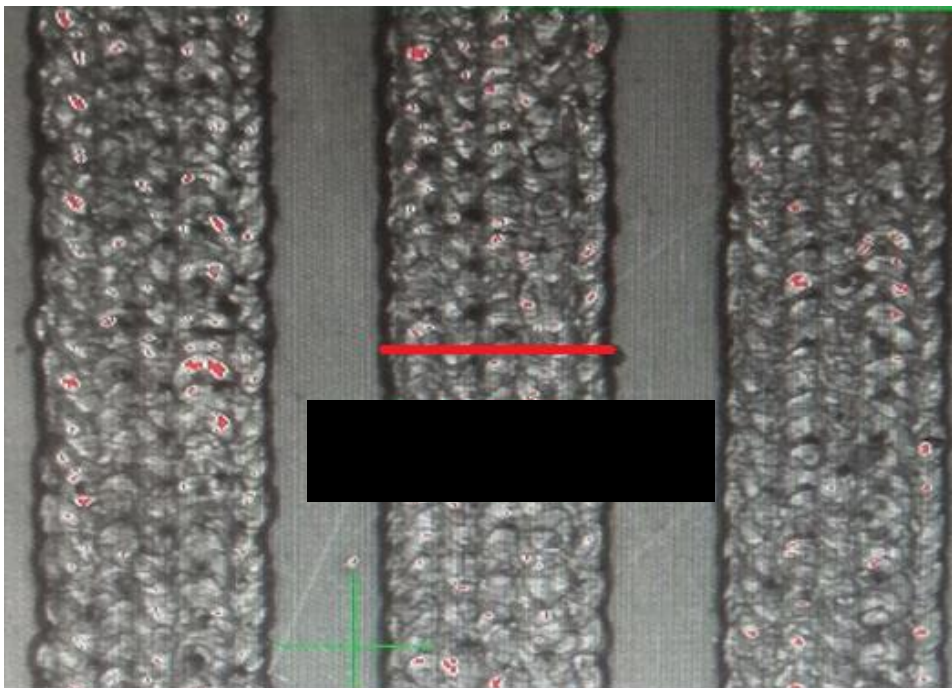


Fig 9 zoom of a region of figure 8 we can easily see that the edges of the rectangle are not straight lines. Images obtained the Confocal Microscope.

As we commented laser causes the expansion of the material during the etching process, so the WS of plot 2 are not exactly 2, 4 or 5, the WS varies from 2.04 to 2.14 for 2 mm, from 4.07 to 4.70 for 4 mm and from 5.18 to 5.09 for 5 mm. This variation depends mainly on the laser intensity used and the velocity of the laser scan, but we also see small variations depending on the particular WW.

The study of the expansion could contribute in two ways:

- We could predict the expansion of the laser and consider it in the design in order to control the WS and the WW.



To study the expansion (E) and see [redacted] we decided to etch some samples using different intensities (Amperes) and different velocities of the laser, the machine of Rofin uses as units of velocity meters/min, so, we will keep these units when talking about the laser velocity for practicality. The *path etched by the laser* (LP) will define WS and the difference between this WS and *the distance between two consecutive lines* (d2) will define the WW (1). See figure 10. In Fig. 11 we can see the results and the evolution of the WS when changing the speed of the laser for a fixed current intensity with three different intensities. The shooting frequency of blinking of the laser was set at 5000 Hz, at this frequency we guarantee that the laser spots overlapped each other for the fastest speed of the laser we used (1300 m/min) and we had a continuous line with no gaps in it.

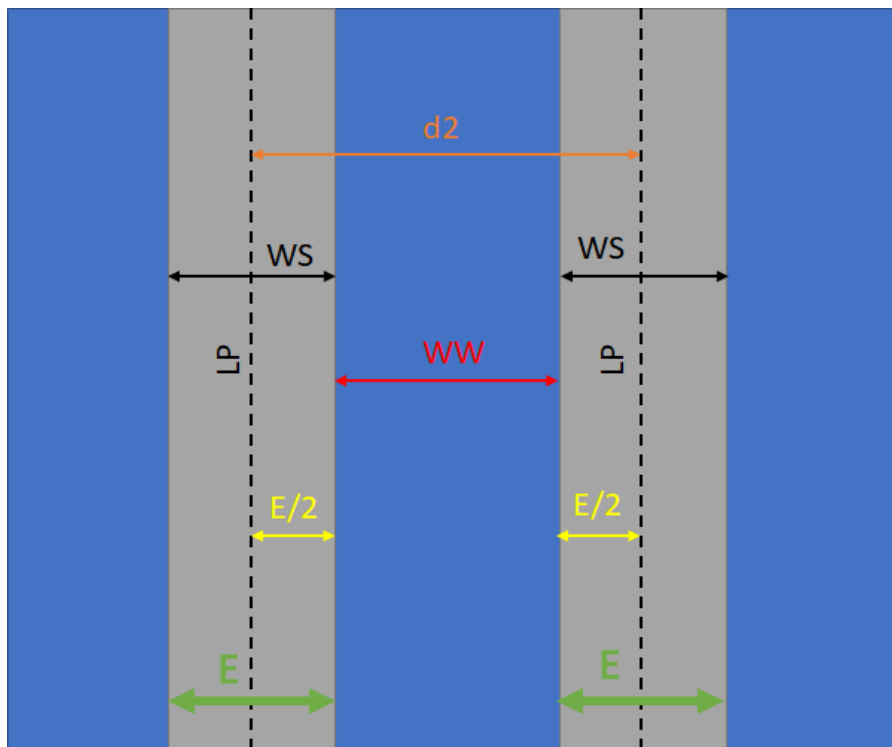


Fig 10. We can see different parameters we need to consider ensuring the design of our circuit.

$$WW = d2 - \left(\frac{E}{2} + \frac{E}{2}\right) = d2 - E \quad (1)$$

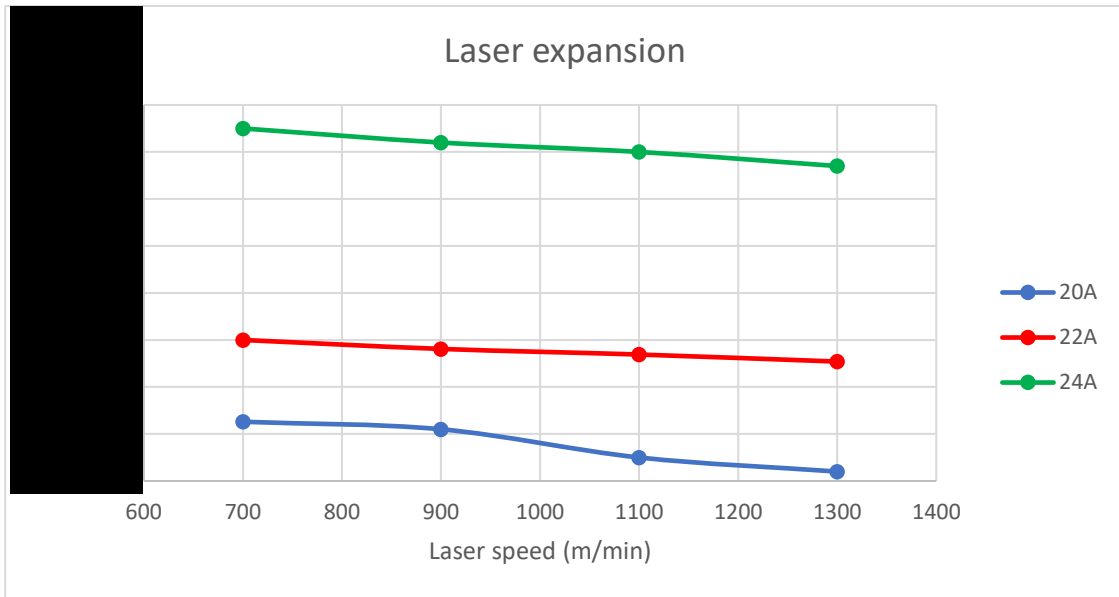


Figure 11. Blue line indicates the evolution of WW for an intensity of the laser of 20A, the Red line for an intensity of 22A and the green line for an intensity of 24A. we can see how WW is reduced when increasing the speed of the laser and it rises when the intensity of the laser rise

Each point of Fig. 11 is an average of six different samples made using the same conditions, the variations of WS between each sample were ± 0.005 mm. In figure 11 we can see clearly that the intensity of the laser is the most important factor for the expansion of the WW. The speed of the laser has also to be considered when designing the circuit, but it is not a key factor.

[REDACTED]

[REDACTED]

On figure 12 we can see clearly that the line is made by consecutive laser circles that are the laser spots. We can observe that the geometric shape of a rectangle is almost vanished. Here we have a rounded tip on the bottom and top side of the line, and the edges have a wave shape representing the overlapping of the laser spots. These differences in the geometry and the expansion of the WW will cause differences between the parameters measured on the real samples and the parameters computed theoretically and from simulations.

5.3.2 Simulations

In this section we use CST studio suite 2019 to perform electromagnetic simulations of our circuit design to help us to find configurations of wires that minimize the radar attenuation and the electrical resistance of our heating system. These simulations are useful to reduce the number of samples we should prepare and characterize to optimize our design and find a useful configuration for our circuit.

To perform the simulation, we will use the parameters found in the previous chapter for sample4 but in this case instead of a homogeneous thin film we will have our configuration of wires as we can see in figure 13.

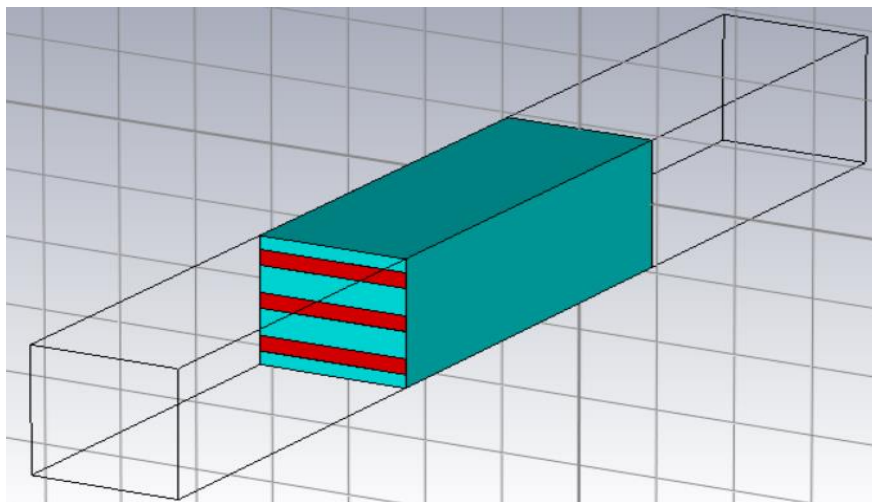


Fig 13. Design of our printed circuit on its glass substrate used to perform the simulations in blue the glass substrate and in red the ABC wires

Because of the boundary condition we applied on the simulation we just need to define a unit cell of our design and the simulation software will extend the results to samples that approaches a full size of the circuit. Obviously, the wires are oriented perpendicular to the electromagnetic radiation coming from the radar, in this case the wires are horizontal placed, and the radar radiation is vertical polarized.

We perform simulations [REDACTED] so for each WW we will obtain 10 configurations of WS, this means that 100 configurations of the etched circuit are simulated and will help us to understand the behavior of the attenuation due to the ABC circuit.

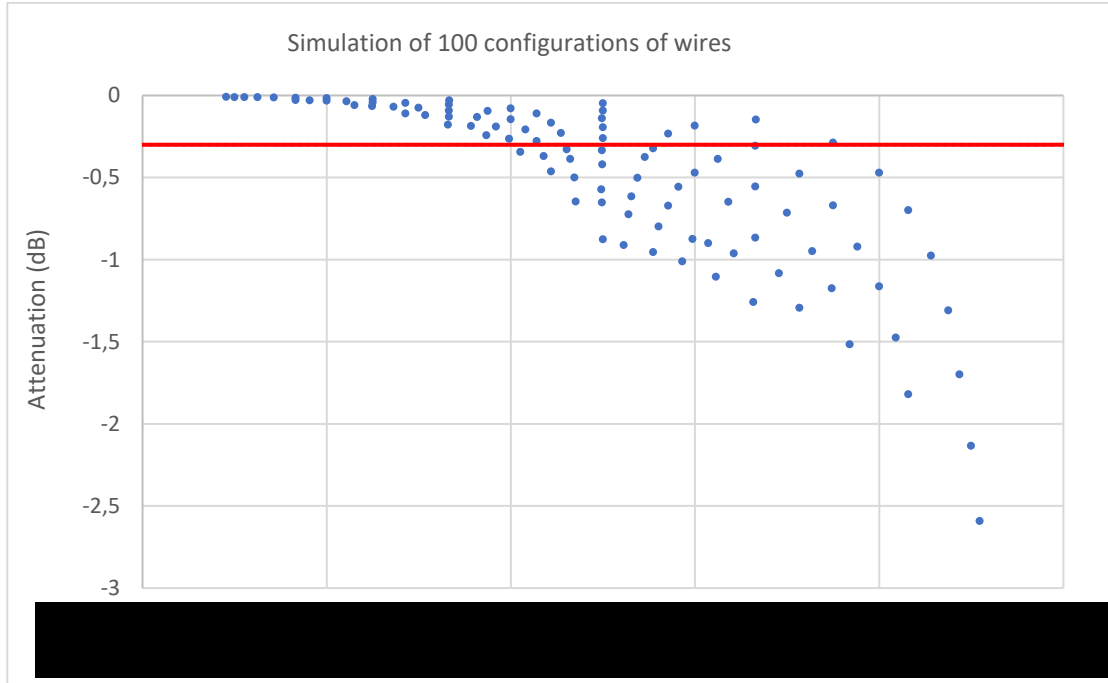


Fig14. Each point represents a configuration of WW and WS. the red line represents the limit of attenuation requirements we have for a one-way measurement. [REDACTED]

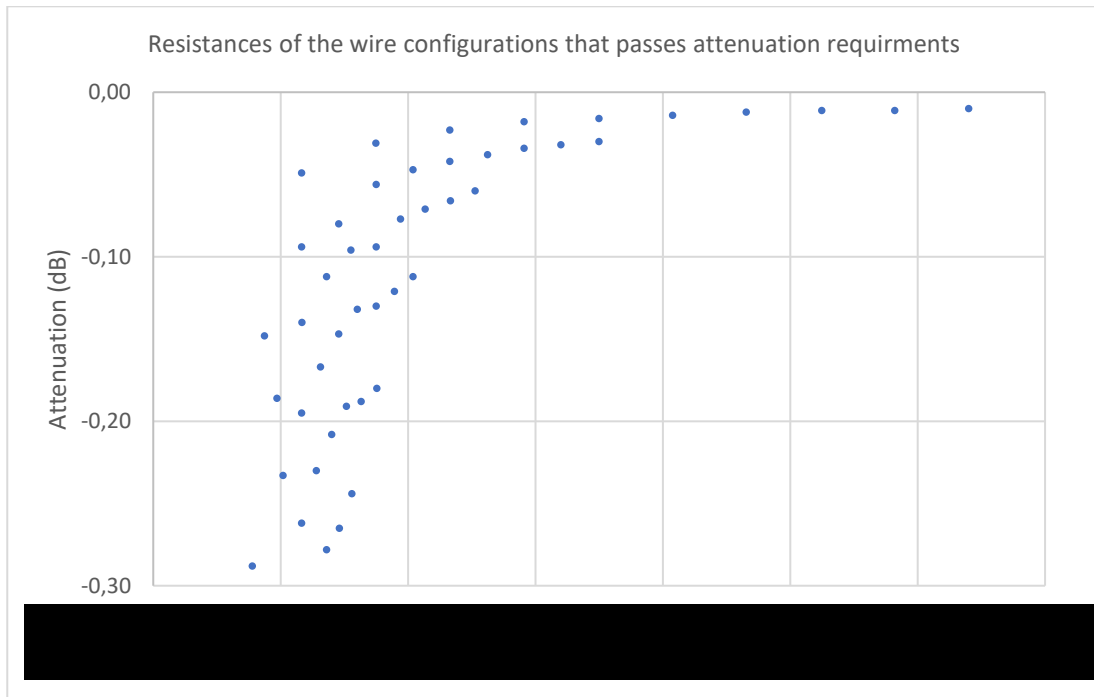


Fig15. Each point represents a configuration of WW and WS that passes the attenuation requirements. [REDACTED]

[REDACTED]

[REDACTED] The red line divides the plot in two parts, in the upper part there are the samples that passes the requirements of attenuation and in the bottom part there are the samples that does not pass the attenuation requirements. Figure 15 shows us the attenuation of the samples that passes the attenuation requirements related to the resistance of the circuit created after etching. This circuit resistance is theoretical since we obtained it considering the number of wires its WW and its conductivity. [REDACTED]

[REDACTED]

[REDACTED]

[REDACTED]

5.4 Real samples results

In this section we will study the attenuation of the radar radiation produced by the samples we made after simulations. Of course, just some of the samples simulated have been reproduced considering the results obtained from simulations and the limitations of the fabrication procedure.

[REDACTED]

[REDACTED]

[REDACTED]

[REDACTED] This means that all configurations simulated that needed a smaller WS were discarded.

The samples were etched at LMS in Vic and we measured the attenuation of the samples at the UPC as commented in chapter 2. We placed all the samples on the same way, so, the ABC wires are perpendicular to the polarization of the electromagnetic radiation of the radar. Here we will see the results for both kind of samples we have done, those made with rectangles and those made by single lines. As we did in chapter 3, the results of attenuation are just the attenuation of the printed circuit because we have subtracted the contribution of the glass substrate.

We applied etching by laser to samples of 3.9Ω using the circuit design geometry reproduced at the beginning of this chapter. The samples commented here made by rectangles are called Y22 and Y32, and the samples made by laser lines are called 015p22v1300, 015p22v1100, 015p20v1100 and 012p20v1100. [REDACTED]

[REDACTED]

[REDACTED]

[REDACTED] Three of these samples passes

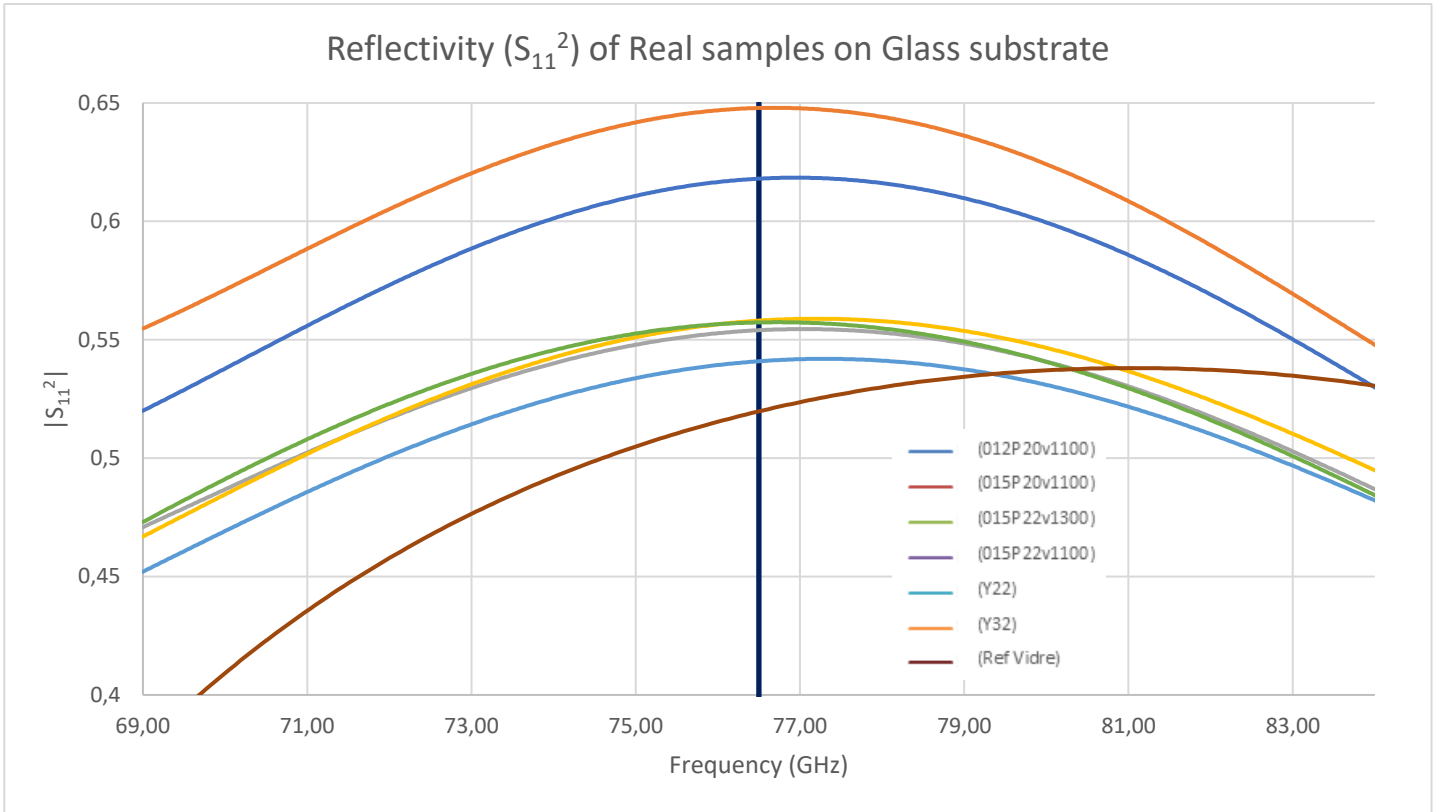


Fig 16. Reflectivity of the Real samples we have made. We can compare the samples with the glass substrate ABC free in brown (Ref Vidre)

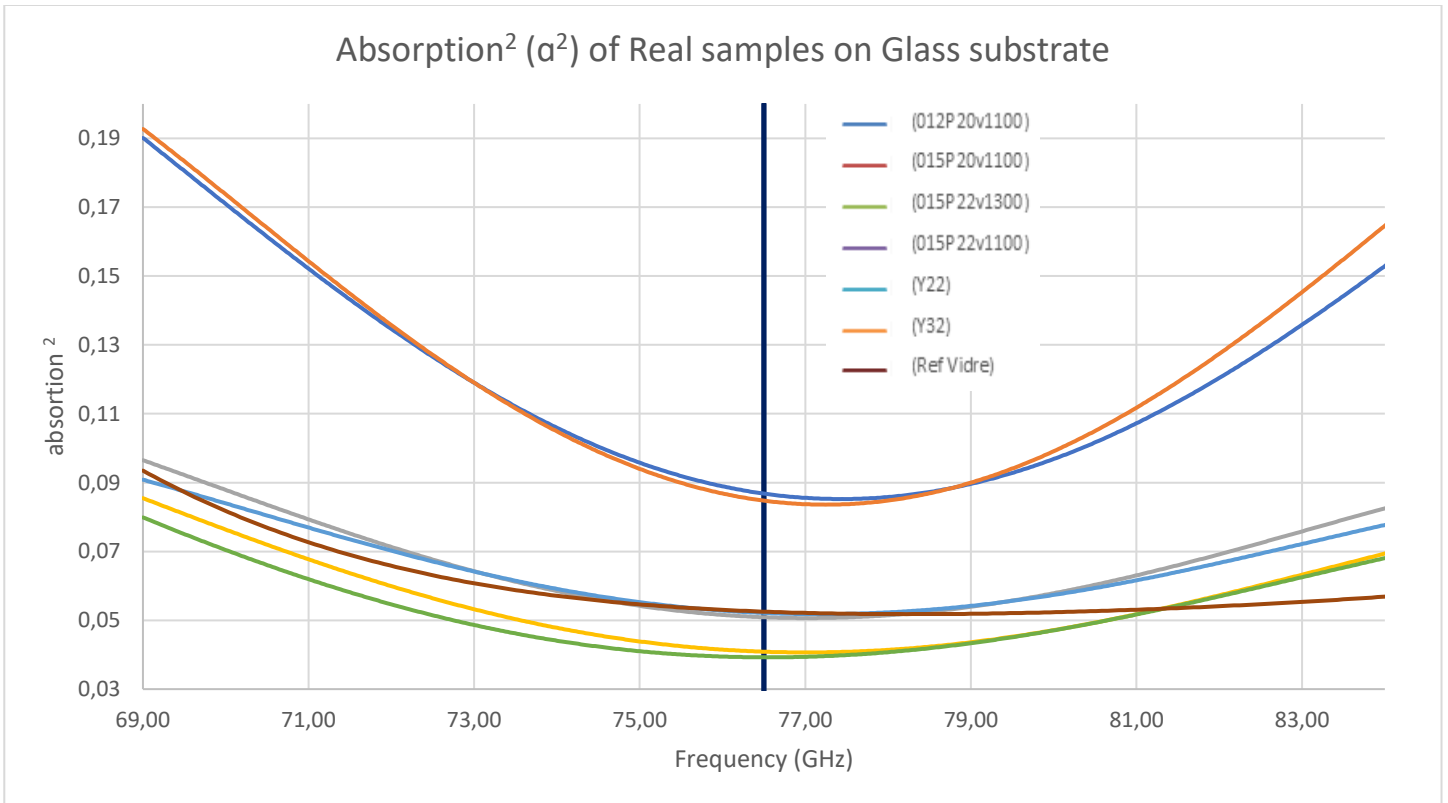


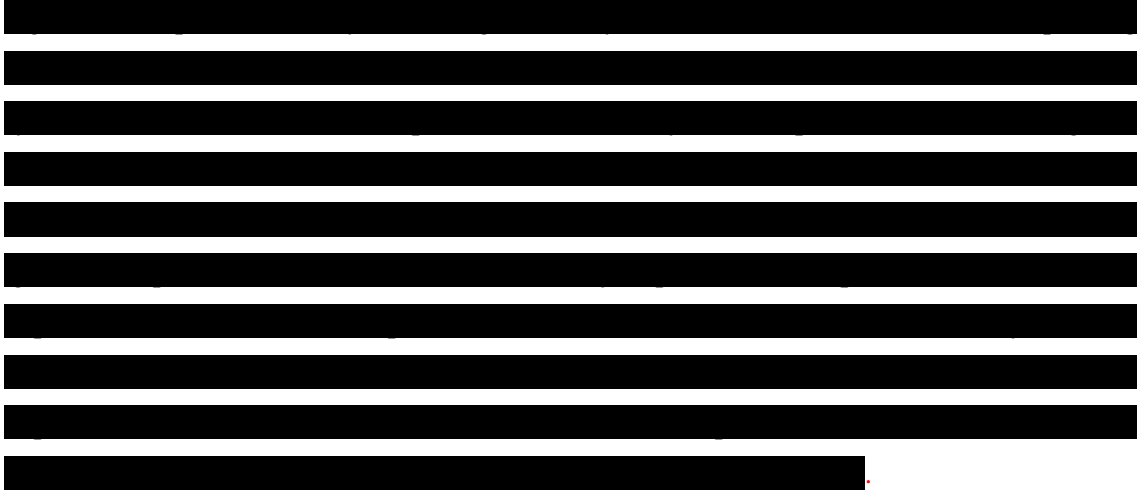
Fig 17. Absorption of the Real samples we have made. We can compare the samples with the glass substrate ABC free in brown (Ref Vidre)

It is worth to remember the equations of S parameters and absorption commented in chapter 3

$$|S_{11}|^2 + |S_{21}|^2 + |\alpha|^2 = 1$$

So

$$1 - |S_{11}|^2 - |\alpha|^2 = |S_{21}|^2$$



5.4.2 Real samples vs Simulated samples

Now for practicality we decide to work just with the samples that have passed the attenuation requirements. To see the differences between the simulation results and real samples we decided to simulate again the three samples using the WW and WS we have on table 2. The results for comparison are shown in table 4:

sample	1-way UPC Attenuation (dB)	1-way Simulation Attenuation (dB)
Y32	-0,24	-0,08
Y22	-0,20	-0,03
015P22v1100	-0,27	-0,03

Table4. shows the different values of attenuation for the three Real samples that passes attenuations requirements and the values of attenuation for the simulated samples

Table 4 shows on the left column the results measured at the UPC for real samples and on the right column the values for attenuation obtained for simulated samples with cst studio 2019. For sample Y32 the measured value is 3 times higher than the simulated sample and for 015P22v1100 sample the attenuation of the real sample is 9 times higher than that of the simulation. We can also plot these results between 71 GHz and 81 GHz and see that we obtain different results from the measurements and the simulations. In this case we decided to use the values of all the sample (circuit + substrate) since the subtracting calculations can introduce small errors that could be ignored in the data showed previously in the different chapters but not in this case that the differences between samples are so small.

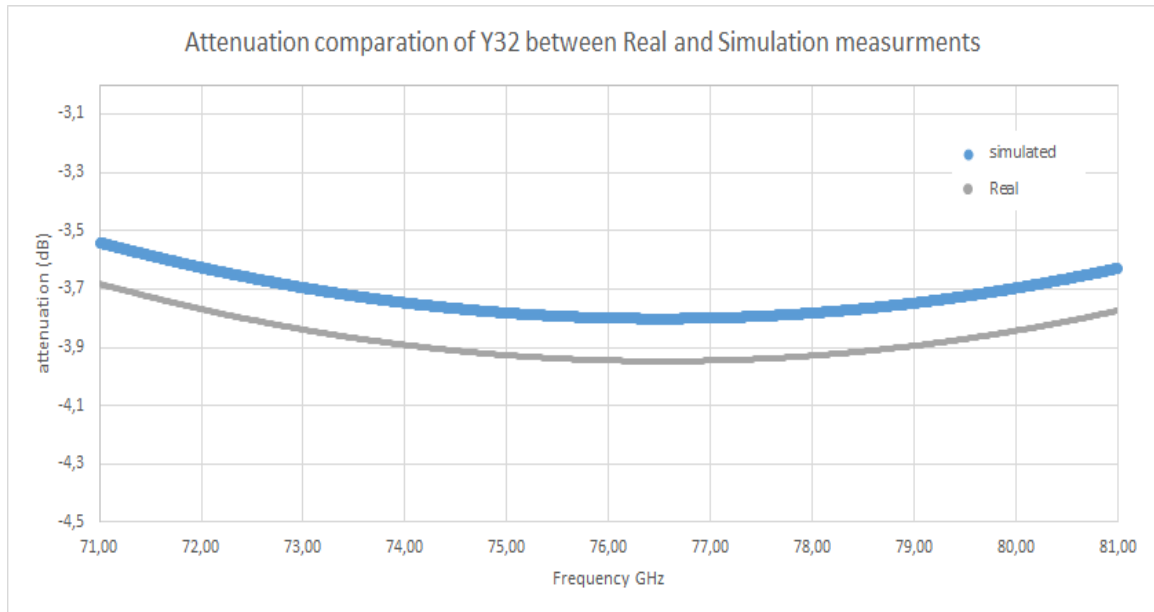


Fig 18. shows the simulated and real attenuation between 71 and 81 GHz in dB for Y32 sample

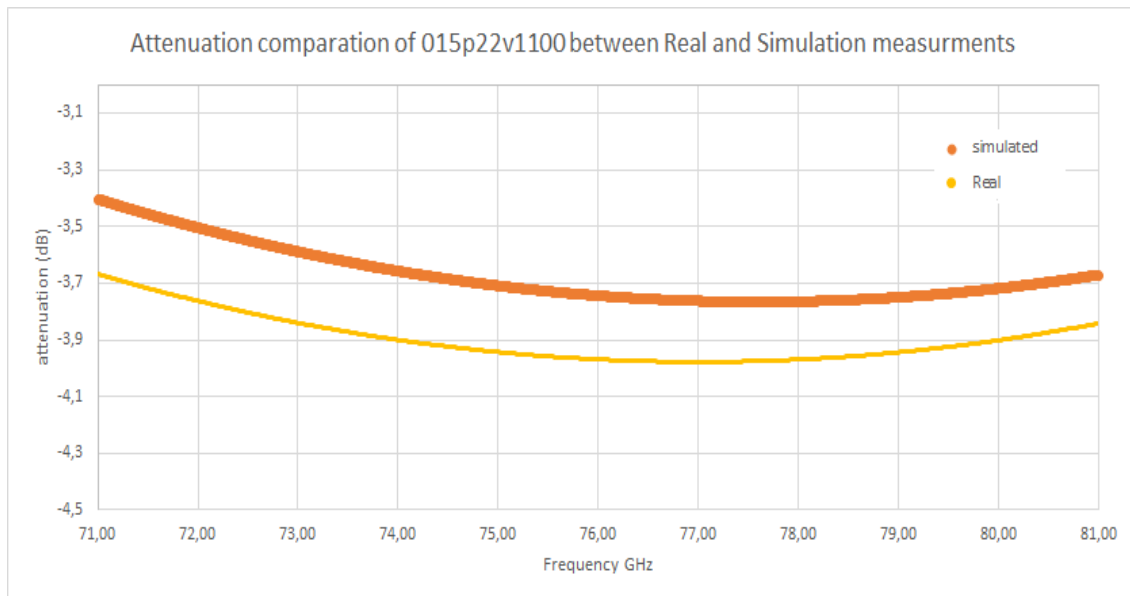


Fig 19. shows the simulated and real attenuation between 71 and 81 GHz in dB for 015p22v1100 sample

Figure 18 and 19 show us the attenuation of samples Y32 and 015p22v1100 measured at the UPC and simulated by CST in this case the attenuation of the glass substrate was not subtracted. We can see that Real samples are moved down between 0.3 and 0.2 dB in the logarithmic scale. To clearly see how different the two measurements are we can compute them linearly and see the difference between intensities:

$$(dB) = 20 \cdot \log_{10} S_i$$

$$(dB_S) - (dB_R) = 20 \cdot \log_{10} S_S - 20 \cdot \log_{10} S_R = 20 \cdot \log_{10} \left(\frac{S_S}{S_R} \right) = 0.3 \text{ dB}$$

$$\frac{S_S}{S_R} = 10^{0.015} \approx 1.035$$

Where suffix *S* refers to simulation sample and the suffix *R* refers to Real samples. So, the intensity that arrive to receiver in the simulation is just 1.035 times higher than the intensity arriving on the real case. So, real case and simulation case are not so different, but logarithmic scale makes them to look very different. Also, the requirements are very restrictive, and this is what makes small differences to be so important in this case.

5.5 Heating tests

In this section, we check if the samples that passes the attenuation requirements also passes the heating requirements. In this heating tests our samples will be introduced in the climatic chamber at -10°C. In this environment the vehicle manufactures' requirements say that the samples should reach 60°C in 5 minutes and the temperature should not go down for the following 5 minutes, so during this second period of 5 minutes temperature can increase from 60°C but it cannot go down.

The tests were performed at the climate chamber of the UB commented in chapter 2. Samples are introduced in the same way that the samples of chapter 3. With figure 20 we remember the scheme.

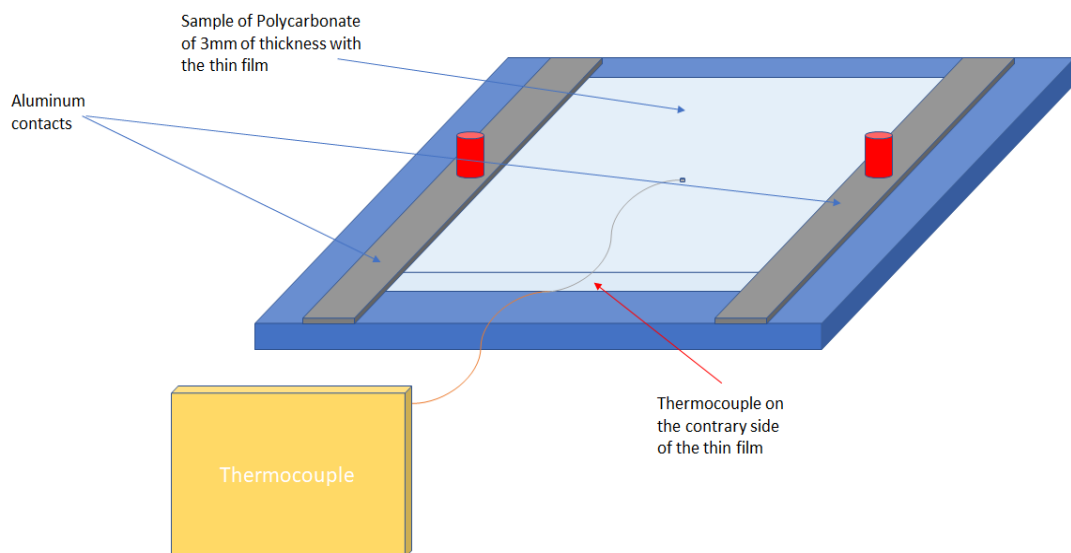


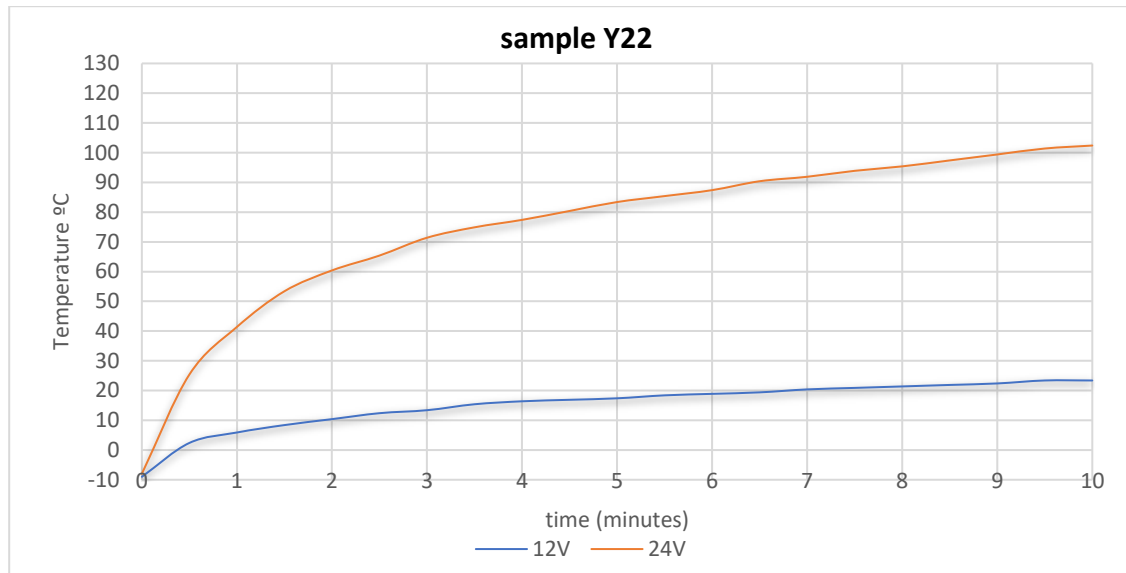
Fig 20. Scheme of how the measurement of temperature was done. The thermocouple had to be placed between the Polycarbonate sample and the HM tool in order that the current going through the thin film do not disturb the measurement

Temperature is measured in the opposite face of the ABC deposition, but we can compute a correction factor as we did in chapter 3 using equation 4 of chapter 3 considering the

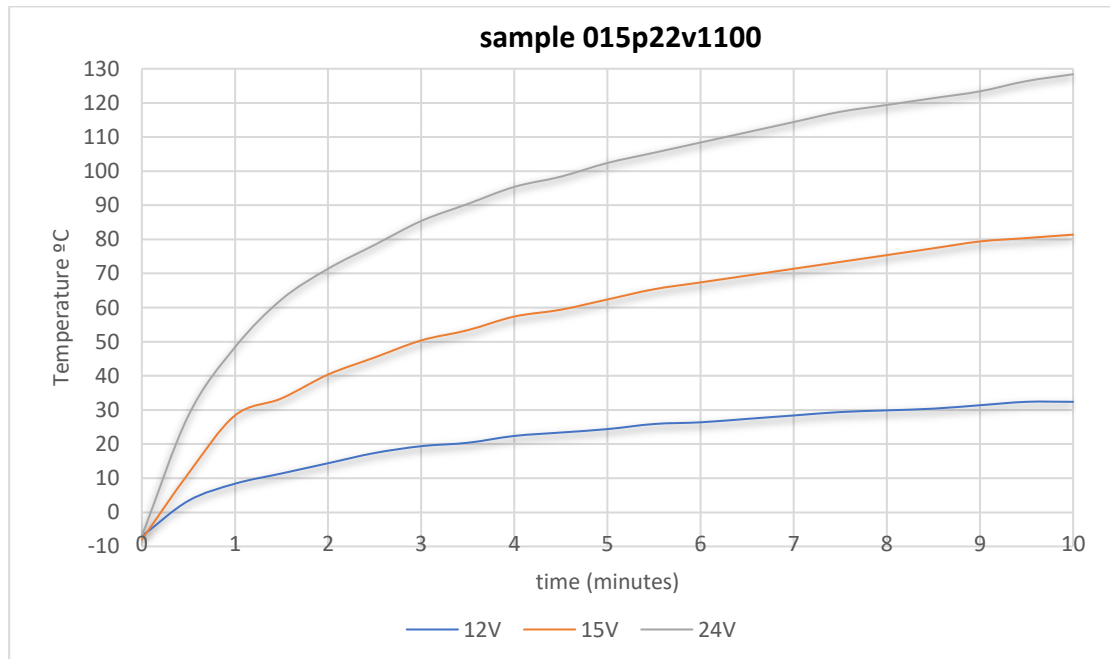
characteristics of the substrate see table 5. The following plots show the temperature achieved by the samples inside the climatic chamber for 10 minutes applying voltages of 12V, 15V and 24V.

Substrate: Soda Lime Float Glass	
thermal conductivity	$\kappa=1.05 \text{ W/m}\cdot\text{K}$
Substrate thickness	1.1 mm
Correction factor	3.387 °C

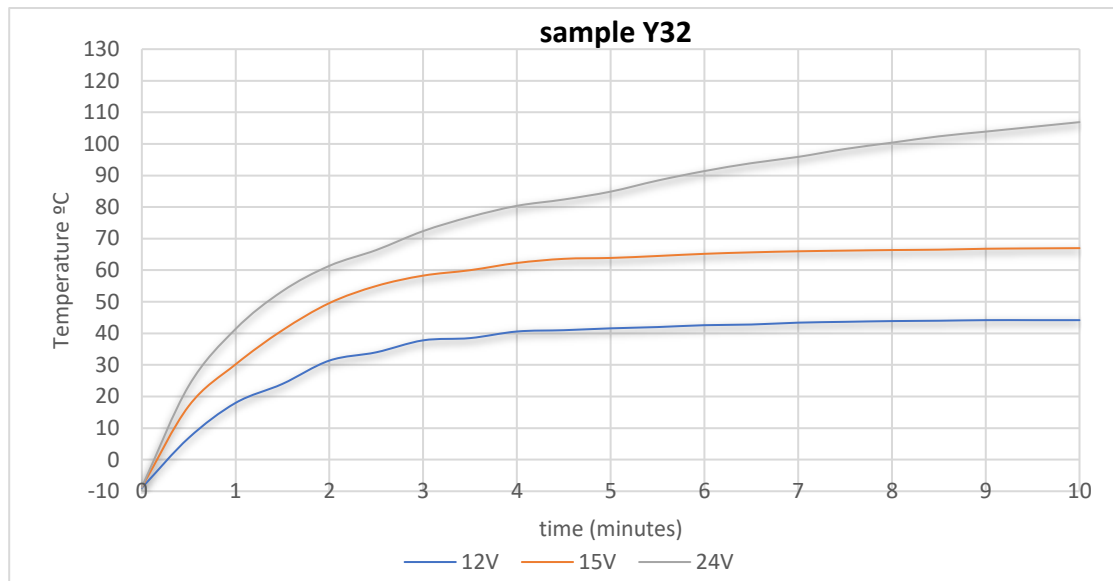
Table5. Thermal parameters and correction factor for glass substrate



Plot10. Evolution of temperature with time, in blue the temperature produced applying a 12V tension on the heating system and in red the temperature applying a 24V tension in th heating system for the sample Y22.



Plot11. Evolution of temperature with time, in blue the temperature achieved applying a 12V tension on the heating system, in red the temperature applying a 15V tension in the heating system and in green the temperature applying a 24V tension in the heating system for the sample 015p22v1100.



Plot12. Evolution of temperature with time, in blue the temperature achieved applying a 12V tension on the heating system, in red the temperature applying a 15V tension in the heating system and in green the temperature applying a 24V tension in the heating system for the sample Y32.

The three samples pass the requirements at 24V but not at 12V. nevertheless Y32 and 015p22v1100 were also tested at 15V since they were the samples with less resistance and they also pass the requirements at low voltage. Today’s vehicles use batteries of voltages in the range of 12V and 24V and, in some cases, batteries can even overpass the 24V. We have already calculated a minimum value for the power needed to melt a film of 1mm of ice for a Radome of 10 cm x 15 cm of surface in chapter 1 that is 18W, taking this value as a reference we can decide which of the samples passes the requirements for each voltage. If we look into the electrical parameters of these test showed in Table 6, we see that all samples overpass this minimum power for 24V and Y32 and 015p22v1100 overpass this minimum value also for 15V

sample voltage (V)	Y22		015p22v1100			Y32		
	12,00	24,00	12,00	15,00	24,00	12,00	15,00	24,00
I_0 (A)	0,81	1,66	1,44	1,82	2,83	1,26	1,58	2,51
I_f (A)	0,81	1,55	1,40	1,75	2,63	1,22	1,48	2,48
P_0 (W)	9,72	39,84	17,28	27,30	67,92	15,12	23,70	60,24
P_f (W)	9,72	37,20	16,80	26,25	63,12	14,64	22,20	59,52
R_r (Ω)	14,81	14,46	8,33	8,24	8,48	9,52	9,49	9,56
R_c (Ω)	10,34		8,17			8,95		

Table 6. Electric parameters measured during the heating test in the climatic chamber measured for each of the samples

Where the suffix 0 and f indicates the starting value and the final value of the parameter during the heating test. Also suffix r for resistances values refers to the real circuit resistance values

computed from the electrical parameters obtained during the tests and suffix c for computed values before doing the heating tests. Values of real resistances are slightly different from the values computed before doing the test with the data obtained in the previous sections of the chapter. Differences of samples Y32 and 015p22v1100 can be attributed to the copper connectors on the bottom and upper side of the samples and the Aluminum contacts of the HM tool that has not been considered when computing the resistances before the heating tests. Also, the geometry of the wires that are not ideal rectangles could bring to small differences between the computed and real values of the resistances. For sample Y22, apart from the commented reasons, we can think that some issues with the glue of the copper foil can be the reason why the differences are bigger than the other two samples.

5.6 Summary and comments

[REDACTED]

This allows us to design a heating system that could work in most common range of voltage for a vehicle between 12V and 15V [REDACTED]

[REDACTED]

Furthermore, this kind of heating system could be use on today's car after a good adaptation to a Polycarbonate substrate.

The etching technic is also a crucial factor on this kind of designs so, new and different etching technics should be tested and compared to improve the heating system. Here, we have used a laser that heats ABC creating a non-expected expansion of the material and a rough surface between wires that can affect electromagnetic radiation from the radar. We have seen how different the results from simulations are from those of the real samples. Simulations works with perfect rectangles, but the confocal images of real samples have shown us that the microstructure we have on our etched circuits is very different from a rectangle. [REDACTED]

[REDACTED]

[REDACTED]

[REDACTED]

[REDACTED]

[REDACTED]

[REDACTED]

[REDACTED]

6 Conclusions

In this thesis we have designed two different heating systems based on TCO with an optical transparency higher than 80% in the range of the human vision. So, we can assure that these two systems will reduce the impact on the image of a car's company. Both systems are based on TCO's, but their characteristics and deposition conditions are very different.

Regarding to [REDACTED] thin film heating system:

We developed it in the facilities of the UB and UZag so, we controlled all the parameters of its deposition and, so, we should be able to easily transfer this development to the Zanini's facilities.

[REDACTED]
[REDACTED]

- [REDACTED]
[REDACTED]. But, by using this design to a real Radome part we will also need to consider the curvature of the Radome to ensure its good heating homogeneity.

- We performed climatic test to ABC14 and Zanini6 but they do not passes the radar attenuation requirements of less than -0.3 dB 1 way. [REDACTED]
[REDACTED] should be use in a real Radomes which implies that [REDACTED]
[REDACTED] This indicates us that perhaps ABC is not the best material for this heating system design since we need better mechanical properties of the film [REDACTED]

- The results obtained in this thesis show us a good behavior of [REDACTED]
[REDACTED] icing conditions in the climatic chamber. But they fail when getting [REDACTED]. We considered that this is a consequence of the difference in thermal expansion between the TCO thin film and the substrate. This is an important point to be considered since depending on the resistance of the thin film to get the suitable attenuation requirements the voltage of work should be increased.

- This heating system requires [REDACTED]
[REDACTED]
[REDACTED]
[REDACTED]
[REDACTED]. This inquiry should be done by Zanini if they decide to go ahead with the internal development of this heating system.

Regarding to the ABC etched circuit:

- This design is ready to work with voltages on the range of common batteries used today in vehicles.
- Here the homogeneity of the heated surface is also improved as compared to the commercial Radomes that use copper wires.
- The ABC wires are placed on the surface of the Radome, so, no internal damages are produced to the plastic part.
- In this case polarization is a key factor for the right work of the radar, so, the dependence on polarization could not be forgot.

[REDACTED]
[REDACTED]
[REDACTED]
[REDACTED]
[REDACTED]

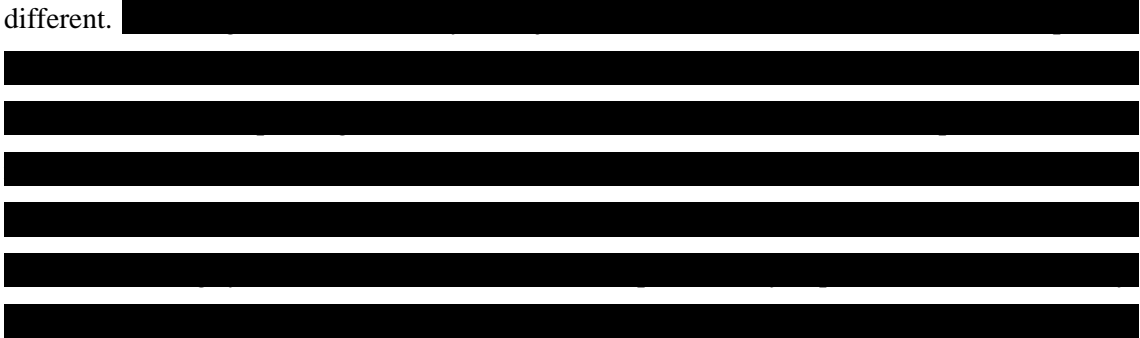
- Simulations can help to understand the behavior of this heating system, but the specific values of attenuation differ a lot from those of the real samples we made. To improve this point and to study if it is possible to have a better agreement between simulation and real cases, other TCO etching methods should be tested. [REDACTED]

[REDACTED]
[REDACTED] In this

context, simulations can be very helpful to focus the study to the most interesting configurations.

- In this case we have seen that reflection is a very important mechanism of attenuation in this heating system, so, a deeper development of this idea should be matched with an adaptation of the thickness of the Radome to minimize the effect of reflectivity.

Considering these conclusions, it is easy to compare both heating systems. Both use thin films of TCO's in a different way, so the industrial processes involved to produce each heating system are different.



REFERENCES

Chapter 0

- [1] https://en.wikipedia.org/wiki/Houdina_Radio_Control
- [2] Autonomous cars: Past, present and future a review of the developments in the last century, the present scenario and the expected future of autonomous vehicle technology - K. Bimbraw, 2015 12th International Conference on Informatics in Control, Automation and Robotics (ICINCO), Colmar, 2015, pp. 191-198.
- [3] LIDARvsRADAR, Ann Neal Fierce Electronics 2018.
<https://www.fierceelectronics.com/components/lidar-vs-radar>
- [4] Indicators for the Signal Degradation and Optimization of Automotive Radar Sensors under Adverse Weather Conditions - Arage Hassen, Alebel, PhD Tesis, Darmstadt, Technische Universität (2007)
- [5] Effects of Water and Ice Layer on Automotive Radar - Alebel Arage, Wolf Steens, G• otz K• uhnle, Rolf Jakoby, German Microwave Conference (GeMiC) 2006, University of Karlsruhe, Germany, 2006.

Chapter 1

- [1] Physics for scientist and engineering Vol 2, Paul A Tipler, Gene Mosca, Reverte, 6th edition, 2010, ISBN: 9788429144307
- [2] Electromagnetisme, Manuel Varela Fernandez, Publicacions i Edicions Universitat de Barcelona, 2006
- [3] Transparent Conductive Oxides - Hosono H., Ueda K. (2017). In: Kasap S., Capper P. (eds) Springer HandBook of Electronic and Photonic Materials. Springer HandBooks. Springer, Cham
- [4] TCO/metal/TCO structures for energy and flexible electronics - C. Guillén, J. Herrero Thin Solid Films, vol. 520, issue 1, pp. 1-17, October 2011.
- [5] HandBook of Transparent Conductors - David S. Ginley et al, Springer (2010).
- [6] Electrical properties and defect model of tin-doped indium oxide layers - Frank, G. & Köstlin, H. Appl. Phys. A (1982) 27: 197. <https://doi.org/10.1007/BF00619080>

[7] [REDACTED]
[REDACTED]

[8] [REDACTED]
[REDACTED]

[9] [REDACTED]
[REDACTED]

[10] [REDACTED]
[REDACTED]
[REDACTED]

[11] [REDACTED]
[REDACTED]
[REDACTED]

[12] A Drop Size Distribution (DSD) Based Model for Evaluating the Performance of Wet Radomes for Dual-Polarized Radars - Salazar, J., Chandrasekas, V., Trabal, J., Siquera, P., Medina, R., Knapp, E., and McLaughlin, D. (2014) J. Atmos. Oceanic Technol., 31:2409–2430

[13] Radome design and experimental characterization of scattering and propagation properties for atmospheric radar applications - Díaz, J.D.; Salazar-Cerreno, J.L.; Mancini, A.; Colom, J.G. Amer. Meteor. Soc. 2014, 819–823.

[14] Radar Signal Attenuation due to Finite due to finite Radome thickness - V. Kepeši and J. Labun, International Journal of Maritime Science, ISSN 0469-6255/2015 DOI 10.17818/NM/2015/SI20

[15] National radio astronomy observatory Tucson, Arizona: Radome study, 1976.
http://library.nrao.edu/public/memos/25/25M/25M_063.pdf

[16] the engineering toolbox - <https://www.engineeringtoolbox.com/>

Chapter 2

[1] Advanced Radome design for automotive applications - Santiago Buitrago, PhD TESIS U.P.C. 2019

[2] FeedBack networks: theory and circuit applications - Choma J. & Chen W.K. (2007). Singapore: World Scientific. Chapter 3, p. 225 ff. ISBN 978-981-02-2770-8.

[3] Keysight Technologies – Two-port Measurements and S-Parameters – Application note 4

[4]

[5] Estudio de propiedades ópticas, eléctricas y térmicas de recubrimientos decorativos aplicados a cocinas de inducción realizados mediante PVD - E. Carretero, PHD tesis, Universidad de Zaragoza, 2016.

[6] <http://www.ajaint.com/atc-orion-series-sputtering-systems.html>

[7] <https://www.weiss-technik.com>

[8] Jandel Manuals

[9] Sensofar PL μ 2300 online Manuals

[10] FIB-SEM of mouse nervous tissue: Fast and slow sample preparation - Methods in Cell Biology, Chapter 1, Anna M. Steyer, Andreas Schertel, Christos Nardis, Wiebke Möbius, Academic Press, Volume 152 Pages 1-21, 2019, ISSN 0091-679X

[11] Focused Ion beam systems - Thermo Fischer and Zeiss manuals

[12] Determination of thickness and optical constants of a-Si:H - R Swanepoel- J. Phys. E: Sci. Instrum. Vol. 16, 1983.

[13] Determining refractive index and thickness of thin films from wavelength measurements only - R Swanepoel - Opt. Soc. Am. A 1339 Vol. 2, No. 8/August 1985/J

[14] Substrate Effect on the Optical Reflectance and Transmittance of Thin-Film Structures - Anatoly Barybin and Victor Shapovalov - Journal of Optics Volume 2010, Article ID 137572, doi:10.1155/2010/137572 -

[15] Structure and optical properties of polycrystalline ZnSe thin films: validity of Swanepol's approach for calculating the optical parameters -MF Hasaneen, ZAAIrowaili and WS Mohamed 2020 Mater. Res. Express 7 016422

[16] Introduction to Solid State Physics - Physics 927, E.Y.Tsymbal - Section 13: Optical properties of solids – University of Nebraska – Lincoln

[17] HandBook of optics Volume I and II – Eric W van Stryland, David R Williams, William L. Wolfe, Michael Bass. Second Edition, Mc Graw-Hill Inc. (1995). ISBN 0-07-047974-7

[18] A simple method for the determination of the optical constants n, k and the thickness of a weakly absorbing thin film - J C Manifacier et al 1976 J. Phys. E: Sci. Instrum. 9 1002

[19] Substrate Effect on the Optical Reflectance and Transmittance of Thin-Film Structures - International Journal of Optics Volume 2010, Article ID 137572, 18 pages doi:10.1155/2010/137572

[20] Structure-Related Optical Characteristics of Thin Metallic Films in the Visible and Ultraviolet - JOURNAL OF RESEARCH of the National Bureau of Standards-A. Physics and Chemistry Vol. BOA, No.4, July-August 1976

Chapter 3

[1] Electrical Resistivity of Ultra-Thin Copper Films - Ernst Schmiedl Peter Wissmann Hans-Ulrich Finzel, Zeitschrift für Naturforschung A 63 (739-711), 2008

[2] [REDACTED]

[3] [REDACTED]

[4] Developing a theoretical relationship between electrical resistivity, temperature, and film thickness for conductors - Lacy, F, Nanoscale Res Lett 6, 636 (2011). <https://doi.org/10.1186/1556-276X-6-636>.

[5] [REDACTED]

[6] Radar absorbing materials based on titanium thin film obtained by sputtering technique - Soethe, Viviane Lilian, Nohara, Evandro Luis, Fontana, Luis César, Cerqueira Rezende, Mirabel, Journal of Aerospace Technology and Management 2011, 3(3), 279-286 ISSN: 1984-9648.

[7] The electrical conductivity of thin metal films with very smooth surfaces - A.A. Cottey, Thin Solid Films, Volume 1, Issue 4, 1968, Pages 297-307, ISSN 0040-6090

[8] [REDACTED]

[9] [REDACTED]

[10] [REDACTED]
[REDACTED]
[REDACTED]
[REDACTED]

[11] [REDACTED]
[REDACTED]
[REDACTED]

[12] [REDACTED]
[REDACTED]

[13] [REDACTED]
[REDACTED]
[REDACTED]

[14] <https://www.goodfellow.com/> specification Polycarbonate information

[15] Performance and Stress Analysis of Metal Oxide Films for CMOS-Integrated Gas Sensors - Lado Filipovic and Siegfried Selberherr, *Sensors* 2015, 15, 7206-7227

[16] Heterostructure of Ferromagnetic and Ferroelectric Materials with Magneto-Optic and Electro-Optic Effects - Guo, X.; Jiang, H.; Li, K.K.; Zou, Y.K. US Patent 8,124,254, 2012.

[17] [REDACTED]
[REDACTED]

[18] Hecht, Eugene. *Óptica*. 3a ed. Madrid: Addison-Wesley Iberoamericana, 2000

Chapter 4

[1] [REDACTED]
[REDACTED]
[REDACTED]
[REDACTED]

[2] [REDACTED]
[REDACTED]
[REDACTED]

[3] [REDACTED]
[REDACTED]
[REDACTED]

[4] [REDACTED]
[REDACTED]
[REDACTED]

[5] Semiconducting Transparent Thin Films - Hans Hartnagel; Bristol [England]; Philadelphia, PA: Institute of Physics Pub., ©1995.

[6] Semiconductor Material and Device Characterization - D. K. Schroder; Wiley, New York, 1990

[7] [REDACTED]
[REDACTED]
[REDACTED]

[8] [REDACTED]
[REDACTED]
[REDACTED]

[9] Electrical and optical properties of thin films consisting of tin-doped indium oxide nanoparticles - Ederth J. et al., (2003), PHYSICAL REVIEW B 68, 155410.

[10] CST STUDIO SUITE ELECTROMAGNETIC FIELD SIMULATION SOFTWARE manuals

[11] Nanofabrication using focused ion beams - Sven Bauerdick Raith GmbH, Konrad-Adenauer-Allee, Wiley Analytical Science, Dortmund, Germany

[12] An Introduction to Focus Ion Beam Nanofabrication. Raith. 2020. ABC Materials Magazine, <https://www.ABCm.com/article.aspx?ArticleID=14895>.

[13] Focused Ion Beams (FIB) — Novel Methodologies and Recent Applications for Multidisciplinary Sciences; chapter from “Modern Electron Microscopy in Physical and Life Sciences” By Meltem Sezen; IntechOpen 2016 DOI: 10.5772/61634

[14] Multispecies focused ion beam lithography system and its applications - Sven Bauerdick, Lars Bruchhaus, Paul Mazarov, Achim Nadzeyka, and Ralf Jede; Journal of Vacuum Science & Technology B 31, 06F404 (2013)

[15] Dual Beam: Focused Ion Beam (FIB) and FESEM- Universitat Politecnica de Valencia – Electron Microcopy Service. <http://www.upv.es/entidades/SME/info/859073normali.html>

[16] Optical properties on the visible range – Practice 4 – Laboratory of Physics of dialectical Materials – Arturo Lousa, Universitat de Barcelona

[17] Physics of Thin Films - L.Eckertova, Plenum ed., N.Y., 1977

Chapter 5

[1] Printed Circuits HandBook - Clyde F. Coombs, Jr.; Happy T. Holden. Seventh Edition (McGraw-Hill Education: New York, Chicago, San Francisco, Athens, London, Madrid, Mexico City, Milan, New Delhi, Singapore, Sydney, Toronto, 2016).

[2] "Lithography". Introduction to Microelectronic Fabrication - Jaeger, Richard C. (2002). (2nd ed.). Upper Saddle River: Prentice Hall.

[3] Etching in Microsystem Technology - Kohler, Michael (1999). John Wiley & Son Ltd.

[4] manuals, Rofin Sinar Power Line D 100D, Rofin, 1999

[5] <https://en.wikipedia.org/wiki/Polarizer>

[6] Polarization - Atkinson G.A. (2014) In: Ikeuchi K. (eds) Computer Vision. Springer, Boston, MA. https://doi.org/10.1007/978-0-387-31439-6_570

[7] Principles of optics: electromagnetic theory of propagation, interference and diffraction of light - Born, Max; Wolf, Emil. 7th expanded ed. Cambridge: Cambridge University Press, 1999

[8] Óptica, Hecht, Eugene. 3a ed. Madrid: Addison-Wesley Iberoamericana, 2000

